Eur. Phys. J. C (2009) 60: 543–583
DOI 10.1140/epjc/s10052-009-0966-6

THE EUROPEAN PHYSICAL JOURNAL C

Regular Article - Theoretical Physics

Revisiting the global electroweak fit of the Standard Model and beyond with Gfitter

The Gfitter Group

H. Flächer[1], M. Goebel[2,3], J. Haller[3], A. Hoecker[1,a], K. Mönig[2], J. Stelzer[2]

[1]CERN, Geneva, Switzerland
[2]DESY, Hamburg and Zeuthen, Germany
[3]Institut für Experimentalphysik, Universität Hamburg, Hamburg, Germany

Received: 12 November 2008 / Revised: 13 February 2009 / Published online: 19 March 2009

Abstract The global fit of the Standard Model to electroweak precision data, routinely performed by the LEP electroweak working group and others, demonstrated impressively the predictive power of electroweak unification and quantum loop corrections. We have revisited this fit in view of (i) the development of the new generic fitting package, *Gfitter*, allowing for flexible and efficient model testing in high-energy physics, (ii) the insertion of constraints from direct Higgs searches at LEP and the Tevatron, and (iii) a more thorough statistical interpretation of the results. Gfitter is a modular fitting toolkit, which features predictive theoretical models as independent plug-ins, and a statistical analysis of the fit results using toy Monte Carlo techniques. The state-of-the-art electroweak Standard Model is fully implemented, as well as generic extensions to it. Theoretical uncertainties are explicitly included in the fit through scale parameters varying within given error ranges.

This paper introduces the Gfitter project, and presents state-of-the-art results for the global electroweak fit in the Standard Model (SM), and for a model with an extended Higgs sector (2HDM). Numerical and graphical results for fits with and without including the constraints from the direct Higgs searches at LEP and Tevatron are given. Perspectives for future colliders are analysed and discussed.

In the SM fit including the direct Higgs searches, we find $M_H = 116.4^{+18.3}_{-1.3}$ GeV, and the 2σ and 3σ allowed regions $[114, 145]$ GeV and $[[113, 168]$ and $[180, 225]]$ GeV, respectively. For the strong coupling strength at fourth perturbative order we obtain $\alpha_S(M_Z^2) = 0.1193^{+0.0028}_{-0.0027}(\text{exp}) \pm 0.0001$ (theo). Finally, for the mass of the top quark, excluding the direct measurements, we find $m_t = 178.2^{+9.8}_{-4.2}$ GeV. In the 2HDM we exclude a charged-Higgs mass below 240 GeV at 95% confidence level. This limit increases towards larger $\tan\beta$, e.g., $M_{H^\pm} < 780$ GeV is excluded for $\tan\beta = 70$.

Contents

[a] e-mail: andreas.hoecker@cern.ch

1 Introduction

Precision measurements allow us to probe physics at much higher energy scales than the masses of the particles directly involved in experimental reactions by exploiting contributions from quantum loops. These tests do not only require accurate and well understood experimental data but also theoretical predictions with controlled uncertainties that match the experimental precision. Prominent examples are the LEP precision measurements, which were used in conjunction with the Standard Model (SM) to predict via multidimensional parameter fits the mass of the top quark [1], prior to its discovery at the Tevatron [2, 3]. Later, when combined with the measured top mass, the same approach led to the prediction of a light Higgs boson [4]. Other examples are fits to constrain parameters of supersymmetric or extended Higgs models, using as inputs the anomalous magnetic moment of the muon, results on neutral-meson mixing, CP violation, rare loop-induced decays of B and K mesons, and the relic matter density of the universe determined from fits of cosmological models to data.

Several theoretical libraries within and beyond the SM have been developed in the past, which, tied to a multi-parameter minimisation program, allowed one to constrain the unbound parameters of the SM [5–8]. However, most of these programs are relatively old, were implemented in outdated programming languages, and are difficult to maintain in line with the theoretical and experimental progress. It is unsatisfactory to rely on them during the forthcoming era of the Large Hadron Collider (LHC) and the preparations for future linear collider projects. Improved measurements of important input observables are expected and new observables from discoveries may augment the available constraints. None of the previous programs were modular enough to easily allow the theoretical predictions to be extended to models beyond the SM, and they are usually tied to a particular minimisation package.

These considerations led to the development of the generic fitting package *Gfitter* [9], designed to provide a framework for model testing in high-energy physics. Gfitter is implemented in C++ and relies on ROOT [10] functionality. Theoretical models are inserted as plug-in packages, which may be hierarchically organised. Tools for the handling of the data, the fitting, and statistical analyses such as toy Monte Carlo sampling are provided by a core package, where theoretical errors, correlations, and inter-parameter dependencies are consistently dealt with. The use of dynamic parameter caching avoids the recalculation of unchanged results between fit steps, and thus significantly reduces the amount of computing time required for a fit.

The first theoretical framework implemented in Gfitter has been the SM predictions for the electroweak precision observables measured by the LEP, SLC and the Tevatron experiments. State-of-the-art calculations have been used, and—wherever possible—the results have been cross-checked against the ZFITTER package [5]. For the W mass and the effective weak mixing angle, which exhibit the strongest constraints on the Higgs mass through radiative corrections, the full second-order corrections are available [11–13]. Furthermore, the corrections of order $\mathcal{O}(\alpha\alpha_S^2)$ and the leading three-loop corrections in an expansion of the top-mass-squared (m_t^2) are included. The full three-loop corrections are known in the large M_H limit, however they turn out to be negligibly small [14, 15]. The partial and total widths of the Z are known to leading order, while for the second order only the leading m_t^2 corrections are available [16]. Among the new developments included in the SM library is the fourth-order (3NLO) perturbative calculation of the massless QCD Adler function [17], contributing to the vector and axial-vector radiator functions in the prediction of the Z hadronic width (and other observables). It allows one to fit the strong coupling constant with unique theoretical accuracy [17, 18].

Among the experimental precision data used are the Z mass, measured with relative precisions of 2×10^{-5}, the hadronic pole cross section at the Z mass and the leptonic decay width ratio of the Z with 10^{-3} relative precision. The effective weak mixing angle $\sin^2\theta_{\mathrm{eff}}^{\ell}$ is known from the LEP experiments and SLD to a relative precision of 7×10^{-4}. The W mass has been measured at LEP and the Tevatron to an overall relative precision of 3×10^{-4}. The mass of the top quark occurs quadratically in loop corrections of many observables. A precision measurement (currently 7×10^{-3}) is mandatory. Also required is the precise knowledge of the electromagnetic and weak coupling strengths at the appropriate scales. Energy-dependent photon vacuum polarisation contributions modify the QED fine structure constant, which at the Z-mass scale has been evaluated to a relative precision of 8×10^{-3}. The Fermi constant, parameterising the weak coupling strength, is known to 10^{-5} relative precision.

We perform global fits in two versions: the *standard ("blue-band") fit* makes use of all the available information except for the direct Higgs searches performed at LEP and the Tevatron; the *complete fit* uses also the constraints from the direct Higgs searches. Results in this paper are commonly derived for both types of fits.

Several improvements are expected from the LHC [19, 20]. The uncertainty on the W-boson and the top-quark masses should shrink to 1.8×10^{-4} and 5.8×10^{-3} respectively. In addition, the Higgs boson should be discovered leaving the SM without an unmeasured parameter (excluding here the massive neutrino sector, requiring at least nine additional parameters, which are however irrelevant for the results discussed in this paper). The primary focus of the global SM fit would then move from parameter estimation to the analysis of the goodness-of-fit with the goal to uncover inconsistencies between the model and the data, indicating

the presence of new physics. Because the Higgs-boson mass enters only logarithmically in the loop corrections, a precision measurement is not required for this purpose. Dramatic improvements on SM observables are expected from the ILC [21]. The top and Higgs masses may be measured to a relative precision of about 1×10^{-3}, corresponding to absolute uncertainties of 0.2 GeV and 50 MeV, respectively. Running at lower energy with polarised beams, the W mass could be determined to better than 7×10^{-5} relative accuracy, and the weak mixing angle to a relative precision of 5×10^{-5}. Moreover, new precision measurements would enter the fit, namely the two-fermion cross section at higher energies and the triple gauge couplings of the electroweak gauge bosons, which are sensitive to models beyond the SM. Most importantly, however, both machines are directly sensitive to new phenomena and thus either provide additional constraints on fits of new physics models or—if the searches are successful—may completely alter our view of the physics at the terascale. The SM will then require extensions, the new parameters of which must be determined by a global fit, whose goodness must also be probed. To study the impact of the expected experimental improvements on the SM parameter determination, we perform fits under the assumption of various prospective setups (LHC, ILC, and ILC with GigaZ option).

As an example for a study beyond the SM we investigate models with an extended Higgs sector of two doublets (2HDM). We constrain the mass of the charged Higgs and the ratio of the vacuum expectation values of the two Higgs doublets using current measurements of observables from the B and K physics sectors and the most recent theoretical 2HDM predictions.

The paper is organised as follows. A disquisition of statistical considerations required for the interpretation of the fit results is given in Sect. 2. It is followed in Sect. 3 by an introduction to the Gfitter project and toolkit. The calculation of electroweak precision observables, the results of the global fit, and its perspectives are described in Sect. 4. Section 5 discusses results obtained for the Two Higgs Doublet Model. Finally, a collection of formulae used in the theoretical libraries of Gfitter is given in the appendix. We have chosen to give rather exhaustive information here for the purpose of clarity and reproducibility of the results presented.

2 The statistical analysis

The fitting tasks are performed with the Gfitter toolkit described in Sect. 3. It features the minimisation of a test statistics and its interpretation using frequentest statistics. Confidence intervals and p-values are obtained with the use of toy Monte Carlo (MC) simulation or probabilistic approximations where mandatory due to resource limitations. This section introduces the three statistical analyses performed in the paper: (i) determination of SM parameters, (ii) probing the overall goodness of the SM, and (iii) probing SM extensions and determining its parameters. The SM part is represented by the global fit at the electroweak scale (Sect. 4), while as example for beyond SM physics we analyse an extension of the Higgs sector to two scalar doublets (Sect. 5). The statistical treatment of all three analyses relies on a likelihood function formed to measure the agreement between data and theory. The statistical discussion below follows in many aspects Refs. [22, 23] with additional input from [24, 25] and other statistical literature.

2.1 Model parameters

We consider an analysis involving a set of N_{exp} measurements $(x_{\text{exp}})_{i=1\ldots N_{\text{exp}}}$, described by a corresponding set of theoretical expressions $(x_{\text{theo}})_{i=1\ldots N_{\text{exp}}}$. The theoretical expressions are functions of a set of N_{mod} model parameters $(y_{\text{mod}})_{j=1\ldots N_{\text{mod}}}$. Their precise definition is irrelevant for the present discussion besides the fact that:

- a subset of (y_{mod}) may be unconstrained parameters of the theory (e.g., the Higgs mass in the SM, if the results from the direct searches are not used);
- another subset of (y_{mod}) are theoretical parameters for which prior knowledge from measurements or calculations is available and used (e.g., the Z-boson mass and the hadronic vacuum polarisation contribution to the running electromagnetic coupling strength);
- the remaining (y_{mod}) parameterise theoretical uncertainties, which are based on hard-to-quantify educated guesswork (e.g., higher-order QCD corrections to a truncated perturbative series).

It may occur that x_{exp} or y_{mod} parameters have statistical *and* theoretical errors, requiring a proper treatment for both of these. In the following we use the shorthand notations y_{mod} $(x_{\text{exp}}, x_{\text{theo}})$ to label both, sets of and individual parameters (measurements, theoretical expressions).

2.2 Likelihood function

We adopt a least-squares-like notation and define the test statistics

$$\chi^2(y_{\text{mod}}) \equiv -2 \ln \mathcal{L}(y_{\text{mod}}), \tag{2.1}$$

where the likelihood function, $\mathcal{L}$, is the product of two contributions

$$\mathcal{L}(y_{\text{mod}}) = \mathcal{L}_{\text{exp}}\big(x_{\text{theo}}(y_{\text{mod}}) - x_{\text{exp}}\big) \cdot \mathcal{L}_{\text{theo}}(y_{\text{mod}}). \tag{2.2}$$

The experimental likelihood, $\mathcal{L}_{\text{exp}}$, measures the agreement between x_{theo} and x_{exp}, while the theoretical likelihood,

$\mathcal{L}_{\rm theo}$, expresses prior knowledge of some of the $y_{\rm mod}$ parameters. In most cases $\mathcal{L}_{\rm exp}$ incorporates well-behaved statistical errors as well as (mostly) non-statistical experimental systematic uncertainties. In some instances it may also include theoretical uncertainties and/or specific treatments that may account for inconsistent measurements. On the contrary, $\mathcal{L}_{\rm theo}$ relies on educated guesswork, akin to experimental systematic errors, but in most cases less well defined. The impact of (mostly strong interactions related) theoretical uncertainties and their treatment on the analysis may be strong, as it is the case for the global CKM fit [22, 23]. The statistical treatment *R*fit [22, 23] (described below) is designed to deal with the problem of theoretical errors in a clear-cut and conservative manner. Evidently though, an ill-defined problem cannot be treated rigorously, and results that strongly depend on theory uncertainties must be interpreted with care. For the present analysis, by virtue of the large electroweak mass scale so that QCD is in the perturbative regime, purely theoretical errors are small and controlled, so that the fit results are well behaved. Increasing experimental precision may alter this picture in the future.

The experimental likelihood

The experimental component of the likelihood is given by the product

$$\mathcal{L}_{\rm exp}\big(x_{\rm theo}(y_{\rm mod}) - x_{\rm exp}\big) = \prod_{i,j=1}^{N_{\rm exp}} \mathcal{L}_{\rm exp}(i,j), \tag{2.3}$$

where the $N_{\rm exp}$ individual likelihood components $\mathcal{L}_{\rm exp}(i,j)$ account for observables that may be independent or not. The model predictions of the observables depend on a subset of the $y_{\rm mod}$ parameters, and are used to constrain those. Ideally, all likelihood components are independent (i.e. $\mathcal{L}_{\rm exp}(i,j) = 0$ for $i \neq j$) Gaussian functions, each with a standard deviation estimating the experimental statistical uncertainty.[1] In practise however, one has to deal with correlated measurements and with additional experimental and theoretical systematic uncertainties. In accordance with the approach adopted by most published analyses, experimental systematic errors are assumed to express Gaussian standard deviations, so that different systematic errors can be added in quadrature.[2] Theoretical errors are treated according to the *R*fit scheme described below.

The theoretical likelihood

The theoretical component of the likelihood is given by the product

$$\mathcal{L}_{\rm theo}(y_{\rm mod}) = \prod_{i=1}^{N_{\rm mod}} \mathcal{L}_{\rm theo}(i). \tag{2.4}$$

The individual components $\mathcal{L}_{\rm theo}(i)$ can be constant everywhere in case of no a priori information, be bound, or may express a probabilistic function when such information is reliably available. Ideally, one should incorporate in $\mathcal{L}_{\rm exp}$ measurements (or equivalent determinations such as Lattice gauge theory, provided well-controlled theoretical assumptions are made) from which constraints on the $y_{\rm mod}$ parameters can be derived. If such constraints are not available, or if a component has been explicitly introduced to parameterise theoretical uncertainty, the $\mathcal{L}_{\rm theo}(i)$ components must be incorporated by hand in (2.4). They are statistically ill-defined and can hardly be treated as probability density functions.

In the *range fit* approach, *R*fit, it is proposed that the theoretical likelihoods $\mathcal{L}_{\rm theo}(i)$ do not contribute to the χ^2 of the fit when the corresponding $y_{\rm mod}$ parameters take values within allowed ranges denoted $[y_{\rm mod}]$. Usually these ranges are identified with the intervals $[\overline{y}_{\rm mod} - \sigma_{\rm theo}\,,\, \overline{y}_{\rm mod} + \sigma_{\rm theo}]$, where $\overline{y}_{\rm mod}$ is a best-guess value, and $\sigma_{\rm theo}$ is the theoretical systematic error assigned to $y_{\rm mod}$. Hence all *allowed* $y_{\rm mod}$ values are treated on equal footing, irrespective of how close they are to the edges of the allowed range. Instances where even only one of the $y_{\rm mod}$ parameters lies outside its nominal range are not considered. This is the unique assumption made in the *R*fit scheme: $y_{\rm mod}$ parameters for which a priori information exists are bound to remain within *predefined* allowed ranges. The *R*fit scheme departs from a perfect frequentest analysis only because the allowed ranges $[y_{\rm mod}]$ do not always extend to the whole physical space.[3] This minimal assumption, is nevertheless a strong constraint: all the results obtained should be understood as valid only if all the assumed allowed ranges contain the true values of their $y_{\rm mod}$ parameters. Because there is in general no guarantee for it being the case, a certain arbitrariness of the results remains and must be kept in mind.[4] Although in general range

[1] The fitting procedure described in Sect. 2.3 uses χ^2 minimisation to obtain the best match between a test hypothesis, represented by a certain parameter set, and the data. This requires the use of *expected* experimental errors corresponding to the test hypothesis in the experimental likelihood, rather than the *measured* experimental errors. However, the expected experimental errors are usually not available for all possible test hypotheses, and the measured experimental errors are used instead. This may be a reasonable approximation for test values in close vicinity of the measured experimental results. Nonetheless, one should expect that for regions that are strongly disfavoured by the likelihood estimator the statistical analysis is less precise, so that large deviations in terms of "sigmas" must be interpreted with care. We shall revisit this point in Sect. 4.2.2 when including results from the direct searches for the Higgs boson in the fit.

[2] This introduces a Bayesian flavour to the statistical analysis.

[3] Some $y_{\rm mod}$ parameters do not have any a priori information and are hence fully unbound in the fit.

[4] If a theoretical parameter is bound to an allowed range, and if this range is narrower than what the fit would yield as constraint for the

errors do not need to be of theoretical origin, but could as well parameterise hard-to-assess experimental systematics, or set physical boundaries, we will collectively employ the term "theoretical (or theory) errors" to specify range errors throughout this paper.

2.3 Parameter estimation

When estimating model parameters one is not interested in the quality of the agreement between data and the theory as a whole. Rather, taking for granted that the theory is correct, one is only interested in the quality of the agreement between data and various realisations (models) of the theory, specified by distinct sets of $y_{\rm mod}$ values. In the following we denote $\chi^2_{\min;\hat{y}_{\rm mod}}$ the absolute minimum value of the χ^2 function of (2.1), obtained when letting all the $y_{\rm mod}$ parameters free to vary within their respective bounds, with a fit converging at the solution $\hat{y}_{\rm mod}$.[5] One now attempts to estimate confidence intervals for the complete $y_{\rm mod}$ set. This implies the use of the offset-corrected test statistics

$$\Delta\chi^2(y_{\rm mod}) = \chi^2(y_{\rm mod}) - \chi^2_{\min;\hat{y}_{\rm mod}}, \tag{2.5}$$

where $\chi^2(y_{\rm mod})$ is the χ^2 for a given set of model parameters $y_{\rm mod}$. Equation (2.5) represents the logarithm of a profile likelihood. The minimum value $\Delta\chi^2(\hat{y}_{\rm mod})$ is zero, by construction. This ensures that, consistent with the assumption that the model is correct, exclusion confidence levels[6] (CL) equal to zero are obtained when exploring the $y_{\rm mod}$ space.

In general, the $y_{\rm mod}$ parameters in (2.5) are divided into relevant and irrelevant ones. The relevant parameters (denoted a) are scanned for estimation purposes, whereas the irrelevant ones (the *nuisance* parameters μ) are adjusted such that $\Delta\chi^2(a,\mu)$ is at a minimum for $\mu = \hat{\mu}$. Since in frequentest statistics one cannot determine probabilities for certain a values to be true, one must derive exclusion CLs. The goal is therefore to set exclusion CLs in the a space irrespective of the μ values.

A necessary condition is that the confidence interval (CI) constructed from the $\Delta\chi^2(y_{\rm mod})$ test statistics provides sufficient coverage, that is, the CI for a parameter under consideration covers the true parameter value with a frequency of at least the CL values at the CI boundaries if the measurement were repeated many times. For a Gaussian problem, the test statistics follows a χ^2 distribution [26] and one finds

$$1 - \mathrm{CL}(a,\hat{\mu}) = \mathrm{Prob}\big(\Delta\chi^2(a,\hat{\mu}), \dim[a]\big), \tag{2.6}$$

where $\dim[a]$ is the dimension of the a space, which is the number of degrees of freedom[7] of the offset-corrected $\Delta\chi^2$. Here the probability density distribution of $\Delta\chi^2$ is independent of μ. In a non-Gaussian case the CI for a must be evaluated with toy MC simulation for any possible set of true μ values using, e.g., a Neyman construction [27] with likelihood-ratio ordering [28, 29].[8] One may then choose for each a the set of μ that gives the smallest $\mathrm{CL}(a)$. This "supremum" approach [24] (also described in Ref. [25] with however a somewhat different meaning) provides the most conservative result, which however overcovers in general. (Note also that the approach depends on the ordering algorithm used [30].) It may lead to the paradoxical situation that μ values excluded by the data may be chosen as the true set to determine $\mathrm{CL}(a)$. As a modification to this scheme, one could only consider μ values that are within predefined $\Delta\chi^2(a,\mu)$ bounds, thus guaranteeing a minimum compatibility with the data [31, 32]. A vast literature on this topic is available (see PhyStat conference proceedings and, e.g., Ref. [25]), mostly attempting to prescribe a limitation of the μ space while maintaining good coverage properties.[9] We point out that the naive "plug-in" approach that consists of using the set of $\hat{\mu}$ that minimises $\Delta\chi^2(a,\hat{\mu})$ in the fit to estimate the true μ is incorrect in general (it is trivially correct if the problem is strictly Gaussian, as then the $\Delta\chi^2$ distribution is μ-independent). It may lead to serious undercoverage if the $\Delta\chi^2(a,\mu)$ frequency distribution is strongly dependent on μ (cf. the analysis of the CKM phase γ [24]).

As a shortcut to avoid the technically challenging full Neyman construction in presence of nuisance parameters,

parameter if let free to float, the best fit value of this (bound) parameter usually occurs on the edge of the allowed range. A modification of this range will thus have immediate consequences for the central values of the fit.

[5] The application of the *R*fit scheme in presence of theoretical uncertainties may lead to a non-unique $\{\hat{y}_{\rm mod}\}$ solution space.

[6] Throughout this paper the term *confidence level* denotes 1 minus the p-value of a given $\Delta\chi^2$ (or χ^2) test statistics, and is hence a measure of the exclusion probability of a hypothesis. This is not to be confounded with a *confidence interval*, which expresses an inclusion probability.

[7] Note that the effective number of degrees of freedom may not always be equal to the dimension of the a space. For example, if $\dim[a] = 2$ but a single observable $\mathcal{O} = f(a)$ is scanned in a, only one of the two dimensions of a is independent, while the other can be derived via $\mathcal{O}$ so that the effective $\dim[a]$ to be used here is one [23]. Similarly, the available observables may only constrain one of the two dimensions of a. Again, the effective dimension to be used in (2.6) would be one. Intermediate cases, mixing strong and weak constraints in different dimensions of a may lead to an ill-posed situation, which can only be resolved by means of a full toy MC analysis. Such an analysis is performed at some instances in this paper (see in particular Sect. 5.2.2 for the two-dimensional case).

[8] An ordering scheme is required because the construction of a Neyman CL belt is not unique. It depends on the definition of the test statistics used.

[9] We recall here the reserve expressed in footnote 1 on p. 546 affecting the accuracy of any approach: the dependence of the measured errors on the outcome of the observables (determined by a and μ)—if significant—must be taken into account.

one may choose a Gaussian interpretation of the profile likelihood $\mathcal{L}(a, \hat{\mu})$ versus a, which corresponds to a MINOS [33] parameter scan. Simple tests suggest satisfying coverage properties of the profile likelihood (see, e.g., [34–36]). Mainly because of its simplicity this assumption will be adopted for most (though not all) of the results presented in this paper.

2.4 Probing the Standard Model

By construction, the parameter estimation via the offset-corrected $\Delta\chi^2$ is unable to detect whether the SM fails to describe the data. This is because (2.5) wipes out the information contained in $\chi^2_{\mathrm{min};\,\hat{y}_{\mathrm{mod}}}$. This value is a test statistics for the best possible agreement between data and theory. The agreement can be quantified by the p-value $\mathcal{P}(\chi^2_{\mathrm{min}} \geq \chi^2_{\mathrm{min};\,\hat{y}_{\mathrm{mod}}}|\mathrm{SM})$, which is the tail probability to observe a test statistics value as large as or larger than $\chi^2_{\mathrm{min};\,\hat{y}_{\mathrm{mod}}}$, if the SM is the theory underlying the data. It hence quantifies the probability of wrongly rejecting the SM hypothesis. In a Gaussian case, $\chi^2_{\mathrm{min};\,\hat{y}_{\mathrm{mod}}}$ can be readily turned into a p-value via $\mathrm{Prob}(\chi^2_{\mathrm{min};\,\hat{y}_{\mathrm{mod}}}, n_{\mathrm{dof}})$.[10] In presence of non-Gaussian effects, a toy MC simulation must be performed. Again, a full frequentest analysis requires the scan of all possible (or "likely") true nuisance parameters, followed by toy MC studies to derive the corresponding p-values. Chosen is the set of true $\hat{y}_{\mathrm{mod}}$ that maximises $\mathcal{P}(\chi^2_{\mathrm{min};\,\hat{y}_{\mathrm{mod}}}|\mathrm{SM})$, where here exact coverage is guaranteed by construction (note that in this phase no explicit parameter determination is performed so that all y_{mod} are nuisance parameters).

Such a *goodness-of-fit* test may not be the most sensitive manner to uncover physics beyond the SM (BSM). If the number of degrees of freedom is large in the global fit, and if observables that are sensitive to the BSM physics are mixed with insensitive ones, the fluctuations in the latter observables dilute the information contained in the global p-value (or deficiencies in the SM description may fake presence of new physics). It is therefore mandatory to also probe specific BSM scenarios.[11]

[10] The corresponding ROOT function is TMath::Prob(...).

[11] This problem is similar to those occurring in goodness-of-fit (GoF) tests in experimental maximum-likelihood analyses. If, for instance, the data sample with respect to which a likelihood analysis is performed is dominated by background events with a small but significant signal excess a successful global GoF test would only reveal agreement with the background model and say little about the signal. Similarly, a small p-value for the null hypothesis may reflect problems in the background description rather than an excess of signal events. A possible remedy here would be to restrict the GoF test to signal-like events, or more specifically, to test the GoF in all likelihood bins independently.

2.5 Probing new physics

If the above analysis establishes that the SM cannot accommodate the data, that is, the p-value is smaller than some critical value, the next step is to probe the BSM physics revealed by the observed discrepancy. The goal is akin to the determination of the SM parameters: it is to measure new sets of physical parameters y_{NP} that complement the y_{mod} SM parameters. The treatment is identical to the one of Sect. 2.3, using $a = \{y_{\mathrm{NP}}\}$. Even if the SM cannot be said to be in significant disagreement with the data, the estimation of y_{NP} remains interesting because the most sensitive observables, and the precision to be aimed at for their determination can only be derived by this type of analysis. Moreover, the specific analysis might be able to faster detect the first signs of a discrepancy between data and the SM if the theoretical extension used in the analysis turns out to be the right one.

3 The Gfitter package

The generic fitting package Gfitter comprises a statistical framework for model testing and parameter estimation problems. It is specifically designed to provide a modular environment for complex fitting tasks, such as the global SM fit to electroweak precision data, and fits beyond the SM. Gfitteris also a convenient framework for averaging problems, ranging from simple weighted means using or not correlated input data, to more involved problems with non-Gaussian PDFs and/or common systematic errors, requiring or not consistent rescaling due to parameter interdependencies.

Software

The Gfitter package [37] consists of abstracted object-oriented code in C++, relying on ROOT functionality [10]. The core fitting code and the physics content are organised in separate packages, each physics model package can be invoked as a plug-in to the framework. The user interfaces Gfitter through data cards in XML format, where all the input data and driving options are defined. The fits are run alternatively as ROOT macros or executables, interactively or in a batch system.

Gfitter parameters and theories

Gfitter defines only a single data container, denoted *parameter*, which can have three distinct manifestations according to its use case.

(A) Measurements x_{exp} that are predicted by the model (e.g., W mass in the SM): parameters of this type are not varied in the fit, but contribute to the log-likelihood function through comparison between the model prediction and the corresponding measurement.

(B) Model parameters y_{mod} that are not predicted by the theory but for which a direct measurement exists (e.g., top mass in the SM): parameters of this type are varied in the fit, and they contribute to the log-likelihood function through comparison between the fit parameter value and the corresponding measurement.

(C) Model Parameters y_{mod} that are not predicted by the theory and for which no direct measurement exist (e.g., Higgs mass in the SM), or which parameterise theoretical uncertainties according to the *R*fit prescription (cf. Sect. 2.2): parameters of this type are varied freely in the fit within bounds (if exist), and they do not contribute themselves to the log-likelihood function.

A parameter is uniquely defined via a name (and optionally an alias to allow the user to declare several correlated measurements of the same parameter, and to design theoretical predictions in a polymorph class hierarchy) in the data card, and stored in a global parameter container. These parameters are objects (of the *GParameter* class) that cannot be destroyed nor be recreated. Upon creation of a parameter, Gfitter searches automatically in the physics libraries for a corresponding theory (an object of the *GTheory* class), identified through the name of the parameter. If a theory is found, the corresponding class object is instantiated[12] and the parameter is categorised as of type (A); if no theory is found, it is of type (B) or (C) depending on the presence of a measurement in the data card.[13] The categorisation of parameters is performed automatically by Gfitter maintaining full transparency for the user.

Parameter errors, ranges, correlations and rescaling

Gfitter distinguishes three types of errors: normal errors following a Gaussian distribution describing statistical and experimental systematic errors, a user-defined log- likelihood functions including statistical and systematic uncertainties, and allowed ranges describing physical limits or hard-to-assess systematic errors (mostly of theoretical origin). All errors can be asymmetric with respect to the central values given. All parameters may have combinations of Gaussian and range errors (but only a single user-defined likelihood function). Parameters of type (A) and (B) do not contribute to the log-likelihood functions if the theory prediction or floating parameter value is compatible with the central value of the parameter within the ranges of the theoretical errors attributed to the parameter (cf. Sect. 2.1 concerning the implications of the term "theoretical error"). Only beyond these ranges, a Gaussian parabolic contribution to the log-likelihood function occurs. For example, the combined log-likelihood function of a parameter with central value x_0, positive (negative) Gaussian error $\sigma^{+}_{\mathrm{Gauss}}$ ($\sigma^{-}_{\mathrm{Gauss}}$), and positive (negative) theoretical error $\sigma^{+}_{\mathrm{theo}}$ ($\sigma^{-}_{\mathrm{theo}}$), for a given set of y_{mod} parameters and theoretical prediction $f(y_{\mathrm{mod}})$ reads[14]

$$
\begin{aligned}
&-2\log\mathcal{L}(y_{\mathrm{mod}}) \\
&= \begin{cases}
0, \\
\quad \text{if: } -\sigma^{-}_{\mathrm{theo}} \le f(y_{\mathrm{mod}}) - x_0 \le \sigma^{+}_{\mathrm{theo}}, \\
\left(\frac{f(y_{\mathrm{mod}})-(x_0+\sigma^{+}_{\mathrm{theo}})}{\sigma^{+}_{\mathrm{Gauss}}}\right)^2, \\
\quad \text{if: } f(y_{\mathrm{mod}}) - x_0 > \sigma^{+}_{\mathrm{theo}}, \\
\left(\frac{f(y_{\mathrm{mod}})-(x_0-\sigma^{-}_{\mathrm{theo}})}{\sigma^{-}_{\mathrm{Gauss}}}\right)^2, \\
\quad \text{if: } x_0 - f(y_{\mathrm{mod}}) > \sigma^{-}_{\mathrm{theo}}.
\end{cases}
\end{aligned}
\tag{3.1}
$$

Parameters of type (C) vary freely within the ranges set by the theoretical errors if available, or are unbound otherwise.

Parameters can have correlation coefficients identified and set in the data card via the parameter names (and alias if any). These correlations are taken into account in the log-likelihood test statistics as well as for the creation of toy MC experiments.

It is possible to introduce dependencies among parameters, which can be used to parameterise correlations due to common systematic errors, or to rescale parameter values and errors with newly available results for parameters on which other parameters depend. For example, in the global SM fit the experimental value used of the parameter $\Delta\alpha^{(5)}_{\mathrm{had}}(M_Z^2)$ depends on $\alpha_S(M_Z^2)$. The value for $\alpha_S(M_Z^2)$ used when evaluating $\Delta\alpha^{(5)}_{\mathrm{had}}(M_Z^2)$ may have been updated in the meantime, or may be updated in each fit step, which leads to a (not necessarily linear) shift of $\Delta\alpha^{(5)}_{\mathrm{had}}(M_Z^2)$ and also to a reduced systematic error (for details see footnote 19 on p. 556). The rescaling mechanism of Gfitter allows one to automatically account for arbitrary functional interdependencies between an arbitrary number of parameters.

Caching

An important feature of Gfitter is the possibility to cache computation results between fit steps. Each parameter holds pointers to the theory objects that depend on it, and the theories keep track of all auxiliary theory objects they depend on.

[12] A GTheory can depend on auxiliary theory objects (derived from GTheory) that are used to outsource complex computation tasks. Caching of results from repetitive calculations also benefits from outsourcing.

[13] Measurement results can be given as central value and Gaussian (possibly asymmetric) and/or theoretical errors, or as a user-defined log-likelihood function encoded in ROOT objects (e.g. histograms, graphs or functions).

[14] In the log-likelihood definition of (3.1), the central value x_0 corresponds to the value with the largest likelihood, which is not necessarily equal to the arithmetic average in case of asymmetric errors.

Upon computation of the log-likelihood function in a new fit step, only those theories (or part of theories) that depend on modified parameters (with respect to the previous fit step) are recomputed. More importantly, time intensive calculations performed by auxiliary theories that are shared among several theories are made only once per fit step. The gain in CPU time of this caching mechanism is substantial and can reach orders of magnitudes in many-parameter fitting problems.

Fitting

The parameter fitting is transparent with respect to the fitter implementation, which by default uses TMinuit [33], but which is extensible via the driving card to the more involved global minima finders Genetic Algorithm and Simulated Annealing, implemented in the ROOT package TMVA [38].

Parameter scans and contours

Gfitter offers the possibility to study the behaviour of the log-likelihood test statistics as a function of one or two parameters by one- or two-dimensional scans, respectively. If a parameter is of type (A), penalty contributions are added to the log-likelihood test statistics forcing the fit to yield the parameter value under study. In addition, two-dimensional contour regions of the test statistics can be computed using the corresponding TMinuit functionality.

Toy Monte Carlo analyses

Gfitter offers the possibility to perform toy Monte Carlo (MC) analyses repeating the minimisation step for input parameter values that are randomly generated around expectation values according to specified errors and correlations. For each MC experiment the fit results are recorded allowing for a statistical analysis, e.g., the determination of a p-value and an overall goodness-of-fit probability. All parameter scans can be optionally performed that way, as opposed to using a Gaussian approximation to estimate the p-value for a given scan point (manifestation of true values).

4 The Standard Model fit to electroweak precision data

In recent particle physics history, coined by the success of the electroweak unification and Quantum Chromodynamics (QCD), fits to experimental precision data have substantially contributed to our knowledge of the Standard Model (SM). The first application of global fits to electroweak data has been performed by the LEP Electroweak Working Group [39] in the last decade of the 20th century, unifying LEP and SLD precision data. The primary results of these fits were a prediction of the top-quark mass (today's fit precision $\simeq$9 GeV) prior to its discovery, an accurate and theoretically well controlled determination of the strong coupling constant at the Z-mass scale (today available at the 3NLO level [17]), and a logarithmic constraint on the Higgs mass establishing that the SM Higgs must be light. Other areas related to particle physics where global fits are performed are neutrino oscillation [40], leading to constraints on mixing parameters and mass hierarchies, flavour physics, with constraints on the parameters of the quark-flavour mixing (CKM) matrix and related quantities [22, 41], and cosmology [42], leading to a large number of phenomenological results such as the universe's curvature, the relic matter and energy density, neutrino masses and the age of the universe. Global fits also exist for models beyond the SM such as supersymmetry [43, 44] with however yet insufficient high-energy data for successfully constraining the parameters of even a minimal model so that simplifications are in order.

We emphasise that the goal of such fits is twofold (cf. Sect. 2): (i) the determination of the free model parameters, and (ii) a goodness-of-fit test measuring the agreement between model and data after fit convergence. This latter goal can be only achieved if the model is overconstrained by the available measurements. The situation is particularly favourable in the CKM sector, where the primary goal of experiments and phenomenological analysis has been moved from CKM parameter determination to the detection of new physics via inconsistencies in the CKM phase determination. The relatively young field of neutrino oscillation measurements on the contrary does not yet provide significant overconstraints of the neutrino flavour mixing matrix.

In the following we revisit the global electroweak fit at the Z-mass scale using the Gfitter package. We recall the relevant observables, their SM predictions, perform fits under various conditions, and discuss the results.

4.1 Formalism and observables

The formal analysis of this section is placed within the framework of the SM. The electroweak fit focuses on the parameters directly related to the Z and W boson properties, and to radiative corrections to these, providing the sensitivity to heavy particles like the top quark and the Higgs boson. The floating parameters of the fit are the Higgs and Z-boson masses, the c, b, and t-quark masses, as well as the electromagnetic and strong coupling strengths at the Z pole. Most of these parameters are also directly constrained by measurements included in the fit.

We have put emphasis on the completeness of the information given in this paper, with a large part of the relevant formulae quoted in the main text and the appendices. Readers seeking for a more pedagogical introduction are referred to the many excellent reviews on this and related topics (see,

e.g., Refs. [16, 45–47]). Section 4.1.1 provides a formal introduction of tree-level relations, and quantum loop corrections sensitive to particles heavier than the Z. The observables used in the global fit and their SM predictions are summarised in Sects. 4.1.2 and 4.1.3 respectively. Theoretical uncertainties are discussed in Sect. 4.1.4.

4.1.1 *Standard Model tree-level relations and radiative corrections*

The tree-level vector and axial-vector couplings occurring in the Z boson to fermion–antifermion vertex $i\overline{f}\gamma_\mu(g^{(0)}_{V,f} + g^{(0)}_{V,f}\gamma_5)fZ_\mu$ are given by[15]

$$g^{(0)}_{V,f} \equiv g^{(0)}_{L,f} + g^{(0)}_{R,f} = I^f_3 - 2Q^f \sin^2\theta_W, \tag{4.1}$$

$$g^{(0)}_{A,f} \equiv g^{(0)}_{L,f} - g^{(0)}_{R,f} = I^f_3, \tag{4.2}$$

where $g^{(0)}_{L(R),f}$ are the left-handed (right-handed) fermion couplings, and Q^f and I^f_3 are respectively the charge and the third component of the weak isospin. In the (minimal) SM, containing only one Higgs doublet, the weak mixing angle is defined by

$$\sin^2\theta_W = 1 - \frac{M^2_W}{M^2_Z}. \tag{4.3}$$

Electroweak radiative corrections modify these relations, leading to an effective weak mixing angle and effective couplings

$$\sin^2\theta^f_{\text{eff}} = \kappa^f_Z \sin^2\theta_W, \tag{4.4}$$

$$g_{V,f} = \sqrt{\rho^f_Z}\big(I^f_3 - 2Q^f \sin^2\theta^f_{\text{eff}}\big), \tag{4.5}$$

$$g_{A,f} = \sqrt{\rho^f_Z} I^f_3, \tag{4.6}$$

where κ^f_Z and ρ^f_Z are form factors absorbing the radiative corrections. They are given in (A.16) and (A.17) of Appendix A.3. Due to non-zero absorptive parts in the self-energy and vertex correction diagrams, the effective couplings and the form factors are complex quantities. The *observable* effective mixing angle is given by the real parts of the couplings

$$\frac{\mathrm{Re}(g_{V,f})}{\mathrm{Re}(g_{A,f})} = 1 - 4|Q_f|\sin^2\theta^f_{\text{eff}}. \tag{4.7}$$

[15]Throughout this paper the superscript '(0)' is used to label tree-level quantities.

Electroweak unification leads to a relation between weak and electromagnetic couplings, which at tree level reads

$$G_F = \frac{\pi\alpha}{\sqrt{2}(M^{(0)}_W)^2\big(1 - \frac{(M^{(0)}_W)^2}{M^2_Z}\big)}. \tag{4.8}$$

Radiative corrections are parameterised by multiplying the r.h.s. of (4.8) with the form factor $(1-\Delta r)^{-1}$. Using (4.3) and resolving for M_W gives

$$M^2_W = \frac{M^2_Z}{2}\left(1 + \sqrt{1 - \frac{\sqrt{8}\pi\alpha}{G_F M^2_Z(1-\Delta r)}}\right). \tag{4.9}$$

The form factors ρ^f_Z, κ^f_Z and Δr depend nearly quadratically on m_t and logarithmically on M_H. They have been calculated including two-loop corrections in the on-shell renormalisation scheme (OMS) [48–50], except for b quarks where an approximate expression, including the full one-loop correction and the known leading two-loop terms $\propto m^4_t$, is provided. The relevant formulae used in this analysis are summarised in Appendix A.3. Since Δr also depends on M_W an iterative method is needed to solve (4.9). The calculation of M_W has been performed including the complete one-loop correction, two-loop and three-loop QCD corrections of order $\mathcal{O}(\alpha\alpha_S)$ and $\mathcal{O}(\alpha\alpha^2_s)$, fermionic and bosonic two-loop electroweak corrections of order $\mathcal{O}(\alpha^2)$, and the leading $\mathcal{O}(G^2_F\alpha_S m^4_t)$ and $\mathcal{O}(G^3_F m^6_t)$ three-loop contributions [11–13]. Four-loop QCD corrections have been calculated for the ρ-parameter [51–53]. Since they affect the W mass by 2 MeV only, they have been neglected in this work.

For the SM prediction of M_W we use the parameterised formula [11]

$$\begin{aligned} M_W = {} & M^{\text{ini}}_W - c_1\mathrm{dH} - c_2\mathrm{dH}^2 + c_3\mathrm{dH}^4 + c_4(\mathrm{dh}-1) \\ & - c_5\mathrm{d}\alpha + c_6\mathrm{dt} - c_7\mathrm{dt}^2 - c_8\mathrm{dHdt} \\ & + c_9\mathrm{dhdt} - c_{10}\mathrm{d}\alpha_S + c_{11}\mathrm{dZ}, \end{aligned} \tag{4.10}$$

with

$$\mathrm{dH} = \ln\left(\frac{M_H}{100\ \text{GeV}}\right), \qquad \mathrm{dh} = \left(\frac{M_H}{100\ \text{GeV}}\right)^2,$$

$$\mathrm{dt} = \left(\frac{m_t}{174.3\ \text{GeV}}\right)^2 - 1, \qquad \mathrm{dZ} = \frac{M_Z}{91.1875\ \text{GeV}} - 1,$$

$$\mathrm{d}\alpha = \frac{\Delta\alpha(M^2_Z)}{0.05907} - 1, \qquad \mathrm{d}\alpha_S = \frac{\alpha_S(M^2_Z)}{0.119} - 1,$$

where here and below all masses are in units of GeV, and where m_t is the top-quark pole mass, M_Z and M_H are the Z and Higgs boson masses, $\Delta\alpha(M^2_Z)$ is the sum of the leptonic and hadronic contributions to the running QED coupling strength at M^2_Z (cf. Appendix A.1), $\alpha_S(M^2_Z)$ is the running strong coupling constant at M^2_Z (cf. Appendix A.2.1),

and where the coefficients $M_W^{\rm ini}, c_1, \ldots, c_{11}$ read

$$
\begin{aligned}
&M_W^{\rm ini} = 80.3799\ \text{GeV}, && c_1 = 0.05429\ \text{GeV},\\
&c_2 = 0.008939\ \text{GeV}, && c_3 = 0.0000890\ \text{GeV},\\
&c_4 = 0.000161\ \text{GeV}, && c_5 = 1.070\ \text{GeV},\\
&c_6 = 0.5256\ \text{GeV}, && c_7 = 0.0678\ \text{GeV},\\
&c_8 = 0.00179\ \text{GeV}, && c_9 = 0.0000659\ \text{GeV},\\
&c_{10} = 0.0737\ \text{GeV}, && c_{11} = 114.9\ \text{GeV}.
\end{aligned}
$$

The parameterisation reproduces the full result for M_W to better than 0.5 MeV over the range 10 GeV $< M_H <$ 1 TeV, if all parameters are within their expected (year 2003) 2σ intervals [11].

The effective weak mixing angle of charged and neutral leptons and light quarks has been computed [12, 13] with the full electroweak and QCD one-loop and two-loop corrections, and the leading three-loop corrections of orders $\mathcal{O}(G_F^2\alpha_S m_t^4)$ and $\mathcal{O}(G_F^3 m_t^6)$. The corresponding parameterisation formula for charged leptons reads

$$
\begin{aligned}
\sin^2\theta_{\rm eff}^{\ell} = {} & s_0 + d_1 L_H + d_2 L_H^2 + d_3 L_H^4 + d_4\bigl(\Delta_H^2 - 1\bigr)\\
& + d_5\Delta_\alpha + d_6\Delta_t + d_7\Delta_t^2 + d_8\Delta_t(\Delta_H - 1)\\
& + d_9\Delta_{\alpha_S} + d_{10}\Delta_Z,
\end{aligned}
\tag{4.11}
$$

with

$$
L_H = \ln\left(\frac{M_H}{100\ \text{GeV}}\right), \qquad \Delta_H = \frac{M_H}{100\ \text{GeV}},
$$

$$
\Delta_\alpha = \frac{\Delta\alpha(M_Z)}{0.05907} - 1, \qquad \Delta_t = \left(\frac{m_t}{178.0\ \text{GeV}}\right)^2 - 1,
$$

$$
\Delta_{\alpha_S} = \frac{\alpha_S(M_Z^2)}{0.117} - 1, \qquad \Delta_Z = \frac{M_Z}{91.1876\ \text{GeV}} - 1,
$$

and the numerical values

$$
\begin{aligned}
&s_0 = 0.2312527, && d_1 = 4.729\times 10^{-4},\\
&d_2 = 2.07\times 10^{-5}, && d_3 = 3.85\times 10^{-6},\\
&d_4 = -1.85\times 10^{-6}, && d_5 = 0.0207,\\
&d_6 = -0.002851, && d_7 = 1.82\times 10^{-4},\\
&d_8 = -9.74\times 10^{-6}, && d_9 = 3.98\times 10^{-4},\\
&d_{10} = -0.655.
\end{aligned}
$$

Equation (4.11) reproduces the full expression with maximum (average) deviation of 4.5×10^{-6} (1.2×10^{-6}), if the Higgs-boson mass lies within 10 GeV $< M_H <$ 1 TeV, and if all parameters are within their expected (year 2003) 2σ intervals [13].

The prediction of the effective weak mixing angle for the remaining light fermions (u, d, s, c quarks and neutrinos) differs slightly from the prediction for charged leptons. Again a parameterisation formula is provided [13], which is used in this analysis. For bottom quarks, new diagrams with additional top-quark propagators enter the calculation and the b quark specific two-loop vertex corrections do not exist.[16] Instead we use (4.4) and the calculation of κ_Z^b (cf. Appendix A.3), which includes the full one-loop correction and the known leading two-loop terms $\propto m_t^4$.

4.1.2 Summary of electroweak observables

The following classes of observables are used in the fit.

Z resonance parameters: Z mass and width, and total $e^+e^- \to Z \to$ hadron production cross section (i.e., corrected for photon exchange contributions).

Partial Z cross sections: Ratios of leptonic to hadronic, and heavy-flavour hadronic to total hadronic cross sections.

Neutral current couplings: Effective weak mixing angle, and left-right and forward-backward asymmetries for universal leptons and heavy quarks.[17]

W boson parameters: W mass and width.

Higgs boson parameters: Higgs mass.

Additional input parameters: Heavy-flavour (c, b, t) quark masses (masses of lighter quarks and leptons are fixed to their world averages), QED and QCD coupling strengths at the Z-mass scale.

4.1.3 Theoretical predictions of electroweak observables

Parity violation in neutral current reactions $e^+e^- \to f\overline{f}$ resulting from the different left- and right-handed Z-boson couplings to fermions leads to fermion polarisation in the initial and final states and thus to observable asymmetry effects. They can be conveniently expressed by the asymmetry parameters

$$
A_f = \frac{g_{L,f}^2 - g_{R,f}^2}{g_{L,f}^2 + g_{R,f}^2} = 2\frac{g_{V,f}/g_{A,f}}{1 + (g_{V,f}/g_{A,f})^2},
\tag{4.12}
$$

where only the real parts of the couplings are considered as the asymmetries refer to pure Z exchange. For instance, the forward-backward asymmetry $A_{\rm FB}^{0,f} = (\sigma_{F,f}^0 - \sigma_{B,f}^0)/(\sigma_{F,f}^0 + \sigma_{B,f}^0)$, where the superscript '0' indicates that the observed values have been corrected for radiative

[16] After completion of this work the two-loop electroweak fermionic corrections to $\sin^2\theta_{\rm eff}^b$ have been published [54]. They will be included in future updates of this analysis.

[17] Left–right and forward–backward asymmetries have been also measured for strange quarks, with however insufficient precision to be included here.

effects and photon exchange, can be determined from the asymmetry parameters (4.12) as follows:

$$A_{\mathrm{FB}}^{0,f} = \frac{3}{4} A_e A_f. \tag{4.13}$$

The A_f are obtained from (4.12) and (4.7) using $\sin^2\theta_{\mathrm{eff}}^f$ from the procedure described in the previous section.

Unlike the asymmetry parameters, the partial decay width $\Gamma_f = \Gamma(Z \to f\overline{f})$ is defined inclusively, i.e., it contains all real and virtual corrections such that the imaginary parts of the couplings must be taken into account. One thus has

$$\Gamma_f = 4N_C^f \Gamma_0 \left|\rho_Z^f\right| \left(I_3^f\right)^2 \left(\left| \frac{g_{V,f}^2}{g_{A,f}^2} \right| R_V^f\left(M_Z^2\right) + R_A^f\left(M_Z^2\right) \right), \tag{4.14}$$

where $N_C^{\ell(q)} = 1(3)$ is the colour factor, $R_V^f(M_Z^2)$ and $R_A^f(M_Z^2)$ are *radiator functions* (defined further below), and Γ_0 is given by

$$\Gamma_0 = \frac{G_F M_Z^3}{24\sqrt{2}\pi}. \tag{4.15}$$

The $\sin^2\theta_{\mathrm{eff}}^f$ term entering through the ratio of coupling constants in (4.14) is modified by the real-valued contribution I_f^2 resulting from the product of two imaginary parts of polarisation operators [6]

$$\sin^2\theta_{\mathrm{eff}}^f \to \sin^2\theta_{\mathrm{eff}}^f + I_f^2, \tag{4.16}$$

where

$$I_f^2 = \alpha^2\left(M_Z^2\right)\frac{35}{18}\left(1 - \frac{8}{3}\,\mathrm{Re}\left(\kappa_Z^f\right)\sin^2\theta_W\right). \tag{4.17}$$

The full expression for the partial leptonic width reads [6]

$$\begin{aligned}\Gamma_\ell = {} & \Gamma_0 \left|\rho_Z^\ell\right| \sqrt{1 - \frac{4m_\ell^2}{M_Z^2}} \\ & \times \left[\left(1 + \frac{2m_\ell^2}{M_Z^2}\right)\left(\left| \frac{g_{V,\ell}}{g_{A,\ell}} \right|^2 + 1 \right) - \frac{6m_\ell^2}{M_Z^2} \right] \\ & \times \left(1 + \frac{3}{4}\frac{\alpha(M_Z^2)}{\pi} Q_\ell^2\right),\end{aligned} \tag{4.18}$$

which includes effects from QED final state radiation. The partial widths for $q\overline{q}$ final states, Γ_q, involve radiator functions that describe the final state QED and QCD vector and axial-vector corrections for quarkonic decay modes. Furthermore, they contain QED $\otimes$ QCD and finite quark-mass corrections. For the massless perturbative QCD correction, the most recent fourth-order result is used [17]. Explicit formulae for the radiator functions are given in Appendix A.4.

The influence of non-factorisable EW $\otimes$ QCD corrections, $\Delta_{\mathrm{EW/QCD}}$, that must be added to the width (4.14) for quark final states is small (less than 10^{-3}). They are assumed to be constant [55, 56], and take the values

$$\Delta_{\mathrm{EW/QCD}} = \begin{cases} -0.113\ \mathrm{MeV} & \text{for } u \text{ and } c \text{ quarks}, \\ -0.160\ \mathrm{MeV} & \text{for } d \text{ and } s \text{ quarks}, \\ -0.040\ \mathrm{MeV} & \text{for the } b \text{ quark}. \end{cases} \tag{4.19}$$

The total Z width for three light neutrino generations obeys the sum

$$\Gamma_Z = \Gamma_e + \Gamma_\mu + \Gamma_\tau + 3\Gamma_\nu + \Gamma_{\mathrm{had}}, \tag{4.20}$$

where $\Gamma_{\mathrm{had}} = \Gamma_u + \Gamma_d + \Gamma_c + \Gamma_s + \Gamma_b$ is the total hadronic Z width. From these the *improved* tree-level total hadronic cross section at the Z pole is given by

$$\sigma_{\mathrm{had}}^0 = \frac{12\pi}{M_Z^2}\frac{\Gamma_e\Gamma_{\mathrm{had}}}{\Gamma_Z^2}. \tag{4.21}$$

To reduce systematic uncertainties, the LEP experiments have determined the partial-Z-width ratios $R_\ell^0 = \Gamma_{\mathrm{had}}/\Gamma_\ell$ and $R_q^0 = \Gamma_q/\Gamma_{\mathrm{had}}$, which are used in the fit.

The computation of the W boson width is similar to that of the Z boson, but it is only known to one electroweak loop. The expression adopted in this analysis can be found in [57]. An improved, gauge-independent formulation exists [58], but the difference with respect to the gauge-dependent result is small (0.01%) compared to the current experimental error (3%).

The value of the QED coupling constant at the Z pole is obtained using three-loop results for the leptonic contribution, and the most recent evaluation of the hadronic vacuum polarisation contribution for the five quarks lighter than M_Z. Perturbative QCD is used for the small top-quark contribution. The relevant formulae and references are given in Appendix A.1.

The evaluation of the running QCD coupling constant uses the known four-loop expansion of the QCD β-function, including three-loop matching at the quark-flavour thresholds (cf. Appendix A.2.1). The running of the b and c quark masses is obtained from the corresponding four-loop γ-function (cf. Appendix A.2.2). All running QCD quantities are evaluated in the modified minimal subtraction renormalisation scheme ($\overline{\mathrm{MS}}$).

4.1.4 *Theoretical uncertainties*

Within the *R*fit scheme, theoretical errors based on educated guesswork are introduced via bound theoretical scale parameters in the fit, thus providing a consistent numerical treatment. For example, the effect from a truncated perturbative series is included by adding a *deviation parameter*, δ_{th}, describing the varying perturbative prediction as a function of

the contribution from the unknown terms. Leaving the deviation parameter floating within estimated ranges allows the fit to adjust it when scanning a parameter, such that the likelihood estimator is increased (thus improving the fit compatibility).

The uncertainties in the form factors ρ_Z^f and κ_Z^f are estimated using different renormalisation schemes, and the maximum variations found are assigned as theoretical errors. A detailed numerical study has been performed in [59] leading to the following real-valued relative theoretical errors

$$\delta_{\text{th}}\rho_Z^f/\left|1-\rho_Z^f\right| \approx 5\times 10^{-3}, \tag{4.22}$$

$$\delta_{\text{th}}\kappa_Z^f/\left|1-\kappa_Z^f\right| \approx 5\times 10^{-4}, \tag{4.23}$$

which vary somewhat depending on the fermion flavour. The corresponding absolute theoretical errors are around 2×10^{-5} for both $\delta_{\text{th}}\rho_Z^f$ and $\delta_{\text{th}}\kappa_Z^f$ and are treated as fully correlated in the fit. These errors, albeit included, have a negligible effect on the fit results.

More important are theoretical uncertainties affecting directly the M_W and $\sin^2\theta_{\text{eff}}^\ell$ predictions. They arise from three dominant sources of unknown higher-order corrections [11, 13]: (i) $\mathcal{O}(\alpha^2\alpha_S)$ terms beyond the known contribution of $\mathcal{O}(G_F^2\alpha_S m_t^4)$, (ii) $\mathcal{O}(\alpha^3)$ electroweak three-loop corrections, and (iii) $\mathcal{O}(\alpha_S^3)$ QCD terms. The quadratic sums of the above corrections amount to

$$\delta_{\text{th}} M_W \approx 4\ \text{MeV}, \tag{4.24}$$

$$\delta_{\text{th}}\sin^2\theta_{\text{eff}}^\ell \approx 4.7\times 10^{-5}, \tag{4.25}$$

which are the theoretical ranges used in the fit. The empirical W mass parameterisation (4.10) is only valid for a relatively light Higgs boson, $M_H \lesssim 300$ GeV, for which the error introduced by the approximation is expected to be negligible [11]. For larger Higgs masses, the total theoretical error used is linearly increased up to $\delta_{\text{th}}M_W = 6$ MeV at $M_H = 1$ TeV, which is a coarse estimate along the theoretical uncertainties given in [11].

Theoretical uncertainties affecting the top mass from non-perturbative colour-reconnection effects in the fragmentation process [60, 61] and due to ambiguities in the top-mass definition [62, 63] have been recently estimated to approximately 0.5 GeV each. The systematic error due to shower effects may be larger [60]. Especially the colour-reconnection and shower uncertainties, estimated by means of a toy model, need to be verified with experimental data and should be included in the top-mass result published by the experiments. Both errors have been neglected for the present analysis.

Other theoretical uncertainties are introduced via the evolution of the QED and QCD couplings and quark masses, and are discussed in Appendices A.1 and A.2.

4.2 Global Standard Model analysis

The last two decades have been proliferous in providing precision experimental data at the electroweak scale. Driven by measurements at LEP, SLC and the Tevatron, and significant theoretical progress, many phenomenological analyses have been performed, of which we re-examine below the global SM fit. The primary goal of this re-analysis is (i) to validate the new fitting toolkit Gfitter and its SM library with respect to earlier results [5–8], (ii) to include the results from the direct Higgs searches at LEP and the Tevatron in the global fit, (iii) to revisit the impact of theoretical uncertainties on the results, and (iv) to perform more complete statistical tests.

4.2.1 Floating fit parameters

The SM parameters relevant for the global electroweak analysis are the coupling constants of the electromagnetic (α), weak (G_F) and strong interactions (α_S), and the masses of the elementary bosons (M_γ, M_Z, M_W, M_H) and fermions (m_f with $f = e, \mu, \tau, \nu_e, \nu_\mu, \nu_\tau, u, c, t, d, s, b,$), where neutrinos are taken to be massless. The fit simplifies with electroweak unification resulting in a massless photon and a relation between the W mass and the electromagnetic coupling α, the Z mass, and the weak coupling G_F, according to (4.8). Further simplification of the fit arises from fixing parameters with insignificant uncertainties compared to the sensitivity of the fit.

- Compared to M_Z the masses of leptons and light quarks are small and/or sufficiently well known so that their uncertainties are negligible in the fit. They are fixed to their world average values [64]. Only the masses of the heavy quarks,[18] $\overline{m}_c$, $\overline{m}_b$ and m_t, are floating in the fit while being constrained to their experimental values. The top-mass uncertainty has the strongest impact on the fit.
- The weak coupling constant G_F has been accurately determined through the measurement of the μ lifetime, giving $G_F = 1.16637(1)\times 10^{-5}\ \text{GeV}^{-2}$ [64]. The parameter is fixed in the fit.
- The leptonic and top-quark vacuum polarisation contributions to the running of the electromagnetic coupling are precisely known or small. Only the hadronic contribution for the five lighter quarks, $\Delta\alpha_{\text{had}}^{(5)}(M_Z^2)$, adds significant uncertainties and replaces the electromagnetic coupling $\alpha(M_Z^2)$ as floating parameter in the fit (cf. Appendix A.1).

With the *R*fit treatment of theoretical uncertainties four deviation parameters are introduced in the fit. They vary freely

[18] In the analysis and throughout this paper we use the $\overline{\text{MS}}$ renormalised masses of the c and b quarks, $\overline{m}_c(\overline{m}_c)$ and $\overline{m}_b(\overline{m}_b)$, at their proper scales. In the following they are denoted with $\overline{m}_c$ and $\overline{m}_b$ respectively.

within their corresponding error ranges (cf. Sect. 4.1.4). The theoretical uncertainties in the predictions of M_W and $\sin^2\theta^\ell_{\rm eff}$ are parameterised by $\delta_{\rm th}M_W$ and $\delta_{\rm th}\sin^2\theta^\ell_{\rm eff}$. The form factors κ^f_Z and ρ^f_Z have theoretical errors $\delta_{\rm th}\kappa^f_Z$ and $\delta_{\rm th}\rho^f_Z$, which are treated as fully correlated in the fit.

In summary, the floating parameters in the global electroweak fit are the coupling parameters $\Delta\alpha^{(5)}_{\rm had}(M^2_Z)$ and $\alpha_S(M^2_Z)$, the masses M_Z, $\overline{m}_c$, $\overline{m}_b$, m_t and M_H, and four theoretical error parameters.

4.2.2 Input data

A summary of the input data used in the fit is given in the second column of Table 4.1, and discussed below.

- The mass and width of the Z boson, the hadronic pole cross section $\sigma^0_{\rm had}$, the partial widths ratio R^0_ℓ, and the forward-backward asymmetries for leptons $A^{0,\ell}_{\rm FB}$, have been determined by fits to the Z-lineshape measured precisely at LEP (see [46] and references therein). Measurements of the τ polarisation at LEP [46] and the left–

Table 4.1 Input values and fit results for parameters of the global electroweak fit. The first and second columns list respectively the observables/parameters used in the fit, and their experimental values or phenomenological estimates (see text for references). The subscript "theo" labels theoretical error ranges. The third column indicates whether a parameter is floating in the fit. The fourth (fifth) column quotes the results of the *standard* (*complete*) *fit* not including (including) the constraints from the direct Higgs searches at LEP and Tevatron in the fit. In case of floating parameters the fit results are directly given, while for observables, the central values and errors are obtained by individual profile likelihood scans. The errors are derived from the $\Delta\chi^2$ profile using a Gaussian approximation. The last column gives the fit results for each parameter without using the corresponding experimental constraint in the fit (indirect determination)

Parameter	Input value	Free in fit	Results from global EW fits		Complete fit w/o exp. input in line
			Standard fit	Complete fit	
M_Z [GeV]	91.1875 ± 0.0021	yes	91.1874 ± 0.0021	91.1877 ± 0.0021	$91.2001^{+0.0174}_{-0.0178}$
Γ_Z [GeV]	2.4952 ± 0.0023	–	2.4959 ± 0.0015	2.4955 ± 0.0015	2.4950 ± 0.0017
$\sigma^0_{\rm had}$ [nb]	41.540 ± 0.037	–	41.477 ± 0.014	41.477 ± 0.014	41.468 ± 0.015
R^0_ℓ	20.767 ± 0.025	–	20.743 ± 0.018	20.742 ± 0.018	$20.717^{+0.029}_{-0.025}$
$A^{0,\ell}_{\rm FB}$	0.0171 ± 0.0010	–	0.01638 ± 0.0002	0.01610 ± 0.9839	0.01616 ± 0.0002
A_ℓ $^{(\star)}$	0.1499 ± 0.0018	–	$0.1478^{+0.0011}_{-0.0010}$	$0.1471^{+0.0008}_{-0.0009}$	–
A_c	0.670 ± 0.027	–	$0.6682^{+0.00046}_{-0.00045}$	$0.6680^{+0.00032}_{-0.00046}$	$0.6680^{+0.00032}_{-0.00047}$
A_b	0.923 ± 0.020	–	$0.93470^{+0.00011}_{-0.00012}$	$0.93464^{+0.00008}_{-0.00013}$	$0.93464^{+0.00008}_{-0.00011}$
$A^{0,c}_{\rm FB}$	0.0707 ± 0.0035	–	0.0741 ± 0.0006	$0.0737^{+0.0004}_{-0.0005}$	$0.0737^{+0.0004}_{-0.0005}$
$A^{0,b}_{\rm FB}$	0.0992 ± 0.0016	–	0.1036 ± 0.0007	$0.1031^{+0.0007}_{-0.0006}$	0.1036 ± 0.0005
R^0_c	0.1721 ± 0.0030	–	0.17224 ± 0.00006	0.17224 ± 0.00006	0.17225 ± 0.00006
R^0_b	0.21629 ± 0.00066	–	$0.21581^{+0.00005}_{-0.00007}$	0.21580 ± 0.00006	0.21580 ± 0.00006
$\sin^2\theta^\ell_{\rm eff}(Q_{\rm FB})$	0.2324 ± 0.0012	–	0.23143 ± 0.00013	$0.23151^{+0.00012}_{-0.00010}$	$0.23149^{+0.00013}_{-0.00009}$
M_H [GeV] $^{(\circ)}$	Likelihood ratios	yes	$80^{+30[+75]}_{-23[-41]}$	$116.4^{+18.3[+28.4]}_{-1.3[-2.2]}$	$80^{+30[+75]}_{-23[-41]}$
M_W [GeV]	80.399 ± 0.025	–	$80.382^{+0.014}_{-0.016}$	80.364 ± 0.010	$80.359^{+0.010}_{-0.021}$
Γ_W [GeV]	2.098 ± 0.048	–	$2.092^{+0.001}_{-0.002}$	2.091 ± 0.001	$2.091^{+0.001}_{-0.002}$
$\overline{m}_c$ [GeV]	1.25 ± 0.09	yes	1.25 ± 0.09	1.25 ± 0.09	–
$\overline{m}_b$ [GeV]	4.20 ± 0.07	yes	4.20 ± 0.07	4.20 ± 0.07	–
m_t [GeV]	172.4 ± 1.2	yes	172.5 ± 1.2	172.9 ± 1.2	$178.2^{+9.8}_{-4.2}$
$\Delta\alpha^{(5)}_{\rm had}(M^2_Z)$ $^{(\dagger\triangle)}$	2768 ± 22	yes	2772 ± 22	2767^{+19}_{-24}	2722^{+62}_{-53}
$\alpha_s(M^2_Z)$	–	yes	$0.1192^{+0.0028}_{-0.0027}$	$0.1193^{+0.0028}_{-0.0027}$	$0.1193^{+0.0028}_{-0.0027}$
$\delta_{\rm th}M_W$ [MeV]	$[-4, 4]_{\rm theo}$	yes	4	4	–
$\delta_{\rm th}\sin^2\theta^\ell_{\rm eff}$ $^{(\dagger)}$	$[-4.7, 4.7]_{\rm theo}$	yes	4.7	-1.3	–
$\delta_{\rm th}\rho^f_Z$ $^{(\dagger)}$	$[-2, 2]_{\rm theo}$	yes	2	2	–
$\delta_{\rm th}\kappa^f_Z$ $^{(\dagger)}$	$[-2, 2]_{\rm theo}$	yes	2	2	–

$^{(\star)}$Average of LEP ($A_\ell = 0.1465 \pm 0.0033$) and SLD ($A_\ell = 0.1513 \pm 0.0021$) measurements. The *complete fit* w/o the LEP (SLD) measurement gives $A_\ell = 0.1472^{+0.0008}_{-0.0011}$ ($A_\ell = 0.1463 \pm 0.0008$). $^{(\circ)}$In brackets the 2σ errors. $^{(\dagger)}$In units of 10^{-5}. $^{(\triangle)}$Rescaled due to α_s dependency

Table 4.2 Correlation matrices for observables determined by the Z-lineshape fit (left), and by heavy flavour analyses at the Z pole (right) [46]

	M_Z	Γ_Z	$\sigma^0_{\rm had}$	R^0_ℓ	$A^{0,\ell}_{\rm FB}$		$A^{0,c}_{\rm FB}$	$A^{0,b}_{\rm FB}$	A_c	A_b	R^0_c	R^0_b
M_Z	1	−0.02	−0.05	0.03	0.06	$A^{0,c}_{\rm FB}$	1	0.15	0.04	−0.02	−0.06	0.07
Γ_Z		1	−0.30	0.00	0.00	$A^{0,b}_{\rm FB}$		1	0.01	0.06	0.04	−0.10
$\sigma^0_{\rm had}$			1	0.18	0.01	A_c			1	0.11	−0.06	0.04
R^0_ℓ				1	−0.06	A_b				1	0.04	−0.08
$A^{0,\ell}_{\rm FB}$					1	R^0_c					1	−0.18

right asymmetry at SLC [46] have been used to determine the lepton asymmetry parameter A_ℓ. The corresponding c and b-quark asymmetry parameters $A_{c(b)}$, the forward–backward asymmetries $A^{0,c(b)}_{\rm FB}$, and the widths ratios R^0_c and R^0_b, have been measured at LEP and SLC [46]. In addition, the forward- backward charge asymmetry ($Q_{\rm FB}$) measurement in inclusive hadronic events at LEP was used to directly determine the effective leptonic weak mixing angle $\sin^2\theta^\ell_{\rm eff}$ [46]. The log-likelihood function used in the fit includes the linear correlation coefficients among the Z-lineshape and heavy-flavour observables given in Table 4.2.

- For the running quark masses $\overline{m}_c$ and $\overline{m}_b$, the world average values derived in [64] are used. The combined top-quark mass is taken from the Tevatron Electroweak Working Group [65].
- For the five-quark hadronic contribution to $\alpha(M_Z^2)$, the most recent phenomenological result is used [66] (see also the discussion in [67]). Its dependence on $\alpha_S(M_Z^2)$ requires a proper rescaling in the fit (cf. Sect. 3).[19]
- The LEP and Tevatron results for the W mass and width are respectively $M_W = (80.376 \pm 0.033)$ GeV, $\Gamma_W = (2.196 \pm 0.083)$ GeV [68], and $M_W = (80.432 \pm 0.039)$ GeV, $\Gamma_W = (2.056 \pm 0.062)$ GeV [69, 70]. Their weighted averages [69], quoted without the correlation coefficient between mass and width, are used in the fit (cf. Table 4.1). Since a modest correlation has insignificant impact on the fit results[20] it is ignored in the following.
- The direct searches for the SM Higgs boson at LEP [71] and at the Tevatron [72, 73] use as test statistics the negative logarithm of a likelihood ratio, $-2\ln Q$, of the SM Higgs signal plus background (s + b) to the background-only (b) hypotheses. This choice guarantees $-2\ln Q = 0$ when there is no experimental sensitivity to a Higgs signal. The corresponding one-sided confidence levels $\mathrm{CL_{s+b}}$ and $\mathrm{CL_b}$ describe the probabilities of upward fluctuations of the test statistics in presence and absence of a signal ($1 - \mathrm{CL_b}$ is thus the probability of a false discovery). They are derived using toy MC experiments.[21]

  In the modified frequentest approach [74–76], a hypothesis is considered excluded at 95% CL if the ratio $\mathrm{CL_s} = \mathrm{CL_{s+b}}/\mathrm{CL_b}$ is equal or lower than 0.05. The corresponding exclusion confidence levels defined by (2.6) are given by $1 - \mathrm{CL_s}$ and $1 - \mathrm{CL_{s+b}}$, respectively. The use of $\mathrm{CL_s}$ leads to a more conservative limit [71] than the (usual) approach based on $\mathrm{CL_{s+b}}$.[22] Using this method the combination of LEP searches [71] has set the lower limit $M_H > 114.4$ GeV at 95% CL. For the Tevatron combination [72, 73], ratios of the 95% CL cross-section limits to the SM Higgs boson production cross section as a function of the Higgs mass are derived, exhibiting a minimum of 1.0 at $M_H = 170$ GeV. The LEP Higgs Working Group provided the observed and expected $-2\ln Q$ curves for the s + b and b hypotheses, and the corresponding values of the aforementioned confidence levels up to $M_H = 120$ GeV. The Tevatron New Phenomena and Higgs Working Group (TEVNPH) made the same

[19] In [66] the light-quark hadronic contribution to $\alpha(M_Z^2)$ was found to be $\Delta\alpha^{(5)}_{\rm had}(M_Z^2) = 0.02768 \pm 0.00022 \pm 0.00002$, where the second error singles out the uncertainty from the strong coupling constant for which $\alpha_S(M_Z^2) = 0.118 \pm 0.003$ was used. Linear rescaling leads to the modified central value $\Delta\alpha^{(5)}_{\rm had}(M_Z^2) = 0.02768 + 0.00002 \cdot (\alpha_S(M_Z^2)_{\rm fit} - 0.118)/0.003$. Since $\alpha_S(M_Z^2)$ is a free fit parameter and has no uncertainty in a certain fit step the error on $\Delta\alpha^{(5)}_{\rm had}(M_Z^2)$ used in the log-likelihood function does no longer include the contribution from $\alpha_S(M_Z^2)$, but the corresponding variation is included in the rescaling of the central value only.

[20] A correlation of 0.2 between W mass and width was reported for the Tevatron Run-I results [46]. Assuming the same correlation for the LEP and Tevatron combined values of W mass and width leads to an increase of the $\chi^2_{\rm min}$ of the *standard fit* (*complete fit*) by 0.09 (0.23). In the *complete fit* the central value of the Higgs mass estimate is unchanged (only the $+1\sigma$ bound slightly reduces by 0.6 GeV), whereas a downward shift of 1.1 GeV of the central value is observed for the *standard fit*. In both fits the changes in the other parameters are negligible.

[21] For a counting experiment with N observed events and N_s ($N_b \gg N_s$) expected signal (background) events, one has $-\ln Q = N_s - N\ln(N_s/N_b + 1) \simeq N_s(1 - N/N_b)$, leading to small $-\ln Q$ values for large N (signal-like) and large $-\ln Q$ values for small N (background-like). For sufficiently large $N_s + N_b$, the test statistics $-\ln Q$ has a symmetric Gaussian probability density function.

[22] Assuming a simple counting experiment with a true number of 100 background and 30 signal events, the one-sided probability $\mathrm{CL_{s+b}}$ to fluctuate to equal or less than 111 observed event is 0.05. The corresponding value $\mathrm{CL_s} = 0.05$ (which does not represent a probability) is however already reached between 105 and 106 events.

information available for 10 discrete data points in the mass range $155 \leq M_H \leq 200$ GeV based on preliminary searches using data samples of up to 3 fb^{-1} integrated luminosity [73]. For the mass range $110 \leq M_H \leq 200$ GeV, Tevatron results based on 2.4 fb^{-1} are provided for $-2\ln Q$ [72], however not for the corresponding confidence levels.

To include the direct Higgs searches in the *complete* SM fit we interpret the $-2\ln Q$ results for a given Higgs mass hypothesis[23] as measurements and derive a log-likelihood estimator quantifying the deviation of the data from the corresponding SM Higgs expectation. For this purpose we transform the one-sided $\mathrm{CL_{s+b}}$ into two-sided confidence levels[24] using $\mathrm{CL_{s+b}^{2\text{-sided}}} = 2\mathrm{CL_{s+b}}$ for $\mathrm{CL_{s+b}} \leq 0.5$ and $\mathrm{CL_{s+b}^{2\text{-sided}}} = 2(1-\mathrm{CL_{s+b}})$ for $\mathrm{CL_{s+b}} > 0.5$. The contribution to the χ^2 estimator of the fit is then obtained via $\delta\chi^2 = 2\cdot[\mathrm{Erf}^{-1}(1-\mathrm{CL_{s+b}^{2\text{-sided}}})]^2$, where Erf^{-1} is the inverse error function,[25] and where the underlying probability density function has been assumed to be symmetric (cf. footnote 21 on p. 556).

For the complete mass range available for the LEP searches ($M_H \leq 120$ GeV), and for the high-mass region of the Tevatron searches ($155 \leq M_H \leq 200$ GeV), we employ the $\mathrm{CL_{s+b}}$ values determined by the experiments. For the low-mass Tevatron results ($110 \leq M_H \leq 150$ GeV), where the $\mathrm{CL_{s+b}}$ values are not provided, they are estimated from the measured $-2\ln Q$ values that are compared with those expected for the s+b hypothesis, and using the errors derived by the experiments for the b hypothesis. We have tested this approximation in the high-mass region, where the experimental values of $\mathrm{CL_{s+b}}$ from the Tevatron are provided, and found a systematic overestimation of the contribution to our χ^2 test statistics of about 30%, with small dependence on the Higgs mass. We thus rescale the test statistics in the mass region where the $\mathrm{CL_{s+b}}$ approximation is used (i.e. $110 \leq M_H \leq 150$ GeV) by the correction factor 0.77.[26] Once made available by the TEVNPH Working Group, this approximation will be replaced by the published $\mathrm{CL_{s+b}}$ values.

Our method follows the spirit of a global SM fit and takes advantage from downward fluctuations of the background in the sensitive region to obtain a more restrictive limit on the SM Higgs production as is obtained with the modified frequentest approach. The resulting χ^2 curves versus M_H are shown in Fig. 4.1. The low-mass exclusion is dominated by the LEP searches, while the information above 120 GeV is contributed by the Tevatron experiments. Following the original figure, the Tevatron measurements have been interpolated by straight lines for the purpose of presentation and in the fit which deals with continuous M_H values.

Constraints on the weak mixing angle can also be derived from atomic parity violation measurements in caesium, thallium, lead and bismuth. For heavy atoms one determines the *weak charge*, $Q_W \approx Z(1-4\sin^2\theta_W) - N$. Because the present experimental accuracy of 0.6% (3.2%) for Q_W from Cs [77, 78] (Tl [79, 80]) is still an order of magnitude away from a competitive constraint on $\sin^2\theta_W$, we do not include it into the fit. (Including it would reduce the error on the fitted Higgs mass by 0.2 GeV.) Due to the same reason we do not include the parity violation left-right asymmetry measurement using fixed target polarised Møller scattering at low $Q^2 = 0.026\ \mathrm{GeV}^2$ [81].[27]

The NuTeV Collaboration measured ratios of neutral and charged current cross sections in neutrino–nucleon scattering at an average $Q^2 \simeq 20\ \mathrm{GeV}^2$ using both muon neutrino and muon anti-neutrino beams [82]. The results derived for the effective weak couplings are not included in this analysis because of unclear theoretical uncertainties from QCD effects such as next-to-leading order corrections and nuclear effects of the bound nucleon parton distribution functions [83] (for reviews see, e.g., Refs. [84, 85]).

Although a large number of precision results for α_S at various scales are available, including recent 3NLO determinations at the τ-mass scale [17, 18, 86, 87], we do not

[23] This procedure only uses the M_H value under consideration, where Higgs-mass hypothesis and measurement are compared. It thus neglects that in the SM a given signal hypothesis entails background hypotheses for all M_H values other than the one considered. An analysis accounting for this should provide a statistical comparison of a given hypothesis with all available measurements. This however would require to know the correlations among all the measurement points (or better: the full experimental likelihood as a function of the Higgs-mass hypothesis), which are not provided by the experiments to date. The difference to the hypothesis-only test employed here is expected to be small at present, but may become important once an experimental Higgs signal appears, which however has insufficient significance yet to claim a discovery (which would allow one to discard all other Higgs-mass hypotheses). We thank Bill Murray (RAL) for bringing this point to our attention.

[24] The experiments integrate only the tail towards larger $-2\ln Q$ values of the probability density function to compute $\mathrm{CL_{s+b}}$ (corresponding to a counting experiment with to too few observed events with respect to the s + b hypothesis), which is later used to derive $\mathrm{CL_s}$ in the modified frequentest approach. They thus quantify Higgs-like (not necessarily SM Higgs) enhancements in the data. In the global SM fit, however, one is interested in the compatibility between the SM hypothesis and the experimental data as a whole, and must hence account for any deviation, including the tail towards smaller $-2\ln Q$ values (corresponding to a counting experiment with too many Higgs candidates with respect to the s + b hypothesis where, s labels the *SM Higgs* signal).

[25] The use of Erf^{-1} provides a consistent error interpretation when (re)translating the χ^2 estimator into a confidence level via $\mathrm{CL} = 1 - \mathrm{Prob}(\chi^2, 1) = \mathrm{Erf}(\sqrt{\chi^2/2})$.

[26] The correction factor reduces the value of the χ^2 test statistics. As described in footnote 32, its application has little impact on the fit results.

[27] The main success of this measurement is to have established the running of the weak coupling strength at the 6.4σ level.

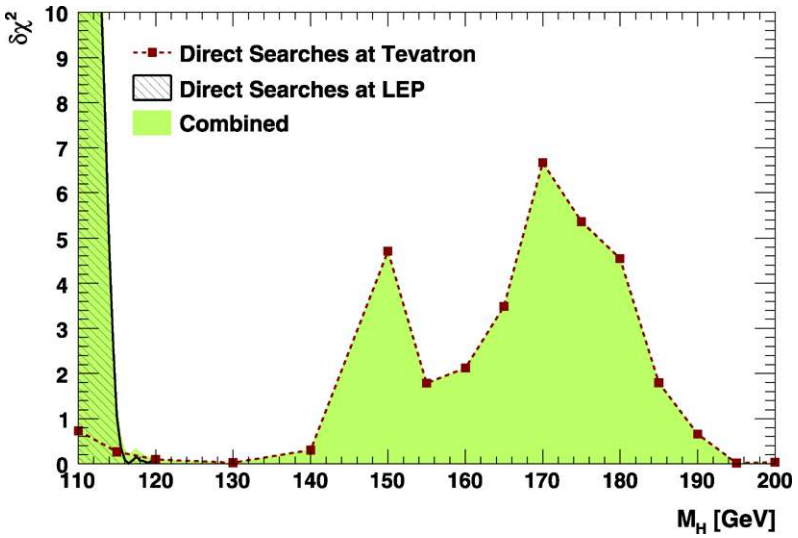

Fig. 4.1 The contribution to the χ^2 estimator versus M_H derived from the experimental information on direct Higgs boson searches made available by the LEP Higgs Boson and the Tevatron New Phenomena and Higgs Boson Working Groups [71–73]. The *solid dots* indicate the Tevatron measurements. Following the original figure they have been interpolated by *straight lines* for the purpose of presentation and in the fit. See text for a description of the method applied

include these in the fit, because—owing to the weak correlation between $\alpha_S(M_Z^2)$ and M_H (cf. Table 4.3)—the gain in precision on the latter quantity is insignificant.[28] Leaving $\alpha_S(M_Z^2)$ free provides thus an independent and theoretically robust determination of the strong coupling at the Z-mass scale.

The anomaly of the magnetic moment of the muon $(g-2)_\mu$ has been measured very accurately to a relative precision of 5×10^{-7}. Because of the small muon mass the interesting weak corrections only set in at a similar size, and this observable is thus not included in the analysis. However, the sensitivity of $(g-2)_\mu$ to physics beyond the SM (expected to couple to the lepton mass-squared) is similar to that of the other observables.

4.2.3 Fit results

All fits discussed in this section minimise the test statistics $\chi^2(y_{\rm mod})$ defined in (2.1). The χ^2 function accounts for the deviations between the observables given in Table 4.1 and their SM predictions (including correlations). Throughout this section we will discuss the results of two fits:

- The *standard ("blue-band") fit*, which includes all the observables listed in Table 4.1, except for results from the direct Higgs searches.
- The *complete fit* includes also the results from the direct searches for the Higgs boson at LEP and the Tevatron using the method described in Sect. 4.2.2.

The *standard* (*complete*) *fit* converges at the global minimum value $\chi^2_{\rm min}=16.4$ ($\chi^2_{\rm min}=18.0$) for 13 (14) degrees of freedom, giving the naive p-value Prob$(\chi^2_{\rm min},13)=0.23$ (Prob$(\chi^2_{\rm min},14)=0.21$). See Sect. 4.2.5 for a more accurate toy-MC-based determination of the p-value. The results for the parameters and observables of the two fits are given in columns four and five of Table 4.1 together with their one standard deviation (σ) intervals derived from the $\Delta\chi^2$ estimator using a Gaussian approximation.[29] We discuss in the following some of the outstanding findings and features of the fits.

Direct and indirect determination of observables, pulls

To test the sensitivity of the SM fit to the various input observables, we consecutively disabled each of the observables in the fit and performed a log-likelihood scan of the disabled observable. The corresponding results and the 1σ intervals are listed in the last column of Table 4.1. Comparing the errors obtained in these indirect determinations with the available measurements reveals their importance for the fit. For example, the measurement of M_Z is a crucial ingredient, albeit the available accuracy is not required. The indirect and direct determinations of M_W are of similar precision, such that an improved measurement would immediately impact the fit. The same is true for the asymmetry A_ℓ. On the other hand, due to an insufficient precision the heavy quark asymmetries A_c and A_b do not significantly impact the fit (the fit outperforms the measurements by almost two orders of magnitude in precision).

For further illustration, the pull values obtained from the difference between the fit result and the measurement divided by the total experimental error (not including the fit

[28] Including the constraint $\alpha_S(M_Z^2)=0.1212\pm0.0011$ [18] into the fit moves the central value of M_H by $+0.6$ MeV, and provides no reduction in the error.

[29] We have verified the Gaussian properties of the fit by sampling toy MC experiments. The results are discussed in Sect. 4.2.4. In the following, unless otherwise stated, confidence levels and error ranges are derived using the Gaussian approximation Prob$(\Delta\chi^2, n_{\rm dof})$.

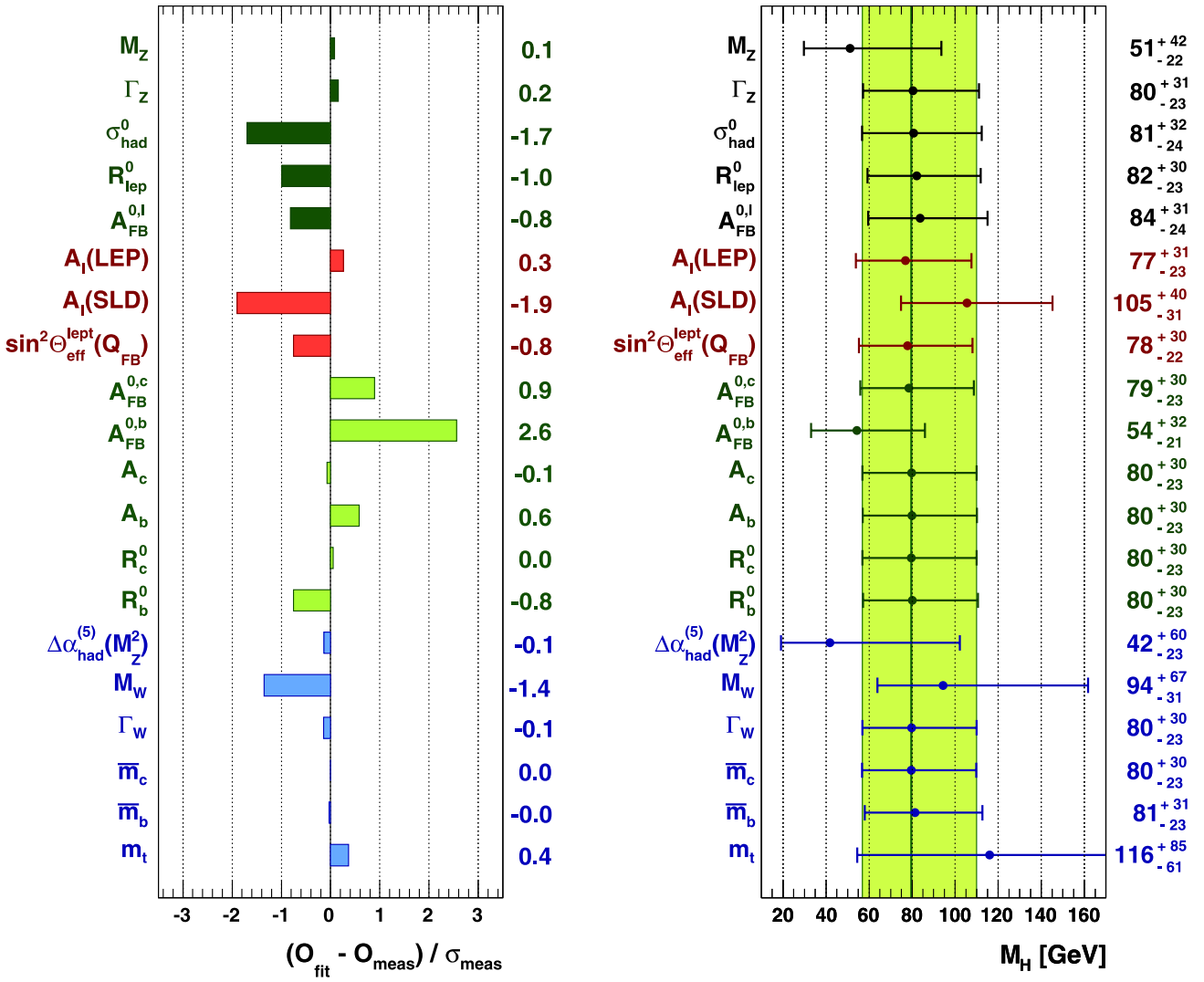

Fig. 4.2 Comparing fit results with direct measurements: pull values for the *complete fit* (*left*), and results for M_H from the *standard fit* excluding the respective measurements from the fit (*right*)

error) are shown for the *complete fit* in the left-hand plot of Fig. 4.2 (the *standard fit* pulls are very similar). They reflect the known tension between the leptonic and hadronic asymmetries, though it is noticeable that no single pull value exceeds 3σ. The pulls of the c and b quark masses are very small indicating that variations of these masses within their respective error estimates has negligible impact on the fit. The same observation applies to M_Z and $\Delta\alpha^{(5)}_{\mathrm{had}}(M_Z^2)$ (and to a lesser extent even to m_t). Thus, without significant impact on the goodness-of-fit fit these parameters could have been fixed.[30]

Correlations

The correlation coefficients between the fit parameters of the *standard fit* are given in Table 4.3. Significant are the correlations of -0.40 ($+0.31$) between $\ln M_H$ and $\Delta\alpha^{(5)}_{\mathrm{had}}(M_Z^2)$ (m_t). An excellent precision of these two latter quantities is hence of primary importance for the Higgs-mass constraint. The correlation between $\Delta\alpha^{(5)}_{\mathrm{had}}(M_Z^2)$ and $\alpha_S(M_Z^2)$ is due to the dependence of the hadronic vacuum polarisation contribution on the strong coupling that is known to the fit (cf. comment in footnote 19 on p. 556). The correlation coefficients obtained with the *complete fit* are very similar.

[30] Fixing $\overline{m}_c$, $\overline{m}_b$, m_t, M_Z and $\Delta\alpha^{(5)}_{\mathrm{had}}(M_Z^2)$ in the fit leads to only an insignificant increase of 0.03 in the overall χ^2_{min}, reflecting the little sensitivity of the fit to these parameters varying within the ranges of their (comparably small) measurement errors. Of course, this does not prevent M_H to strongly depend on the m_t and $\Delta\alpha^{(5)}_{\mathrm{had}}(M_Z^2)$ input values.

Table 4.3 Correlation coefficients between the free fit parameters in the *standard fit*. The correlations with and between the varying theoretical error parameters $\delta_{\rm th}$ are negligible in all cases. The correlation between M_H and the input parameter M_W amounts to -0.49

Parameter	$\ln M_H$	$\Delta\alpha^{(5)}_{\rm had}(M_Z^2)$	M_Z	$\alpha_S(M_Z^2)$	m_t	$\overline{m}_c$	$\overline{m}_b$
$\ln M_H$	1	−0.395	0.113	0.041	0.309	−0.001	−0.006
$\Delta\alpha^{(5)}_{\rm had}(M_Z^2)$		1	−0.006	0.101	−0.007	0.001	0.003
M_Z			1	−0.019	−0.015	−0.000	0.000
$\alpha_S(M_Z^2)$				1	0.021	0.011	0.043
m_t					1	0.000	−0.003
$\overline{m}_c$						1	0.000

Prediction of the Higgs mass

The primary target of the electroweak fit is the prediction of the Higgs mass. The main results are discussed in this paragraph, while more detailed aspects concerning the statistical properties of the Higgs mass prediction are presented in Sect. 4.2.4. The *complete fit* represents the most accurate estimation of M_H considering all available data. We find

$$M_H = 116.4^{+18.3}_{-1.3}\ \text{GeV} \tag{4.26}$$

where the error accounts for both experimental and theoretical uncertainties. The theory parameters $\delta_{\rm th}$ lead to an uncertainty of 8 GeV on M_H, which does however not yet significantly impact the error in (4.26) because of the spread among the input measurements that are sensitive to M_H (cf. Fig. 4.3).[31] As seen in Fig. 4.12 of Sect. 4.3, once the measurements are (made) compatible, the theoretical errors become visible by the uniform plateau around the $\Delta\chi^2$ minimum, and also fully contribute to the fit error. The 2σ and 3σ allowed regions of M_H, including all errors, are [114, 145] GeV and [[113, 168] and [180, 225]] GeV, respectively.[32] The result for the *standard fit* without the direct Higgs searches is

$$M_H = 80^{+30}_{-23}\ \text{GeV} \tag{4.27}$$

and the 2σ and 3σ intervals are respectively [39, 155] GeV and [26, 209] GeV. The 3σ upper limit is tighter than for the complete fit because of the increase of the best fit value of M_H in the *complete fit*. The contributions from the various measurements to the central value and error of M_H in the *standard fit* are given in the right-hand plot of Fig. 4.2, where all input measurements except for the ones listed in a given line are used in the fit. It can be seen that, e.g., the measurements of m_t and M_W are essential for an accurate estimation of the M_H.

Figure 4.3 gives the complementary information. Among the four observables providing the strongest constraint on M_H, namely A_ℓ(LEP), A_ℓ(SLD), $A^{0,b}_{\rm FB}$ and M_W, only the one indicated in a given row of the plot is included in the fit.[33] The compatibility among these measurements (cf. Fig. 4.3) can be estimated by (for example) repeating the global fit where the least compatible of the measurements (here $A^{0,b}_{\rm FB}$) is removed, and by comparing the $\chi^2_{\rm min}$ estimator obtained in that fit to the one of the full fit (here the *standard*

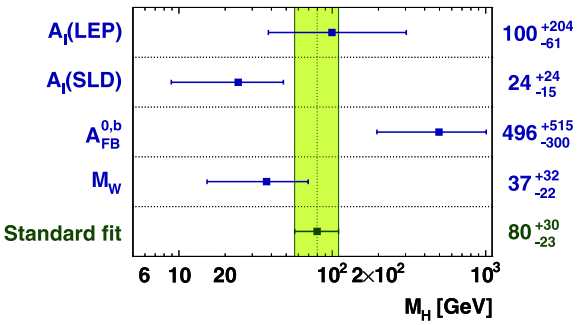

Fig. 4.3 Determination of M_H excluding all the sensitive observables from the *standard fit*, except for the one given. The results shown are not independent. The information in this figure is complementary to the one in the right-hand plot of Fig. 4.2

[31] This is a subtle feature of the *R*fit treatment that we shall illustrate by mean of a simple example. Consider two identical uncorrelated measurements of an observable A: $1 \pm 1 \pm 1$ and $1 \pm 1 \pm 1$, where the first errors are statistical and the second theoretical. The weighted average of these measurements gives $\langle A\rangle = 1 \pm 0.7 \pm 1 = 1 \pm 1.7$, where for the last term statistical and theoretical errors (likelihoods) have been combined. If the two measurements only barely overlap within their theoretical errors, e.g., $1 \pm 1 \pm 1$ and $3 \pm 1 \pm 1$, their weighted average gives $\langle A\rangle = 2 \pm 1$. Finally, if the two measurements are incompatible, e.g., $1 \pm 1 \pm 1$ and $5 \pm 1 \pm 1$, one finds $\langle A\rangle = 3 \pm 0.7$, i.e., the theoretical errors are only used to increase the global likelihood value of the average, without impacting the error. This latter situation occurs in the M_H fits discussed here (although the theoretical errors in these fits are attached to the theory predictions rather than to the measurements, which however does not alter the conclusion).

[32] A fit in which the estimated $\rm CL_{s+b}$ values of the Tevatron searches in the mass region $110 \le M_H \le 150$ GeV are not rescaled with the correction factor 0.77 (cf. Sect. 4.2.2) leads to a significant increase of the $\Delta\chi^2$ value only for $M_H = 150$ GeV. At lower masses the χ^2 contributions of the direct searches at the Tevatron are small. The central value of M_H as well as the 1σ and 3σ allowed regions are unchanged; only the 2σ interval is slightly reduced to [114, 144] GeV without the correction factor.

[33] The uncertainty in the $y_{\rm mod}$ parameters that are correlated to M_H (mainly $\Delta\alpha^{(5)}_{\rm had}(M_Z^2)$ and m_t) contributes to the errors shown in Fig. 4.3, and generates a correlations between the four M_H values found.

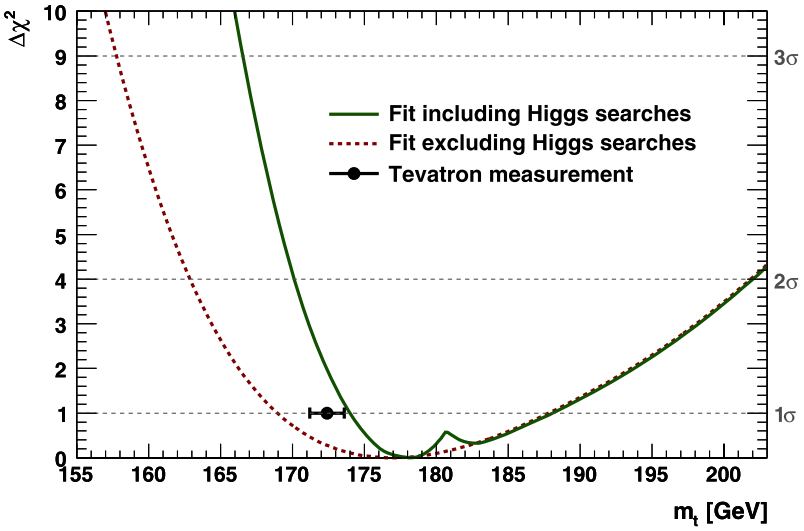

Fig. 4.4 $\Delta\chi^2$ versus m_t for the *complete fit* (*solid line*) and the *standard fit* (*dashed*), both excluding the direct m_t measurement which is indicated by the dot with 1σ error bars

fit). To assign a probability to the observation, the $\Delta\chi^2_{\rm min}$ obtained this way must be gauged with toy MC experiments to take into account the "look-elsewhere" effect introduced by the explicit selection of the pull outlier. We find that in $(1.4 \pm 0.1)\%$ ("2.5σ") of the toy experiments, the $\Delta\chi^2_{\rm min}$ found exceeds the $\Delta\chi^2_{\rm min} = 8.0$ observed in current data.

In spite of the significant anticorrelation between M_H and $\Delta\alpha^{(5)}_{\rm had}(M_Z^2)$, the present uncertainty in the latter quantity does not strongly impact the precision obtained for M_H. Using the theory-driven, more precise phenomenological value $\Delta\alpha^{(5)}_{\rm had}(M_Z^2) = (277.0 \pm 1.6) \times 10^{-4}$ [88], we find for the *standard fit* $M_H = 80^{+28}_{-22}$ GeV. For comparison, with $\Delta\alpha^{(5)}_{\rm had}(M_Z^2) = (275.8 \pm 3.5) \times 10^{-4}$ [89], we find $M_H = 83^{+34}_{-26}$ GeV, reproducing the result form the LEP Electroweak Working Group [39].

Prediction of the top mass

Figure 4.4 shows the $\Delta\chi^2 = \chi^2 - \chi^2_{\rm min}$ profile as a function of m_t obtained for the *complete fit* (solid line) and the *standard fit* (dashed line), both excluding the direct measurement of the top-quark mass from the fit. The one, two and three standard deviations from the minimum are indicated by the crossings with the corresponding horizontal lines. From the *complete fit* we find

$$m_t = 178.2^{+9.8}_{-4.2}\ \text{GeV}, \tag{4.28}$$

which, albeit less precise, agrees with the experimental number indicated in Fig. 4.4 by the dot with 1σ error bars (cf. Table 4.1). The corresponding result for the *standard fit* is $m_t = 177.0^{+10.8}_{-8.0}$ GeV. The insertion of the direct (LEP) Higgs searches leads to a more restrictive constraint towards small top-quark masses. Because of the floating Higgs mass, and its positive correlation with m_t, the $\Delta\chi^2$ profile of the *standard fit* exhibits an asymmetry (the constraint is less restrictive towards *larger* m_t values), which is opposite to the naive expectation from the dominantly quadratic m_t dependence of the loop corrections.

The strong and electromagnetic couplings

From the *complete fit* we find for the strong coupling at the Z-mass scale

$$\alpha_S\big(M_Z^2\big) = 0.1193^{+0.0028}_{-0.0027} \pm 0.0001, \tag{4.29}$$

where the first error is experimental (including also the propagated uncertainties from the errors in the c and b quark masses) and the second due to the truncation of the perturbative QCD series. It includes variations of the renormalisation scale between $0.6M_Z < \mu < 1.3M_Z$ [18], of massless terms of order $\alpha_S^5(M_Z)$ and higher, and of quadratic massive terms of order and beyond $\alpha_S^4(M_Z)$ (cf. Appendix A.4).[34] Equation (4.29) represents the theoretically most robust determination of α_S to date. It is in excellent agreement with the recent 3NLO result from τ decays [17, 18], $\alpha_S(M_Z^2) = 0.1212 \pm 0.0005 \pm 0.0008 \pm 0.0005$, where the errors are experimental (first) and theoretical (second and third), the latter error being further subdivided into contributions from the prediction of the τ hadronic width (and spectral moments), and from the evolution to the Z-mass scale.[35] Because of their precision, and the almost two orders of magnitude scale difference, the τ and Z-scale mea-

[34] The uncertainty related to the ambiguity between the use of fixed-order perturbation theory and the so-called contour-improved perturbation theory to solve the contour integration of the complex Adler function has been found to be very small (3×10^{-5}) at the Z-mass scale [18].

[35] Another analysis exploiting the τ hadronic width and its spectral functions, but using a different set of spectral moments than [18], finds

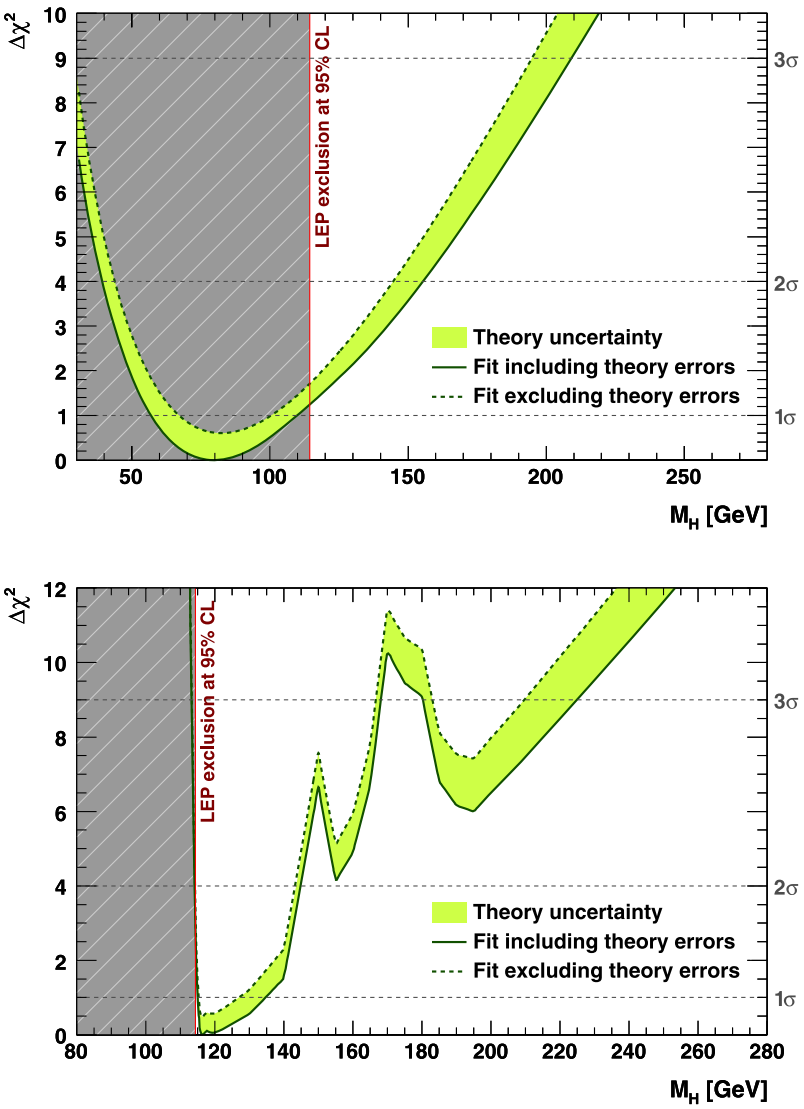

Fig. 4.5 $\Delta\chi^2$ as a function of M_H for the *standard fit* (*top*) and the *complete fit* (*bottom*). The *solid* (*dashed*) *lines* give the results when including (ignoring) theoretical errors. The minimum $\chi^2_{\min}$ of the fit including theoretical errors is used for *both curves* in *each plot* to obtain the offset-corrected $\Delta\chi^2$

surements of α_S represent the best current test of the asymptotic freedom property of QCD.

Finally, the fit result for $\Delta\alpha^{(5)}_{\rm had}(M_Z^2)$ without using the constraint from the phenomenological analysis in the fit (but including the constraint from the direct Higgs searches, cf. Table 4.1) precisely establishes a running QED coupling,[36] and can be translated into the determination $\alpha^{-1}(M_Z)|_{\rm fit} = 128.99 \pm 0.08$. The result is in agreement with the phenomenological value $\alpha^{-1}(M_Z)|_{\rm ph} = 128.937 \pm 0.030$ [66].

4.2.4 *Properties of the Higgs-mass constraint*

We proceed with studying the statistical properties of the constraints (4.26) and (4.27). Figure 4.5 (top) shows the $\Delta\chi^2$ profile versus M_H obtained for the *standard fit* (outermost envelope). Also shown is the 95% CL exclusion region obtained from the direct searches at LEP [71]. It exceeds the best fit value of the *standard fit*. The *R*fit approach provides an inclusive treatment of all types of theoretical uncertainties considered in the fit. Fixing the $\delta_{\rm th}$ parameters at zero in the fit (which is equivalent to ignoring the corresponding theoretical uncertainties) results in a narrower log-likelihood curve, with a +0.6 larger global $\chi^2_{\min}$ value, and a shift in M_H at this minimum of +2.4 GeV with respect to the result of the *standard fit*. The difference between the two envelopes obtained with freely varying and fixed $\delta_{\rm th}$ parameters is highlighted by the shaded band in Fig. 4.5 (top).

$\alpha_S(M_Z^2) = 0.1187 \pm 0.0016$ [87]. An analysis of the τ hadronic width relying on fixed-order perturbation theory finds $\alpha_S(M_Z^2) = 0.1180 \pm 0.0008$, where all errors have been added in quadrature [86].

[36] This result is complementary (though more precise) to the LEP measurements of the scale dependence of α using, e.g., small and large-angle Bhabha scattering at low energy [90, 91] and high energies [92], respectively, or cross-section and asymmetry measurements at high energies [93].

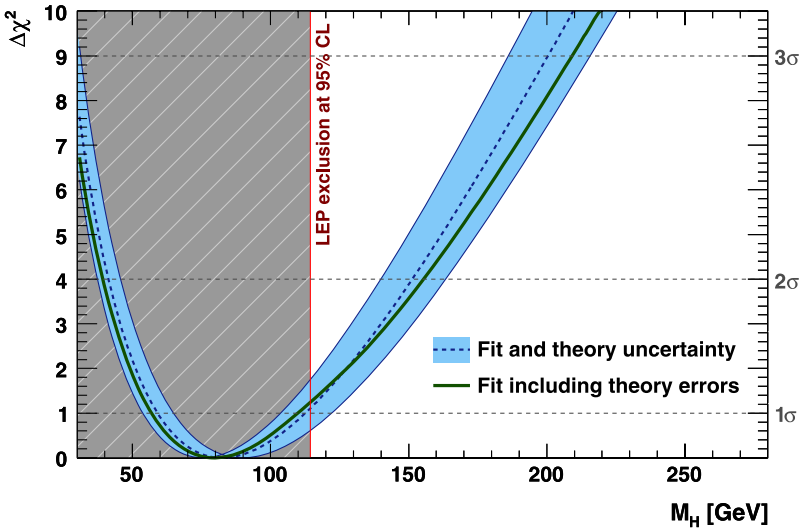

Fig. 4.6 $\Delta\chi^2$ versus M_H with an alternative treatment of theory uncertainties [94]. Shown are the results of the *standard fit* ignoring theoretical uncertainties (*dotted line*), the regions determined from the maximum deviation in $\Delta\chi^2$ achieved by shifting the SM predictions of all observables according to 1 "standard deviation" of the various theory uncertainties (*shaded band*) and for comparison the result of the *standard fit* (*solid curve*) in which theoretical uncertainties are included in the χ^2 calculation

In previous electroweak fits [94] theoretical uncertainties were accounted for by independently shifting the SM prediction of each affected observable by the size of the estimated theoretical uncertainty, and taking the maximum observed cumulative deviation in M_H as theoretical error. The error envelope obtained this way is shown in Fig. 4.6. The dotted curve in the middle of the shaded band is the result of a fit ignoring all theoretical uncertainties. The shaded band illustrates the maximum deviations of the $\Delta\chi^2$ curves obtained with shifted predictions. Including the systematic uncertainties in this way yields a 1σ interval of [55, 122] GeV and 95% (99%) CL upper limits of 162 GeV(192 GeV) respectively. For comparison the solid curve in Fig. 4.6 shows the result of the *standard fit* using the *R*fit scheme.[37] More detailed studies of systematic theoretical uncertainties are reported in [59].

The $\Delta\chi^2$ curve versus M_H for the *complete fit* is shown in Fig. 4.5 (bottom). Again the shaded band indicates the difference between the two envelopes obtained with freely varying and fixed $\delta_{\rm th}$ parameters, both normalised to the same $\chi^2_{\rm min}$ (from the fit with free $\delta_{\rm th}$ parameters). The inclusion of the direct Higgs search results from LEP leads to a strong rise of the $\Delta\chi^2$ curve below $M_H = 115$ GeV. The data points from the direct Higgs searches at the Tevatron, available in the range $110 < M_H < 200$ GeV with linear interpolation between the points, increases the $\Delta\chi^2$ estimator for Higgs masses above 140 GeV beyond that obtained from the *standard fit*.

We have studied the Gaussian (parabolic) properties of the $\Delta\chi^2$ estimator to test whether the interpretation of the profile likelihood in terms of confidence levels can be simplified. Figure 4.7 gives the $1 - {\rm CL}$ derived for $\Delta\chi^2$ as a function of the M_H hypothesis for various scenarios: Gaussian approximation ${\rm Prob}(\Delta\chi^2, 1)$ of the *standard fit* including theory errors (dashed/red line), Gaussian approximation of the *standard fit* ignoring theory errors, i.e., fixing all $\delta_{\rm th}$ parameters at zero (solid/black line), and an accurate evaluation using toy MC experiments ignoring theory errors (shaded/green area). Also shown is the *complete fit* result with Gaussian approximation. The toy experiments are sampled using as underlying model the best fit parameters (and corresponding observables) obtained for each M_H hypothesis. As described in Sect. 2.4, such a hypothesis is incomplete from a frequentest point of view because the true values of the nuisance parameters are unknown.[38] However, the persuasively Gaussian character of the fit makes us confident that our assumption is justified in the present case (cf. the additional discussion and tests in Sect. 4.2.5). The correlations given in Table 4.2 are taken into account for the generation of the toy experiments. Theoretical errors being of non-statistical origin have been excluded from this test, which aims at gauging the statistical properties of the test

[37] The inclusion of the theory errors via freely varying parameters (*R*fit) leads to a decrease in the global $\chi^2_{\rm min}$ of the fit. Incompatibilities in the input observables (which may be due to statistical fluctuations) thus attenuate the numerical effect of the theoretical errors on the fitted parameter (here M_H). See footnote 31 on p. 560 for an illustration of this effect.

[38] Examples from other particle physics areas, such as the determination of the CKM phase γ via direct CP violation measurements in B decays involving charm, show that this approximation can lead to severe undercoverage of the result [24]. As described in Sect. 2, the full treatment would require a numerical minimisation of the exclusion CL with respect to any true SM (nuisance) parameter set used to generate the toy MC samples (cf. Refs. [24, 25]). More formally, this corresponds to solving ${\rm CL}(M_H) = \min_\mu {\rm CL}_\mu(M_H)$, where μ are the nuisance parameters of the fit and ${\rm CL}_\mu(M_H) = \int_0^{\Delta\chi^2(M_H;{\rm data})} F(\Delta\chi^2|M_H,\mu)\,d\Delta\chi^2$, and where $F(\Delta\chi^2|M_H,\mu)$ is the probability density function of $\Delta\chi^2$ for true M_H and μ determined from toy MC simulation.

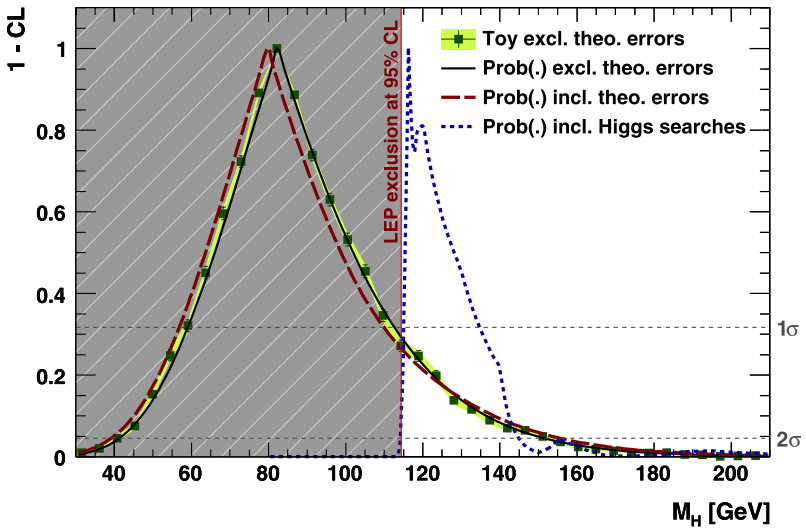

Fig. 4.7 The $1-\mathrm{CL}$ function derived from the $\Delta\chi^2$ estimator versus the M_H hypothesis (cf. Fig. 4.5 (*top*) for $\Delta\chi^2$ versus M_H) for the *standard fit*. Compared are the Gaussian approximation Prob$(\Delta\chi^2, 1)$ for the *standard fit* with (*dashed/red line*) and without theoretical errors (*solid/black line*), respectively, to an evaluation based on toy MC simulation for which theoretical errors have been ignored. Also given is the result using Prob(.) for the *complete fit* (*dotted/blue line*)

statistics. The curves in Fig. 4.7 show agreement between the Gaussian approximation without theoretical errors, and the toy MC result. It proves that the fit is well behaved, and the $\Delta\chi^2$ estimator can be interpreted as a true χ^2 function.

Figure 4.8 shows the 68%, 95% and 99% CL contours for the variable pairs m_t vs. M_H (top) and $\Delta\alpha^{(5)}_{\mathrm{had}}(M_Z^2)$ vs. M_H (bottom), exhibiting the largest correlations in the fits. The contours are derived from the $\Delta\chi^2$ values found in the profile scans using Prob$(\Delta\chi^2, 2)$ (cf. discussion in Sect. 2.3). Three sets of fits are shown in these plots: the largest/blue (narrower/purple) allowed regions are derived from the *standard fit* excluding (including) the measured values (indicated by shaded/light green horizontal bands) for respectively m_t and $\Delta\alpha^{(5)}_{\mathrm{had}}(M_Z^2)$ in the fits. The correlations seen in these plots are approximately linear for $\ln M_H$ (cf. Table 4.3). The third set of fits, providing the narrowest constraints, uses the *complete fit*, i.e., including in addition to all available measurements the direct Higgs searches. The structure of allowed areas reflects the presence of local minima in the bottom plot of Fig. 4.5.

Figure 4.9 compares the direct measurements of M_W and m_t, shown by the shaded/green 1σ bands, with the 68%, 95% and 99% CL constraints obtained with again three fit scenarios. The largest/blue (narrowest/green) allowed regions are again the result of the *standard fit* (*complete fit*) excluding (including) the measured values of M_W and m_t. The results of the *complete fit* excluding the measured values are illustrated by the narrower/yellow allowed region. The allowed regions of the indirect determination is significantly reduced with the insertion of the direct Higgs searches. Good agreement is observed between (i) indirect determination without (largest/blue area) and with (narrower/yellow area) the direct Higgs searches, and (ii) the direct measurements (shaded/green bands).

4.2.5 *Probing the standard model*

We evaluate the p-value of the global SM fit following the prescription outlined in Sect. 2.4. A toy MC sample with 10 000 experiments has been generated using as true values for the SM parameters the outcomes of the global fit (see the remarks below and in Sect. 2.4 and footnote 38 on page 563 about the limitation of this method). For each toy simulation, the central values of all the observables used in the fit are generated according to Gaussian distributions around their expected SM values (given the parameter settings) with standard deviations equal to the full experimental errors taking into account all correlations.[39] It is assumed that central values and errors are independent. The *R*fit treatment of theoretical uncertainties allows the fit to adjust theoretical predictions and parameters at will within the given error ranges, and—as opposed to measurements—the theoretical parameters cannot be described by a probability density distribution and are thus not fluctuated in the toy MC. For each toy MC sample, the *complete fit* is performed (i.e., including the results from the direct Higgs searches) yielding the χ^2_{min} distribution shown by the light shaded histogram in Fig. 4.10. The distribution obtained when fixing the δ_{th} parameters at zero is shown by the dark shaded/green histogram. Including the theoretical uncertainties reduces the number of degrees of freedom in the data and hence shifts the distribution to lower values. Overlaid is the χ^2 function expected for Gaussian observables and 14 degrees of freedom. Fair agreement with the empirical toy MC distribution for fixed δ_{th} is observed.

[39] Since only bounds on M_H are available with no probability density information given within these bounds, a random generation of M_H toy measurements is not possible. This experimental input is thus kept unchanged for all toy MC experiments.

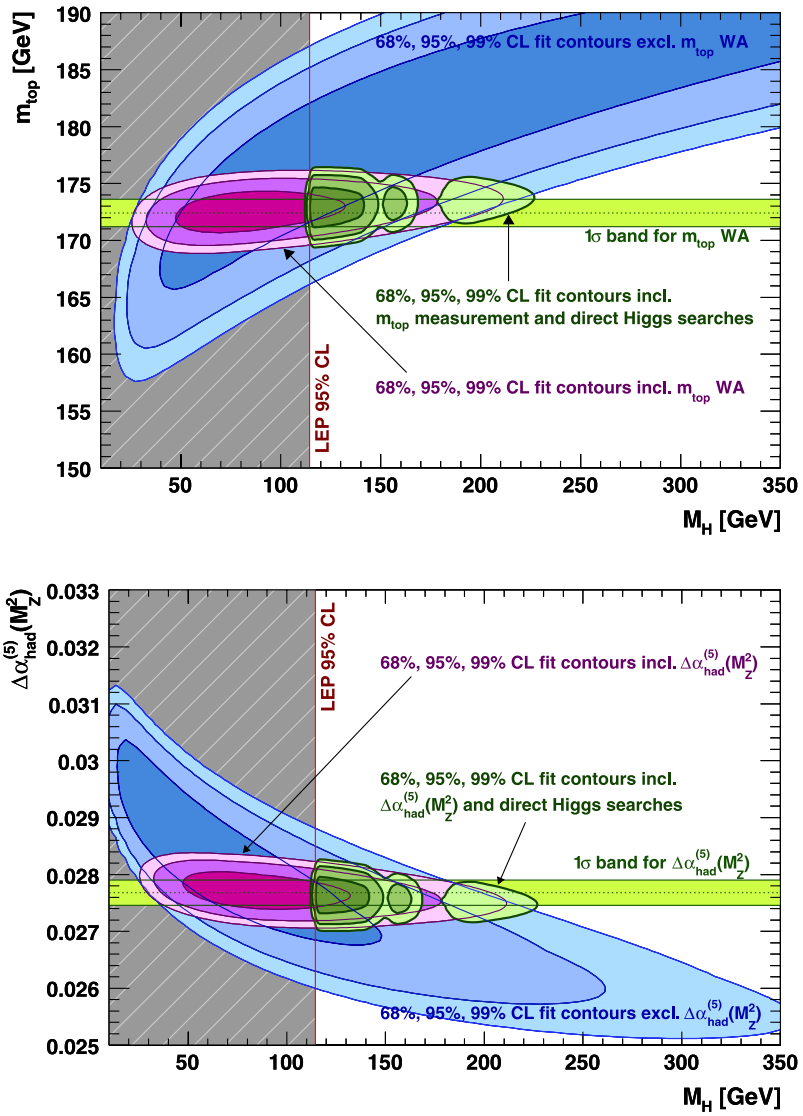

Fig. 4.8 Contours of 68%, 95% and 99% CL obtained from scans of fits with fixed variable pairs m_t vs. M_H (*top*) and $\Delta\alpha^{(5)}_{\mathrm{had}}(M_Z^2)$ vs. M_H (*bottom*). The *largest/blue* (*narrower/purple*) allowed *regions* are the results of the *standard fit* excluding (including) the measurements of m_t (*top*) and $\Delta\alpha^{(5)}_{\mathrm{had}}(M_Z^2)$ (*bottom*). The narrowest/green areas indicate the constraints obtained for the *complete fit* including all the available data. The *horizontal bands* indicate the 1σ regions of respectively the m_t measurement and $\Delta\alpha^{(5)}_{\mathrm{had}}(M_Z^2)$ phenomenological determination

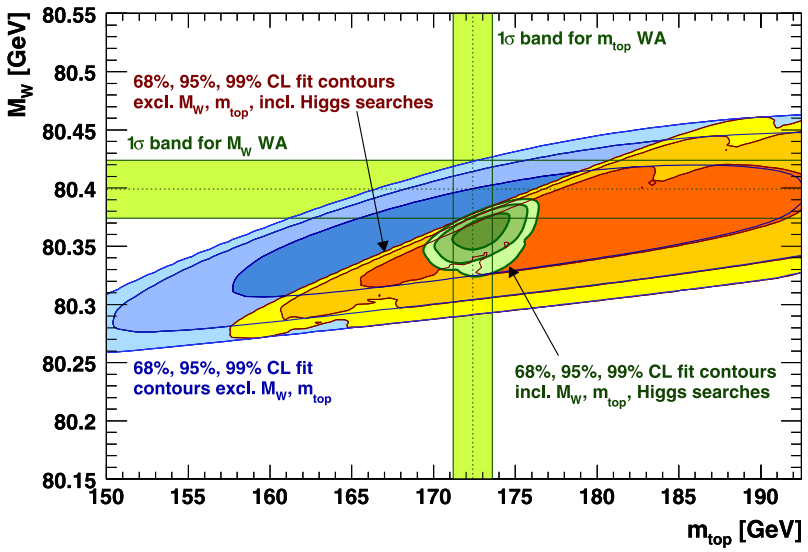

Fig. 4.9 Contours of 68%, 95% and 99% CL obtained from scans of fits with fixed variable pairs M_W vs. m_t. The *largest/blue* allowed *regions* are the results of the *standard fit* excluding the measurements of M_W and m_t. The *narrow/yellow* (*narrowest/green*) *areas* indicate the constraints obtained for the *complete fit* excluding (including) the corresponding measurements. The *horizontal bands* indicate the 1σ regions of the measurements (world averages)

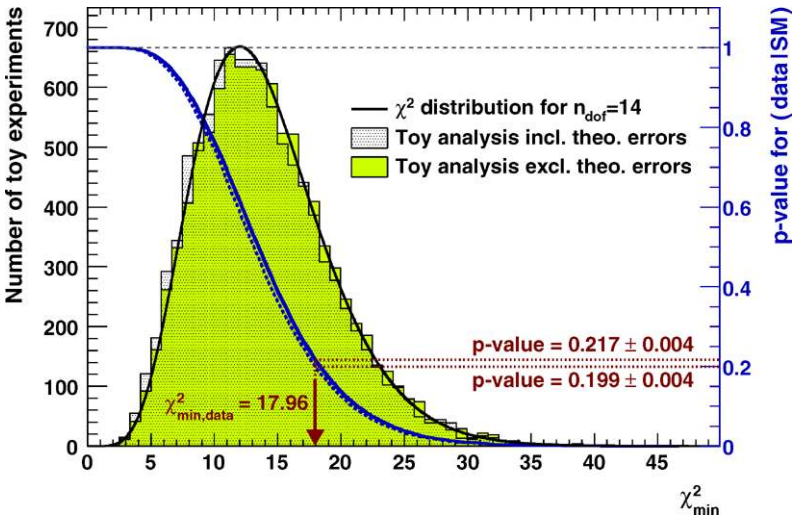

Fig. 4.10 Result of the MC toy analysis of the *complete fit*. Shown are the χ^2_{min} distribution of a toy MC simulation (*open histogram*), the corresponding distribution for a *complete fit* with fixed δ_{th} parameters at zero (*shaded/green histogram*), an ideal χ^2 distribution assuming a Gaussian case with $n_{\text{dof}} = 14$ (*black line*) and the p-value as a function of the χ^2_{min} of the global fit

The monotonously decreasing curves in Fig. 4.10 give the p-value of the SM fit as a function of χ^2_{min}, obtained by integrating the sampled normalised χ^2 function between χ^2_{min} and infinity. The value of the global SM fit is indicated by the arrow. Including theoretical errors in the fit gives

$$\text{p-value (data|SM)} = 0.22 \pm 0.01_{-0.02}, \tag{4.30}$$

where the first error is statistical, determined by the number of toy experiments performed, and the second accounts for the shift resulting from fixed δ_{th} parameters. The probability of falsely rejecting the SM, expressed by the result (4.30), is sufficient and no significant requirement for physics beyond the SM can be inferred from the fit. To validate the $p_{\mu-\text{best fit}} \approx \min_\mu p_\mu$ assumption used in the above study, we have generated several true parameter sets (μ) in the vicinity of the best fit result (varying parameters incoherently by $\pm 1\sigma$ around their measurement errors), and repeated the toy-MC-based p-value evaluation for each of them. The χ^2 probability density distributions derived from these tests have been found to be compatible with each other, leading to similar p-values in all cases studied. It supports the robustness of the result (4.30).

We have extended the above analysis by deriving p-values for the *standard fit* as a function of the true Higgs mass. The results are shown in Fig. 4.11. For values of M_H around 80 GeV, corresponding to the χ^2_{min} of the *standard fit*, p-values of about 0.25 are found.[40] With higher M_H the p-value drops reaching the 2σ level at $M_H = 190$ GeV and the 3σ level at $M_H = 270$ GeV.

[40] By fixing M_H the number of degrees of freedom of the fit is increased compared to the *standard fit* resulting in a larger average χ^2_{min} and thus in a larger p-value.

4.3 Prospects for the LHC and ILC

The next generation of particle colliders, namely LHC and ILC, have the potential to significantly increase the precision of most electroweak observables that are relevant to the fit. This will improve the predictive power of the fit, and—in case of a Higgs discovery—its sensitivity to physics beyond the SM by directly confronting theory and experiment, and by testing the overall goodness-of-fit of the SM.

At the LHC the masses of the W boson and the top quark are expected to be measured with precisions reaching $\sigma(M_W) = 15$ MeV and $\sigma(m_t) = 1.0$ GeV [19, 20, 95, 96], respectively.[41] At the ILC it is expected that the top mass can be measured to an experimental precision of approximately $\sigma(m_t) = 50$ MeV using a threshold scan and an adapted mass definition [21, 99]. This should translates into an error of 100–200 MeV on the $\overline{\text{MS}}$-mass depending on the accuracy of the strong coupling constant [21, 99, 100]. More improvements are expected for a linear collider running with high luminosity and polarised beams at the Z

[41] CMS expects a systematic (statistical) precision of better than 20 MeV (10 MeV) for an integrated luminosity of 10 fb^{-1} [20, 97]. It uses a method based on solely the reconstruction of the charged lepton transverse momentum, which has reduced systematic uncertainties compared to reconstructing the transverse W mass, with the downside of a smaller statistical yield. In an earlier study using the transverse-mass method, ATLAS finds a systematic (statistical) uncertainty of better than 25 MeV (2 MeV), for the same integrated luminosity [19]. Combining both, lepton channels and experiments, a final uncertainty of about 15 MeV is anticipated in [95], which is used here. A recent ATLAS study [98], superseding their previous results, finds that uncertainties of $\sigma(M_W) \approx 7$ MeV may be achievable for each lepton channel (with similar uncertainties for both aforementioned experimental approaches), by heavily relying on the calibration of the lepton momenta and reconstruction efficiencies at the Z pole. Using this $\sigma(M_W)$ in the fit improves the M_H determination for the LHC prospective from $M_H = 120^{+42}_{-33}$ to $M_H = 120^{+31}_{-26}$ (using the improved $\Delta\alpha^{(5)}_{\text{had}}(M_Z^2)$ error of 7×10^{-5} for both fits, cf. Table 4.4).

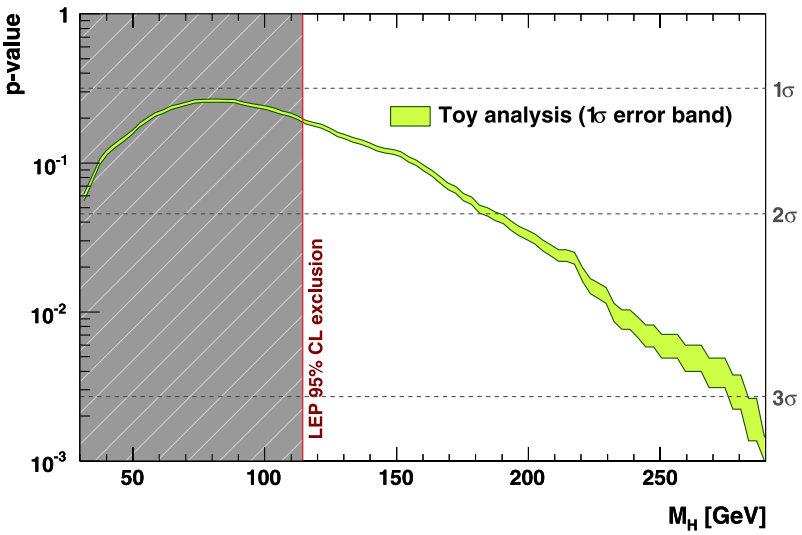

Fig. 4.11 P-value of the electroweak fit versus M_H as obtained from toy MC simulation. The error band represents the statistical error from the MC sampling

resonance (GigaZ). The W-mass can be measured to 6 MeV from a scan of the WW threshold [21]. The effective weak mixing angle for leptons can be measured to a precision of 1.3×10^{-5} from the left-right asymmetry, A_{LR} [21, 101]. At the same time, the ratio of the Z leptonic to hadronic partial decay widths, R_ℓ^0, can be obtained to an absolute experimental precision of 0.004 [102]. These numbers do not include theoretical uncertainties since it is assumed that substantial theoretical progress will be realised in the years left before these measurements are possible.

At the time when the new measurements from the LHC experiments, and later the ILC, become available, an improved determination of $\Delta\alpha^{(5)}_{\mathrm{had}}(M_Z^2)$ will be needed to fully exploit the new precision data. This in turn requires a significant improvement in the quality of the hadronic cross-section data at energies around the $c\bar{c}$ resonances and below, and a better knowledge of the c and b quark masses entering the perturbative prediction of the cross sections where applicable, which serve as input to the dispersion integral. Reference [103] quotes expected uncertainties of $\sigma(\Delta\alpha^{(5)}_{\mathrm{had}}(M_Z^2)) \sim 7 \times 10^{-5}$ and 5×10^{-5}, compared to presently 22×10^{-5}, if the relative precision on the cross sections attains 1% below the J/ψ and the Υ resonances, respectively. The former estimate will be used for the present study. Since most of present data is dominated by systematic uncertainties, measurements of state-of-the-art experiments with better acceptance and control of systematics are needed. High-statistics ISR analyses performed at the B and Φ factories already provided promising results on many exclusive hadronic channels. New data will also come from the BESIII experiment at the BEPCII e^+e^- collider that starts operation in Summer 2008.

The dominant theoretical uncertainties affecting the electroweak fit arise from the missing higher-order corrections in the predictions of M_W and $\sin^2\theta^\ell_{\mathrm{eff}}$ (cf. Sect. 4.1.4), which contribute similarly to the error on M_H. They amount to 10 GeV (13 GeV) at $M_H = 120$ GeV (150 GeV). Significant theoretical effort is needed to reduce these.

A summary of the current and anticipated future uncertainties on the quantities M_W, m_t, $\sin^2\theta^\ell_{\mathrm{eff}}$, R_ℓ^0, and $\Delta\alpha^{(5)}_{\mathrm{had}}(M_Z^2)$, for the LHC, ILC, and the ILC with GigaZ option, is given in Table 4.4. By using these improved measurements the global SM fit (not using the results from direct Higgs searches nor measurements of $\alpha_S(M_Z^2)$) results in the constraints on the Higgs mass and $\alpha_S(M_Z^2)$ quoted in Table 4.4. For all four scenarios the true Higgs mass has been assumed to be $M_H = 120$ GeV and the central values for all observables are adjusted such that they are consistent with this M_H value. All fits are performed using respectively the present uncertainty on $\Delta\alpha^{(5)}_{\mathrm{had}}(M_Z^2)$, and assuming the above-mentioned improvement. For the latter case results for M_H are given including (parentheses) and excluding [brackets] theory uncertainties. With the GigaZ option, the uncertainty from $\Delta\alpha^{(5)}_{\mathrm{had}}(M_Z^2)$ would dominate the overall fit error on M_H if no improvement occurred. We emphasise that due (by part) to the logarithmic dependence, the error obtained on M_H is strongly M_H dependent: with the same precision on the observables, but central values that are consistent with a true value of 150 GeV, one would find $M_H = 150^{+66}_{-49}$ GeV in average, i.e., an error increase over the $M_H = 120$ GeV case of almost 30%. With the GigaZ option and the resulting improvement for R_ℓ^0 the uncertainty on $\alpha_S(M_Z^2)$ from the fit is reduced by a factor of four.

The M_H scans obtained for the four scenarios, assuming the improved $\Delta\alpha^{(5)}_{\mathrm{had}}(M_Z^2)$ precision to be applicable for all future (LHC and beyond) scenarios, are shown in Fig. 4.12.

Table 4.4 Measurement prospects at future accelerators for key observables used in the electroweak fit, and their impact on the electroweak fit. The columns give, from the left to the right: present errors, the expected uncertainties for the LHC with 10 fb^{-1} integrated luminosity, the ILC without and with the option to run at the Z resonance and along the W-pair production threshold (GigaZ) for one year of nominal running. The estimated improvement for $\Delta\alpha^{(5)}_{\rm had}(M_Z^2)$ (given in parenthesis of the corresponding line) over the current uncertainty is unrelated to these accelerators, and must come from new low-energy hadronic cross-section measurements and a more accurate theory (see text). The lower rows give the results obtained for M_H and $\alpha_S(M_Z^2)$. For M_H are also given the results with improved $\Delta\alpha^{(5)}_{\rm had}(M_Z^2)$ precision (parentheses—this has no impact on $\alpha_S(M_Z^2)$), and when in addition ignoring the theoretical uncertainties [brackets]. Note that all errors obtained on M_H are strongly central value dependent (see text)

Quantity	Expected uncertainty			
	Present	LHC	ILC	GigaZ (ILC)
M_W [MeV]	25	15	15	6
m_t [GeV]	1.2	1.0	0.2	0.1
$\sin^2\theta^\ell_{\rm eff}$ [10^{-5}]	17	17	17	1.3
R^0_ℓ [10^{-2}]	2.5	2.5	2.5	0.4
$\Delta\alpha^{(5)}_{\rm had}(M_Z^2)$ [10^{-5}]	22 (7)	22 (7)	22 (7)	22 (7)
$M_H(=120$ GeV) [GeV]	$^{+56}_{-40}$ ($^{+52}_{-39}$) [$^{+39}_{-31}$]	$^{+45}_{-35}$ ($^{+42}_{-33}$) [$^{+30}_{-25}$]	$^{+42}_{-33}$ ($^{+39}_{-31}$) [$^{+28}_{-23}$]	$^{+27}_{-23}$ ($^{+20}_{-18}$) [$^{+8}_{-7}$]
$\alpha_S(M_Z^2)$ [10^{-4}]	28	28	27	6

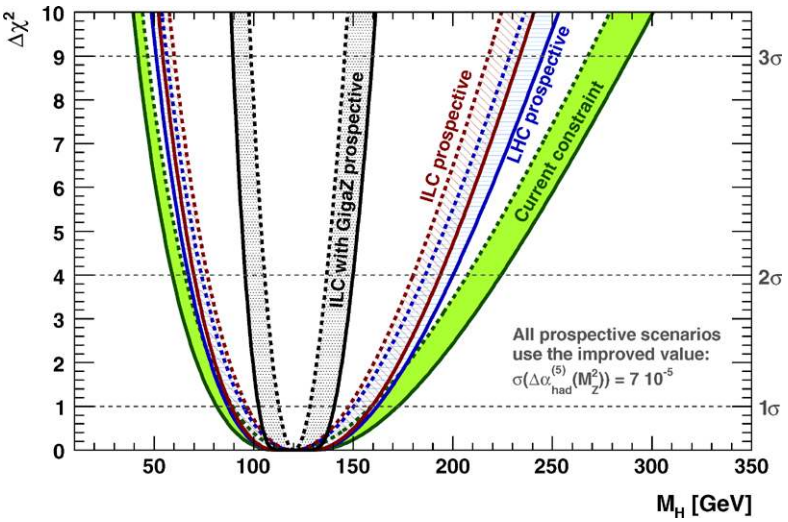

Fig. 4.12 Constraints on M_H obtained for the four scenarios given in Table 4.4, assuming the improvement $\sigma(\Delta\alpha^{(5)}_{\rm had}(M_Z^2)) = 7\times10^{-5}$ for all prospective curves. Shown are, from wider to narrower $\Delta\chi^2$ curves: present constraint, LHC expectation, ILC expectations with and without GigaZ option. The 1σ errors for M_H given in Table 4.4 correspond to the $\Delta\chi^2 = 1$ intervals obtained from these graphs. The *shaded bands* indicate the effect of theoretical uncertainties

The shaded bands indicate the effect of the current theoretical uncertainties. As expected the theoretical errors included with the Rfit scheme are visible by a broad plateau around the $\Delta\chi^2$ minimum.

A discovery of the Higgs boson at the LHC in the clean decay mode $H\to\gamma\gamma$ ($H\to 2\ell 2\ell'$) for a light (heavy) Higgs would soon allow for a precision measurement of M_H beyond the percent level. Inserting the measurement into the global electroweak fit would lead to a prediction of the W boson mass with 13 MeV error, of which 5 MeV is theoretical. Prediction and measurement could be directly confronted. More inclusively, the p-value of the data given the SM could be determined as a direct test of the goodness of the SM fit.

5 Extending the SM Higgs sector—the two Higgs doublet model

Two Higgs Doublet Models (2HDM) [104] are simple extensions to the SM Higgs sector, only introducing an additional $SU(2)_L\times U(1)_Y$ Higgs doublet with hypercharge $Y=1$, leading to five physical Higgs bosons. Three Higgs bosons (A^0, h^0, H^0) are electrically neutral and the two remaining ones ($H^\pm$) are electrically charged. The free parameters of the 2HDM are the Higgs boson masses M_{A^0}, M_{h^0}, M_{H^0} and $M_{H^\pm}$, the ratio of the vacuum expectation values of the two Higgs doublets $\tan\beta = v_2/v_1$, occurring in the mixing of charged and neutral Higgs fields, and the angle α, governing the mixing of the neutral CP-even Higgs fields. It should be noted that, in the most general

2HDM, $\tan\beta$ and hence the corresponding Higgs couplings and mass matrix elements depend on the choice of basis for the Higgs fields [105, 106].

Models with two Higgs doublets intrinsically fulfil the empirical equality $M_W^2 \approx M_Z^2 \cos^2\theta_W$. They also increase the maximum allowed mass of the lightest neutral Higgs boson for electroweak baryogenesis scenarios to values not yet excluded by LEP (see, e.g., [107]), and introduce CP violation in the Higgs sector. Flavour changing neutral currents can be suppressed with an appropriate choice of the Higgs-fermion couplings (see e.g., Refs. [108, 109]). For example, in the *Type-I* 2HDM this is achieved by letting only one Higgs doublet couple to the fermion sector. In the *Type-II* 2HDM [110], which is chosen for this analysis, one Higgs doublet couples to the up-type quarks and leptons only, while the other one couples only to the down-type quarks and leptons. The Type-II 2HDM resembles the Higgs sector in the Minimal Supersymmetric Standard Model. It fixes the basis of the Higgs fields and promotes $\tan\beta$ to a physical parameter.

Our analysis is restricted to the CP conserving 2HDM scalar potential and furthermore we only consider observables that are sensitive to corrections from the exchange of a charged Higgs boson. In the Type-II 2HDM the charged Higgs-fermion interaction Lagrangian is given by [108, 109]

$$\mathcal{L}_{H^\pm ff} = \frac{g}{2\sqrt{2}m_W}\big(H^+\bar{U}\big(M_U K(1-\gamma_5)\cot\beta + K M_D(1+\gamma_5)\tan\beta\big)D + \text{h.c.}\big), \tag{5.1}$$

where U and D are column matrices of three generation up-type and down-type quark fields, respectively, M_U and M_D are the corresponding diagonal mass matrices, and K is the Cabibbo–Kobayashi–Maskawa quark-mixing matrix. The charged Higgs interaction has the same structure as the charged current mediated by the W. Significant charged Higgs couplings to light quarks can occur for large values of $\tan\beta$.

By investigating observables that are sensitive to corrections from a charged Higgs exchange we derive constraints on the allowed charged-Higgs mass $M_{H^\pm}$ and $\tan\beta$. Direct searches for the charged Higgs have been performed at LEP and the Tevatron. LEP has derived a lower limit of $M_{H^\pm} > 78.6$ GeV at 95% CL [111], for any value of $\tan\beta$.

5.1 Input observables

The constraints on the charged Higgs are currently dominated by indirect measurements, as opposed to direct searches at high-energy accelerators. A multitude of heavy flavour observables mainly from B-meson decays is available whose sensitivity to the 2HDM parameters varies however substantially, either due to limited experimental precision in case of rare decays, or because specific 2HDM contributions are strongly suppressed. The most relevant observables for the search of Type-II 2HDM signals are the electroweak precision variable R_b^0, branching fractions of rare semileptonic B, D and K decays, and loop-induced radiative B decays.[42] A summary of the experimental input used for this analysis is given in Table 5.1.

5.1.1 *Hadronic branching ratio of Z to b quarks* R_b^0

The sensitivity of R_b^0 to a charged Higgs boson arises from an exchange diagram modifying the $Zb\bar{b}$ coupling. The corresponding corrections of the SM prediction have been calculated in Ref. [115] and are given in (6.3) and (6.4) thereof. The left- (right-) handed corrections to the effective couplings $\delta g^{L(R)}$ are proportional to $\cot^2\beta$ ($\tan^2\beta$) and to $R/(R-1) - R\log R/(R-1)^2$, where $R = m_t^2/M_{H^\pm}^2$. The charged-Higgs exchange leads to a decrease of R_b^0. Neutral Higgs contributions can be neglected for small $\tan\beta$. For the SM prediction we use the result from the *complete* electroweak fit, $R_{b,\text{SM}}^0 = 0.21580 \pm 0.00006$, where the direct measurement of R_b^0 has been excluded (cf. Table 4.1). It is confronted in the fit with the experimental value $R_{b,\text{exp}}^0 = 0.21629 \pm 0.00066$, obtained at LEP [46], giving $\Delta R_b^0 = R_{b,\text{exp}}^0 - R_{b,\text{SM}}^0 = 0.00049 \pm 0.00066$.

5.1.2 *The decay* $B \to X_s\gamma$

The decay $B \to X_s\gamma$ is an effective flavour changing neutral current process occurring only at loop-level in the SM. The SM prediction for its branching fraction ($\mathcal{B}$) at NNLO accuracy is $(3.15 \pm 0.23) \times 10^{-4}$ [116], where the theoretical uncertainty is estimated by studying (in decreasing order of importance) nonperturbative, parametric, higher-order and m_c interpolation ambiguity effects, and where all errors have been added in quadrature. Averaging branching fraction measurements from the BABAR, Belle and CLEO Collaborations gives $\mathcal{B}(B \to X_s\gamma) = (3.52 \pm 0.23 \pm 0.09) \times 10^{-4}$ [117], where the first error is experimental and the second stems from the modelling of the photon energy spectrum. The improved NNLO calculation yields a branching fraction approximately 1.5σ lower than the NLO calculation [118], resulting in a small tension with the experimental average and thus leading to less stringent constraints on the charged Higgs mass. The 2HDM contribution to the $\mathcal{B}(B \to X_s\gamma)$ arises from a charged Higgs replacing the

[42] Decays of τ and μ leptons can also occur through charged-Higgs tree diagrams giving anomalous contributions to the decay parameters (*Michel parameters* [112]) measured in these decays. Their present sensitivity is however not competitive with the other observables (a 95% CL limit of $M_{H^\pm} > 1.9$ GeV $\cdot \tan\beta$ is currently achieved from τ decays [113], see also [114] for a review of the μ decay parameters).

$W^\pm$ in the loop from which the photon is radiated and is always positive in the type-II model. For the prediction of $\mathcal{B}(B \to X_s\gamma)$ in the 2HDM we have used parameterised formulae [119] reproducing the result of [116] within 0.2%. While the value of the branching fraction changes with $M_{H^\pm}$ and, to a lesser extent with $\tan\beta$, the associated theoretical uncertainty stays to good approximation constant at 7%. Since it has been derived by quadratically combining several error estimates, we treat it as an additional Gaussian systematic error in the fit.

5.1.3 Leptonic decays of charged pseudoscalar mesons

In the SM the leptonic decay of charged pseudoscalar mesons proceeds via the annihilation of the heavy meson into a W boson and its subsequent leptonic decay. Angular momentum conservation leads to a helicity suppression factor that is squared in the lepton mass. Competitive contributions from the charged Higgs sector can therefore occur. Neglecting photon radiation, the leptonic decay rate of a pseudoscalar meson P has the form

$$\Gamma(P \to \ell\nu) = \frac{\mathcal{B}(P \to \ell\nu)}{\tau_P} = \frac{G_F^2}{8\pi} f_P^2 m_\ell^2 m_P \left(1 - \frac{m_\ell^2}{m_P^2}\right)^2 |V_{q_1q_2}|^2, \quad (5.2)$$

where m_P (m_ℓ) is the mass of the pseudoscalar meson (lepton), $|V_{q_1q_2}|$ is the magnitude of the CKM matrix element of the constituent quarks in P, and f_P is the weak decay constant.

For $P = B$ (implying $B^\pm = B_u^\pm$) we use [117] $\tau_{B^\pm} = (1.639 \pm 0.009)$ ps and $|V_{ub}| = (3.81 \pm 0.47) \times 10^{-3}$, where the latter result has been averaged over inclusive and exclusive measurements. For the B decay constant we use the value $f_B = (216 \pm 22)$ MeV, obtained by the HPQCD Collaboration from unquenched Lattice QCD calculations [120]. For meson and lepton masses we use the values of Ref. [64]. With these inputs, we find the SM predictions $\mathcal{B}(B \to \tau\nu) = 1.53^{+0.46}_{-0.38} \times 10^{-4}$ and $\mathcal{B}(B \to \mu\nu) = 0.69^{+0.21}_{-0.17} \times 10^{-7}$.

An alternative approach uses for the r.h.s. of (5.2) additional constraints from the global CKM fit enhancing the information on $|V_{ub}|$ beyond that of the direct measurement through the fit of the Wolfenstein parameters $\overline{\rho}, \overline{\eta}$, and on f_B through the measurement of the $B^0\overline{B}^0$ mixing frequency. This assumes that the measurements entering the fit are free from significant new physics contributions. It is certainly the case for the charged Higgs but cannot be excluded for the CP-violation and neutral-B mixing observables. Hence, albeit using the global CKM fit is an interesting test, it cannot replace the direct SM prediction of (5.2) based on tree-level quantities and lattice calculations only. Not using the direct measurements, the global CKM fit gives $|V_{ub}| = (3.44^{+0.22}_{-0.17}) \times 10^{-3}$, and for the complete prediction $\mathcal{B}(B \to \tau\nu) = 0.83^{+0.27}_{-0.10}$ [121]. This latter result is about 1.9σ below the one from the "tree-level" determination, and a similar discrepancy is found for $B \to \mu\nu$ (cf. Table 5.1).

The charged-Higgs amplitude contributes to the leptonic decays modifying (5.2) by a scaling factor r_H. In the Type-II 2HDM the b quark couples only to one of the Higgs doublets at tree level so that the scaling factor for the decays $B \to \tau\nu$ and $B \to \mu\nu$ reads [122]

$$r_H = \left(1 - m_B^2 \frac{\tan\beta}{M_{H^\pm}}\right)^2, \quad (5.3)$$

which can lead to both, an increase and a decrease in the branching fraction, depending on whether the $W^\pm$ and $H^\pm$ amplitudes interfere constructively or destructively.

The rare leptonic decay $B \to \tau\nu$ has been observed by the BABAR and Belle Collaborations [123–125], with an average branching fraction[43] of $\mathcal{B}(B \to \tau\nu) = (1.51 \pm 0.33) \times 10^{-4}$. Only upper limits are available for the muon channel so far, the tightest one, $\mathcal{B}(B \to \mu\nu) < 1.3 \times 10^{-6}$ at 90% CL (-12 ± 20 fitted events), being found by BABAR [127]. For lack of an experimental likelihood we use the measured branching fraction of $(-5.7 \pm 7.1_{\text{stat}} \pm 6.8_{\text{syst}}) \times 10^{-7}$.

For $P = K$, contributions from a charged Higgs are suppressed by $(m_K/m_B)^2$ relative to leptonic B decays. Moreover, due to the smaller phase space for hadronic final states, leptonic decays have large branching fractions, which—on the other hand—have been measured to an excellent 0.2% relative accuracy for $\ell = \mu$. We follow the approach of Ref. [128] and compare $|V_{us}|$ determined from helicity suppressed $K \to \mu\nu$ decays and helicity allowed $K \to \pi\mu\nu$ decays, considering the expression

$$R_{\ell 23} = \left|\frac{V_{us}(K \to \mu\nu)}{V_{ud}(\pi \to \mu\nu)} \frac{V_{ud}(0^+ \to 0^+)}{V_{us}(K \to \pi\mu\nu)}\right| \quad (5.4)$$

which in the SM is equal to 1. The ratio $\mathcal{B}(K \to \mu\nu)/\mathcal{B}(\pi \to \mu\nu) \sim (V_{us} f_K)/(V_{ud} f_\pi)$ is used to reduce the theoretical uncertainties from the kaon decay constant f_K, and from electromagnetic corrections in the decay $K \to \mu\nu$ [128]. The dominant uncertainty in V_{us} from $K \to \pi\mu\nu$ decays stems from the $K \to \pi$ vector form factor at zero momentum transfer, $f_+(0)$, while V_{ud} determined from super-allowed nuclear beta decays ($0^+ \to 0^+$) is known with very high precision [129].

[43] Updated results from BABAR and Belle have been presented at the recent workshops CKM 2008 and Tau 2008 [126], leading to the new average $\mathcal{B}(B \to \tau\nu) = (1.73 \pm 0.35) \times 10^{-4}$. They will be included in future updates of this analysis.

Table 5.1 Experimental results and SM predictions for the input observables used in the analysis of the charged-Higgs sector of the Type-II 2HDM

Parameter	Experimental value	Ref.	SM prediction	Ref.
R_b^0	0.21629 ± 0.00066	[46]	0.21580 ± 0.00006	This work
$\mathcal{B}(B \to X_s\gamma)$ $[10^{-4}]$	$3.52 \pm 0.23 \pm 0.09$	[117]	3.15 ± 0.23	[116]
			$1.53^{+0.46}_{-0.38}$ $[f_B, \lvert V_{ub}\rvert]$	This work
$\mathcal{B}(B \to \tau\nu)$ $[10^{-4}]$	1.51 ± 0.33	[125]	$0.83^{+0.27}_{-0.10}$ [CKM fit]	[121]
			$0.69^{+0.21}_{-0.17}$ $[f_B, \lvert V_{ub}\rvert]$	This work
$\mathcal{B}(B \to \mu\nu)$ $[10^{-7}]$	$-5.7 \pm 6.8 \pm 7.1$	[127]	$0.37^{+0.12}_{-0.04}$ [CKM fit]	[121]
$R_{D\tau/e}$	$0.42 \pm 0.12 \pm 0.05$	[131]	0.28 ± 0.02	[130]
$R_{\ell 23}$	1.004 ± 0.007	[128]	1	–

In the 2HDM of Type-II the dependence of $R_{\ell 23}$ due to charged Higgs exchange is given by [128]

$$R^H_{\ell 23} = \left| 1 - \left(1 - \frac{m_d}{m_s}\right) \frac{m^2_{K^+}}{m^2_{H^+}} \tan^2\beta \right|, \tag{5.5}$$

where we use $m_d/m_s = 19.5 \pm 2.5$ [64]. Experimentally, a value of $R^{\text{exp}}_{\ell 23} = 1.004 \pm 0.007$ is found [128], where $(f_K/f_\pi)/f_+(0)$ has been taken from lattice calculations. It dominates the uncertainty on $R_{\ell 23}$.

5.1.4 The semileptonic decay $B \to D\tau\nu$

Similar to the $B \to \tau\nu$ decay, the semileptonic decay $B \to D\tau\nu$ can be mediated by a charged Higgs. We follow the arguments of Ref. [130] and use the ratio $R_{D\tau/e} = \mathcal{B}(B \to D\tau\nu)/\mathcal{B}(B \to De\nu)$ to reduce theoretical uncertainties from hadronic form factors occurring in the predictions of the individual branching fractions. In the Type-II 2HDM the ratio $R_{D\tau/e}$ can be expressed in the following compact form [130]:

$$R^H_{D\tau/e} = (0.28 \pm 0.02) \cdot \left[1 + (1.38 \pm 0.03) \cdot \text{Re}\left(C^\tau_{\text{NP}}\right) + (0.88 \pm 0.02) \cdot \left|C^\tau_{\text{NP}}\right|^2\right], \tag{5.6}$$

where $C^\tau_{\text{NP}} = -m_b m_\tau \tan^2\beta/m^2_{H^\pm}$. As for leptonic decays the 2HDM contribution can either lead to an increase or decrease in the branching fraction. Equation (5.6) is the result of an integration of the partial width $d\Gamma(B \to D\ell\nu)/dw$, assuming no Higgs contribution to $B \to De\nu$, and where $w = v_B v_D$ with v_B (v_D) being the four-velocity of the B (D) meson.

The ratio of branching fractions has been measured by BABAR to be $R^{\text{exp}}_{D\tau/e} = 0.42 \pm 0.12_{\text{stat}} \pm 0.05_{\text{syst}}$ [131].

5.2 Results and discussion

The theoretical predictions of the Type-II 2HDM for the various observables sensitive to corrections from the exchange of charged Higgs bosons have been implemented in a separate library integrated as a plug-in into the Gfitter framework. Exclusion confidence levels have been derived in two ways: (i) for each observable separately, and (ii) in a combined fit.

5.2.1 Separate constraints from individual observables

Constraints in the two-dimensional model parameter plane $(\tan\beta, M_{H^\pm})$ have been derived using the individual experimental measurements and the corresponding theoretical predictions of the Type-II 2HDM. Figure 5.1 displays the resulting two-sided 68% (yellow/light), 95% (orange) and 99% CL (red/dark) *excluded* regions separately for each of the observables given in Table 5.1. The confidence levels are derived assuming Gaussian behaviour of the test statistics, and using one degree of freedom (cf. discussion in footnote 7 on p. 547), i.e., Prob$(\Delta\chi^2, 1)$. Also indicated in the plots is the 95% CL exclusion limit resulting from the direct searches for a charged Higgs at LEP [111] (hatched area).

The figures show that R_b is mainly sensitive to $\tan\beta$ excluding small values (below $\simeq$1). $\mathcal{B}(B \to X_s\gamma)$ is only sensitive to $\tan\beta$ for values below $\simeq$1. For larger $\tan\beta$ it provides an almost constant area of exclusion of a charged Higgs lighter than $\simeq$260 GeV. (All exclusions at 95% CL.) The leptonic observables lead to triangle-shaped excluded areas in the region of large $\tan\beta$ and small $m_{H^\pm}$ values. $\mathcal{B}(B \to \tau\nu)$ gives the strongest constraint.[44] For these observables the 2HDM contribution can be either positive or negative, because magnitudes of signed terms occur in the predictions of the branching fractions giving a two-fold ambiguity in the $(\tan\beta, M_{H^\pm})$ plane.

[44] The stronger constraint obtained from the global CKM fit for $\mathcal{B}(B \to \tau\nu)$ is a result of the increased theoretical precision and, more importantly, the 1.9σ deviation with respect to the "tree-level" determination (cf. Table 5.1).

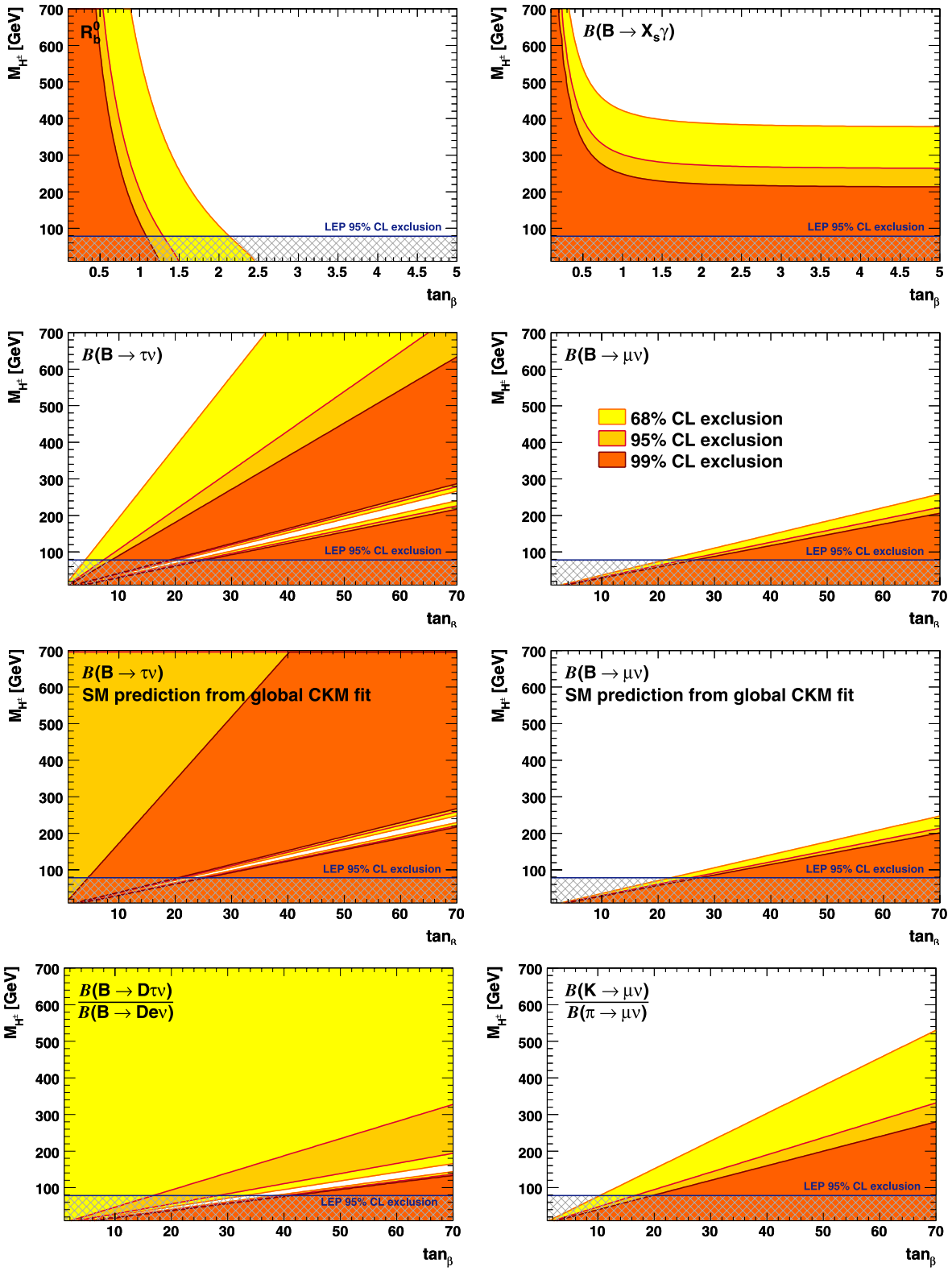

Fig. 5.1 Two-sided 68%, 95% and 99% CL *exclusion* regions obtained for the various observables (see text) in the 2HDM parameter plane $M_{H^\pm}$ versus $\tan\beta$

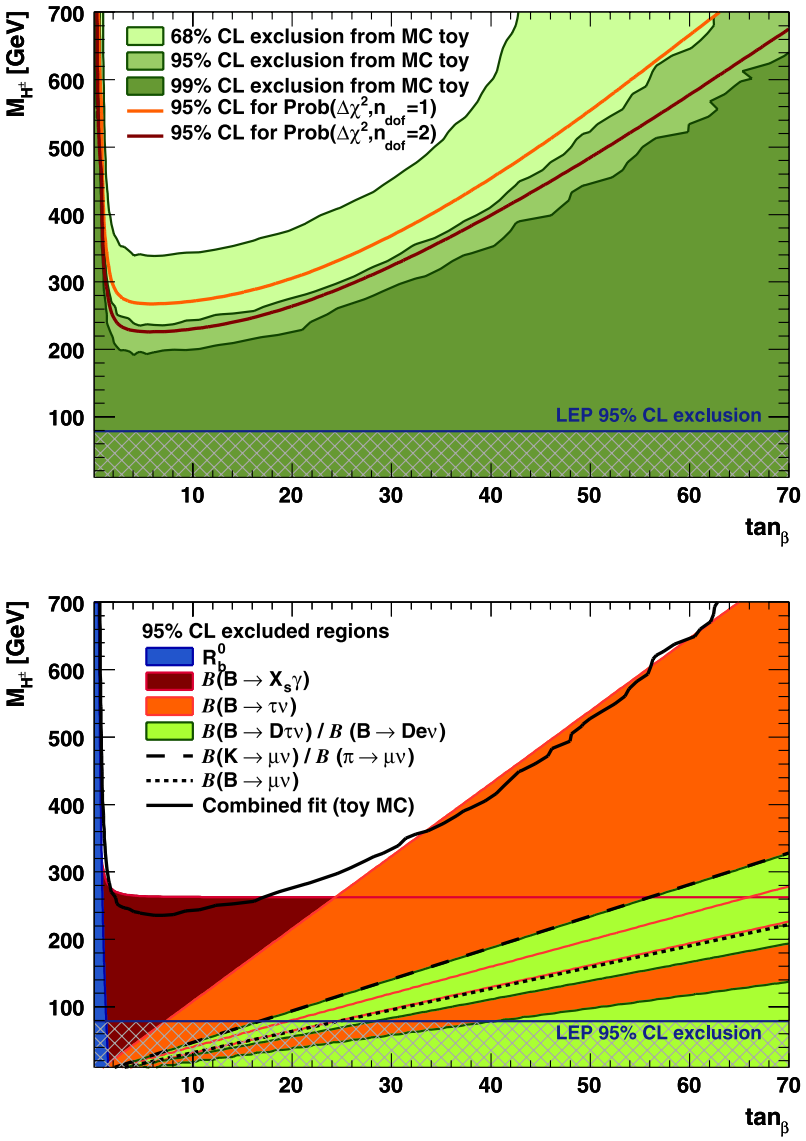

Fig. 5.2 Exclusion regions in the $(\tan\beta, M_{H^\pm})$ plane. The *top plot* displays the 68%, 95% and 99% CL excluded regions obtained from the combined fit using toy MC experiments. For comparison the 95% CL contours using $\text{Prob}(\Delta\chi^2, n_{\text{dof}})$ for $n_{\text{dof}} = 1$ and $n_{\text{dof}} = 2$ are also shown (see discussion in text). The *bottom plot* shows the 95% CL excluded regions from the individual constraints given in Table 5.1, and the toy-MC-based result from the combined fit overlaid

5.2.2 *Combined fit*

We have performed a global Type-II 2HDM fit combining all the available observables (and using the tree-level SM predictions for the leptonic B decays). We find a global minimum $\chi^2_{\text{min}} = 3.9$ at $M_{H^\pm} = 860$ GeV and $\tan\beta = 7$. Since the number of effective constraints varies strongly across the $(\tan\beta, M_{H^\pm})$ plane, it is not straightforward to determine the proper number of degrees of freedom to be used in the calculation of the CL—even if the test statistic follows a χ^2 distribution. According to the discussion in footnote 7 on p. 547 we avoid this problem by performing 2 000 toy-MC experiments in each scan point to determine the associated p-value. The upper plot of Fig. 5.2 shows the 68%, 95% and 99% CL excluded regions obtained from the toy-MC analysis of the combined fit. For comparison the 95% CL contours using $\text{Prob}(\Delta\chi^2, n_{\text{dof}})$ for $n_{\text{dof}} = 1$ and $n_{\text{dof}} = 2$ are also shown. As expected, the $n_{\text{dof}} = 2$ approximation is more accurate in regions where several observables contribute to the combined fit, while $n_{\text{dof}} = 1$ is better when a single constraint dominates over all the others (very small and very large values of $\tan\beta$). For comparison the lower plot of Fig. 5.2 shows again the 95% CL excluded region obtained from the toy-MC analysis of the combined fit (hatched area) together with the corresponding regions obtained from the individual constraints. It can be seen that due to the increased number of effective degrees of freedom the combined fit does not necessarily lead to stronger constraints.

The combination of the constraints excludes the high-$\tan\beta$, low-$M_{H^\pm}$ region spared by the $B \to \tau\nu$ constraint. We can thus exclude a charged-Higgs mass below 240 GeV independently of $\tan\beta$ at 95% confidence level. This limit

increases towards larger $\tan\beta$, e.g., $M_{H^\pm} < 780$ GeV are excluded for $\tan\beta = 70$ at 95% CL.

5.2.3 Perspectives

Improvements on the low-energy B-meson observables are expected from the KEKB and Belle upgrade program with an initial (final) target of 10 ab^{-1} (50 ab^{-1}) integrated luminosity [132–134]. Parallel developments envision the construction of a new SuperB accelerator with similar target luminosities [135]. With respect to the 2HDM analysis, these programs are particularly interesting for the decays $B \to \tau\nu$, $B \to \mu\nu$ and $B \to D\tau\nu$ whose present branching fraction measurements are statistically dominated. Further improvement can also be expected for the measurement of $\mathcal{B}(B \to X_s\gamma)$ with however less prominent effect on the 2HDM parameter constraints due to the size of the theoretical uncertainties. The measurement of the ratio of partial Z widths, R_b^0, could be improved at an ILC running at the Z resonance (GigaZ, cf. Sect. 4.3). The authors of Ref. [101] estimate a factor of five increase over the current precision, mostly by virtue of the increased statistical yield, and the excellent impact parameter resolution suppressing background from charm quarks.

The LHC experiments will attempt to directly detect signals from charged-Higgs production, either via $t \to bH^\pm$ decays, if $M_{H^\pm} < m_t$, and/or via gluon–gluon and gluon–bottom fusion to $t(b)H^\pm$, and the subsequent decay $H^\pm \to \tau\nu$, or, if $M_{H^\pm} > m_t$, via $H^\pm \to tb$. The full $\tan\beta$ parameter space is expected to be covered for $H^\pm$ lighter than top (a scenario already strongly disfavoured by the current indirect constraints, especially the one from $\mathcal{B}(B \to X_s\gamma)$), while the discovery of a heavy $H^\pm$ requires a large $\tan\beta$, which rapidly increases with rising $M_{H^\pm}$ [19, 20, 136].

6 Conclusions and perspectives

The wealth of available precision data at the electroweak scale requires consistent phenomenological interpretation via an overall (*global*) fit of the Standard Model and beyond. Such fits, mainly determining the top-quark mass, the Higgs-boson mass, the strong coupling constant, and the overall consistency of the model, have been performed by several groups in the past. The fit has sensitivity to confirm electroweak unification and the Brout–Englert–Higgs mechanism [137, 138] of spontaneous electroweak symmetry breaking for the dynamical generation of the fermion and boson masses, while posing problems for alternatives such as technicolour in its simplest form [139], requiring more involved scenarios. Other theories, like supersymmetry, are decoupling from the Standard Model if their masses are large. For such models the high energy precision data as well as constraints obtained from rare decays, flavour mixing and CP-violating asymmetries in the B and K-meson sectors, the anomalous magnetic moment of the muon, and electric dipole moments of electron and neutron, exclude a significant part of the parameter space. However, the models can be adjusted to become consistent with the experimental data as long as these data agree with the Standard Model predictions.

In this paper, we have revisited the global electroweak fit, and a simple extension of the Higgs sector to two doublets, using the new generic fitting toolkit Gfitter and its corresponding electroweak and 2HDM libraries. We have included the constraints from direct Higgs searches by the LEP and Tevatron experiments in the former fit. Emphasis has been put on a consistent treatment of theoretical uncertainties, using no assumptions other than their respective ranges, and a thorough frequentest statistical analysis and interpretation of the fit results.

Gfitter is an entirely new fitting framework dedicated to model testing in high-energy physics. It features transparent interfaces to model parameters and measurements, theory libraries, and fitter implementations. Parameter caching significantly increases the execution speed of the fits. All results can be statistically interpreted with toy Monte Carlo methods, treating consistently correlations and rescaling due to parameter dependencies.

For the *complete fit*, including the results from direct Higgs searches, we find for the mass of the Higgs boson the 2σ and 3σ intervals $[114, 145]$ GeV and $[[113, 168]$ and $[180, 225]]$ GeV, respectively. The corresponding results without the direct Higgs searches in the *standard fit* are $[39, 155]$ GeV and $[26, 209]$ GeV. Theoretical errors considered in the fit parameterise uncertainties in the perturbative predictions of M_W and $\sin^2\theta^f_{\text{eff}}$, and the renormalisation scheme ambiguity. They contribute with approximately 8 GeV to the total fit error obtained for M_H for the *standard fit*. In a fit excluding the measurement of the top-quark mass (but including the direct Higgs searches) we find $m_t = 178.2^{+9.8}_{-4.2}$ GeV, in fair agreement with the experimental world average. Finally, the strong coupling constant to 3NLO order at the Z-mass scale is found to be $\alpha_S(M_Z^2) = 0.1193^{+0.0028}_{-0.0027}$, with negligible theoretical error (0.0001) due to the good convergence of the perturbative series at that scale.

We have probed the goodness of the Standard Model fit to describe the available data with toy Monte Carlo simulation. For the fit including the direct Higgs searches it results in a p-value of $0.22 \pm 0.01_{-0.02}$, where the first error accounts for the limited Monte Carlo statistics, and the second for the impact of theoretical uncertainties (without these, the p-value is reduced by 0.04). The p-value for the fit without direct Higgs searches is similar (the reduced number of degrees of freedom approximately countervails the better

χ^2 value). The compatibility of the most sensitive measurements determining M_H has been estimated by evaluating the probability for a consistent set of measurements to find a single measurement that increases the overall χ^2 of the global fit by as much as is observed in data, when adding the least compatible measurement (here $A_{\mathrm{FB}}^{0,b}$). An analysis with toy MC experiments finds that this occurs in $(1.4 \pm 0.1)\%$ of the cases.

We have analysed the perspectives of the electroweak fit considering three future experimental scenarios, namely the LHC and an international linear collider (ILC) with and without high luminosity running at lower energies (GigaZ), all after years of data taking and assuming a good control over systematic effects. For a 120 GeV Higgs boson, the improved M_W and m_t measurements expected from the LHC would reduce the error on the M_H prediction by up to 20% with respect to the present result. The ILC could further reduce the error by about 25% over the LHC, and—if the hadronic contribution to $\alpha(M_Z^2)$ can be determined with better precision (requiring better hadronic cross-section measurements at low and intermediate energies)—a 30% improvement is possible. The largest impact on the fit accuracy can be expected from an ILC with GigaZ option. Together with an improved $\alpha(M_Z^2)$, the present fit error on M_H could be reduced by more than a factor of two. We point out however that, in order to fully exploit the experimental potential, in particular the anticipated improvements in the accuracy of M_W, theoretical developments are mandatory. If the Higgs is discovered, the improved electroweak fit will serve as a sensitive test for the Standard Model and its extensions.

By extending the Standard Model Higgs sector to two scalar doublets (2HDM of Type-II), we have studied the experimental constraints on the charged-Higgs mass $M_{H^\pm}$ and on $\tan\beta$, using as input branching fractions of the rare B decays $B \to X_s\gamma$, $B \to \tau\nu$, $B \to \mu\nu$, and $B \to De\nu$, the kaon decay $K \to \mu\nu$, and the electroweak precision observable R_b^0. Exclusion confidence levels have been derived by carrying out toy experiments for every point on a fine grid of the $(M_{H^\pm}, \tan\beta)$ parameter space. At 95% confidence level we exclude charged Higgs masses $M_{H^\pm} < 240$ GeV for any value of $\tan\beta$, and $M_{H^\pm} < 780$ GeV for $\tan\beta = 70$.

Inputs and numerical and graphical outputs of the Gfitter Standard Model and 2HDM analyses are available on the Gfitter web site: http://cern.ch/gfitter. They will be kept in line with the experimental and theoretical progress. Apart from these update commitments, new theoretical libraries such as the minimal supersymmetric extension of the Standard Model will be included and analysed.

Acknowledgements We are indebted to the LEP-Higgs and Tevatron-NPH working groups for providing the numerical results of the direct Higgs-boson searches. We thank Daisuke Nomura and Thomas Teubner for information on their analysis of the hadronic contribution to the running $\alpha(M_Z^2)$. We are grateful to Malgorzata Awramik for providing detailed information about the SM electroweak calculations, and to Bogdan Malaescu for help on the evaluation of theoretical errors affecting the determination of $\alpha_S(M_Z^2)$. We are obliged to the DESY Summer Student Kieran Omahony for his work on the fit automation and the Gfitter web page. We thank the CKMfitter group for providing the best-effort predictions of the rare leptonic B decays used in the 2HDM analysis, and Paolo Gambino, Ulrich Haisch and Mikolaj Misiak for valuable discussions and exchanges regarding the constraints on the 2HDM parameters. Finally, we wish to thank Jérôme Charles, Stefan Schmitt and Stéphane T'Jampens for helpful discussions on statistical problems.

Appendix A: Standard Model formulae

This section gives the relevant formulae for the calculation of the electroweak observables used in the global electroweak fit. We discuss the scale evolution of the QED and QCD couplings and quark masses, and give expressions for the electroweak form factors and radiator functions.

A.1 Running QED coupling

The electroweak fit requires the knowledge of the electromagnetic coupling strength at the Z-mass scale to an accuracy of 1% or better. The evolution of $\alpha(s)$ versus the mass scale-squared s is conventionally parameterised by

$$\alpha(s) = \frac{\alpha(0)}{1 - \Delta\alpha(s)}, \tag{A.1}$$

following from an all-orders resummation of vacuum polarisation diagrams, sole contributors to the running α. Here $\alpha = \alpha(0) = 1/137.035999679(94)$ is the fine structure constant in the long-wavelength Thomson limit [140], and the term $\Delta\alpha(s)$ controls the evolution. It is conveniently decomposed into leptonic and hadronic contributions

$$\Delta\alpha(s) = \Delta\alpha_{\mathrm{lep}}(s) + \Delta\alpha_{\mathrm{had}}^{(5)}(s) + \Delta\alpha_{\mathrm{top}}(s), \tag{A.2}$$

where the hadronic term has been further separated into contributions from the five light quarks (with respect to M_Z) and the top quark. The leptonic term in (A.2) is known up to three loops in the $q^2 \gg m_\ell^2$ limit [141]. The dominant one-loop term at the Z-mass scale reads

$$\begin{aligned}\Delta\alpha_{\mathrm{lep}}^{(1\text{-loop})}\left(M_Z^2\right) &= \alpha \sum_{\ell=e,\mu,\tau} \left(-\frac{5}{9} + \frac{1}{3}\ln\frac{M_Z^2}{m_\ell^2} - 2\frac{m_\ell^2}{M_Z^2} + \mathcal{O}\left(\frac{m_\ell^4}{M_Z^4}\right)\right) \\ &\approx 314.19 \times 10^{-4}. \end{aligned} \tag{A.3}$$

Adding the sub-leading loops gives a total of $\Delta\alpha_{\mathrm{lep}}(s) = 314.97 \times 10^{-4}$, with negligible uncertainty.[45]

[45] While the two-loop leptonic contribution of 0.78×10^{-4} is significant (roughly one third of the uncertainty in the hadronic contribution), the third-order term, 0.01×10^{-4}, is very small.

The hadronic contribution for quarks with masses smaller than M_Z cannot be obtained from perturbative QCD alone because of the low-energy scale involved. Its computation relies on analyticity and unitarity to express the photon vacuum polarisation function as a dispersion integral involving the total cross section for e^+e^- annihilation to hadrons at all time-like energies above the two-pion threshold. In energy regions where perturbative QCD fails to locally predict the inclusive hadronic cross section, experimental data is used. The accuracy of the calculations has therefore followed the progress in the quality of the corresponding data. Recent calculations improved the precision by extending the use of perturbative QCD to energy regions of relatively low scales, benefiting from global quark–hadron duality. For the fits in this paper we use the most recent value, $\Delta\alpha^{(5)}_{\mathrm{had}}(M_Z^2) = (276.8 \pm 2.2) \times 10^{-4}$, from Ref. [66]. The error is dominated by systematic uncertainties in the experimental data used to calculate the dispersion integral. A small part of the error, 0.14×10^{-4}, is introduced by the uncertainty in $\alpha_S(s)$ (the authors of [66] used the value $\alpha_S(M_Z^2) = 0.1176 \pm 0.0020$ [142]). We include this dependence in the fits via the parameter rescaling mechanism implemented in Gfitter (cf. Sect. 3).

The small top-quark contribution at M_Z^2 up to second order in α_S reads [143–146]

$$\begin{aligned}\Delta\alpha_{\mathrm{top}}\big(M_Z^2\big) = {} & -\frac{4}{45}\frac{\alpha}{\pi}\frac{M_Z^2}{m_t^2}\Bigg\{1 + 5.062 a_S^{(5)}\big(\mu^2\big) \\ & + \left(28.220 + 9.702 \ln\frac{\mu^2}{m_t^2}\right)\big(a_S^{(5)}\big(\mu^2\big)\big)^2 \\ & + \frac{M_Z^2}{m_t^2}\Bigg[0.1071 + 0.8315 a_S^{(5)}\big(\mu^2\big) \\ & + \left(6.924 + 1.594 \ln\frac{\mu^2}{m_t^2}\right)\big(a_S^{(5)}\big(\mu^2\big)\big)^2\Bigg]\Bigg\}, \\ \approx {} & -0.7 \times 10^{-4}, \end{aligned} \tag{A.4}$$

where the short-hand notation $a_S = \alpha_S/\pi$ is used, and where $\alpha_S^{(5)}$ is the strong coupling constant for five active quark flavours, and μ is an arbitrary renormalisation scale, chosen to be $\mu = M_Z$ in the fit.

The uncertainty on $\alpha(M_Z^2)$ is dominated by the hadronic contribution $\Delta\alpha^{(5)}_{\mathrm{had}}(M_Z^2)$, which is a floating parameter of the fit constrained to its phenomenological value. The errors due to uncertainties in M_Z, m_t and α_S are properly propagated throughout the fit. Other uncertainties are neglected.

A.2 QCD renormalisation

Like in QED, the subtraction of logarithmic divergences in QCD is equivalent to renormalising the coupling strength ($\alpha_S \equiv g_s^2/4\pi$), the quark masses ($m_q$), etc., and the fields in the bare (superscript B) Lagrangian such as $\alpha_S^B = s^\varepsilon Z_{\alpha_S}\alpha_S$, $m_q^B = s^\varepsilon Z_m m_q$, etc. Here s is the renormalisation scale-squared, ε the dimensional regularisation parameter, and Z denotes a series of renormalisation constants obtained from the generating functional of the bare Green's function. Renormalisation at scale μ introduces a differential renormalisation group equation (RGE) for each renormalised quantity, governing its running. All formulae given below are for the modified minimal subtraction renormalisation scheme ($\overline{\mathrm{MS}}$) [147, 148].

A.2.1 The running strong coupling

The RGE for $\alpha_S(\mu^2)$ reads

$$\begin{aligned}\frac{d\alpha_S}{d\ln\mu^2} &= \beta(\alpha_S) \\ &= -\beta_0\alpha_S^2 - \beta_1\alpha_S^3 - \beta_2\alpha_S^4 - \beta_3\alpha_S^5 - \cdots, \end{aligned} \tag{A.5}$$

The perturbative expansion of the β-function is known up to four loops (see [149, 150] and references therein), with the coefficients

$$\beta_0 = \frac{1}{4\pi}\left[11 - \frac{2}{3}n_f\right], \tag{A.6}$$

$$\beta_1 = \frac{1}{(4\pi)^2}\left[102 - \frac{38}{3}n_f\right], \tag{A.7}$$

$$\beta_2 = \frac{1}{(4\pi)^3}\left[\frac{2857}{2} - \frac{5033}{18}n_f + \frac{325}{54}n_f^2\right], \tag{A.8}$$

$$\begin{aligned}\beta_3 = {} & \frac{1}{(4\pi)^4}\Bigg[\left(\frac{149753}{6} + 3564\zeta_3\right) \\ & - \left(\frac{1078361}{162} + \frac{6508}{27}\zeta_3\right)n_f \\ & + \left(\frac{50065}{162} + \frac{6472}{81}\zeta_3\right)n_f^2 + \frac{1093}{729}n_f^3\Bigg], \end{aligned} \tag{A.9}$$

where n_f is the number of active quark flavours with masses smaller than μ, and where $\zeta_3 \simeq 1.2020569$. Solving (A.5) for α_S introduces a constant of integration, $\Lambda^{(n_f)}$, with dimension of energy. The solution in the ultraviolet limit reads [151, 152]

$$\begin{aligned}\alpha_S\big(\mu^2\big) = {} & \frac{1}{\beta_0 L}\Bigg\{1 - \frac{\beta_1}{\beta_0^2}\frac{\ln L}{L} \\ & + \frac{1}{\beta_0^2 L^2}\left[\frac{\beta_1^2}{\beta_0^2}\big(\ln^2 L - \ln L - 1\big) + \frac{\beta_2}{\beta_0}\right] \\ & + \frac{1}{\beta_0^3 L^3}\Bigg[\frac{\beta_1^3}{\beta_0^3}\left(-\ln^3 L + \frac{5}{2}\ln^2 L + 2\ln L - \frac{1}{2}\right) \\ & - 3\frac{\beta_1\beta_2}{\beta_0^2}\ln L + \frac{\beta_3}{2\beta_0}\Bigg]\Bigg\}, \end{aligned} \tag{A.10}$$

where $L = 2\ln(\mu/\Lambda^{(n_f)}) \gg 1$.

As α_S evolves it passes across quark-flavour thresholds. Matching conditions at these thresholds connect $\alpha_S^{(n_f)}$ of the full theory with n_f flavours to the effective strong coupling constant $\alpha_S^{(n_f-1)}$, where the heaviest quark decouples. The coupling constant of the full theory is developed in a power series of the coupling constant of the effective theory with coefficients that depend on $x = 2\ln(\mu/\overline{m}_q)$ [151, 153–155]:

$$a_S^{(n_f)} = a_S^{(n_f-1)}\big[1 + C_1(x)\big(a_S^{(n_f-1)}\big) + C_2(x)\big(a_S^{(n_f-1)}\big)^2 + C_3(x)\big(a_S^{(n_f-1)}\big)^3\big], \tag{A.11}$$

with $a_S = \alpha_S/\pi$ (recalled), and

$$\begin{aligned} C_1(x) &= \frac{x}{6}, \\ C_2(x) &= c_{2,0} + \frac{19}{24}x + \frac{x^2}{36}, \\ C_3(x) &= c_{3,0} + \left(\frac{241}{54} + \frac{13}{4}c_{2,0} - \left(\frac{325}{1728} + \frac{c_{2,0}}{6}\right)n_f\right)x \\ &\quad + \frac{511}{576}x^2 + \frac{x^3}{216}. \end{aligned} \tag{A.12}$$

The integration coefficients $c_{i,0}$ computed in the $\overline{\text{MS}}$ scheme at the scale of the quark masses are

$$\begin{aligned} c_{2,0} &= -\frac{11}{72}, \\ c_{3,0} &= \frac{82043}{27648}\zeta_3 - \frac{575263}{124416} + \frac{2633}{31104}n_f. \end{aligned} \tag{A.13}$$

The solution of the RGE (A.5) at arbitrary scale requires α_S to be known at some reference scale, for which the Z pole is commonly chosen. Three evolution procedures are implemented in Gfitter, which lead to insignificant differences in the result. The first uses numerical integration of the RGE with a fourth-order Runge–Kutta method. The second (the one chosen for this paper) determines $\Lambda^{(5)}$ at M_Z by numerically evaluating the root of (A.10), and the values for $\Lambda^{(n_f\neq 5)}$ are obtained via the matching conditions. Both methods use $\alpha_S(M_Z^2)$ as floating parameter in the fit. In the third approach, $\Lambda^{(5)}$ is directly determined by the fit without explicit use of $\alpha_S(M_Z^2)$.

A.2.2 Running quark masses

The $\overline{\text{MS}}$ RGE for massive quarks is governed by the γ-function defined by

$$\begin{aligned} \frac{1}{\overline{m}_q}\frac{d\overline{m}_q}{\ln\mu^2} &= \gamma(\alpha_S) \\ &= -\gamma_0\alpha_S - \gamma_1\alpha_S^2 - \gamma_2\alpha_S^3 - \gamma_3\alpha_S^4 - \cdots. \end{aligned} \tag{A.14}$$

Its perturbative expansion has been computed to four loops (see [156] and references therein), which for the c- and b-quark flavours reads [156]

$$\begin{aligned} \overline{m}_c(\mu^2) &= \hat{m}_c a_S^{12/25}\big[1 + 1.0141a_S + 1.3892a_S^2 + 1.0905a_S^3\big], \\ \overline{m}_b(\mu^2) &= \hat{m}_b a_S^{12/23}\big[1 + 1.1755a_S + 1.5007a_S^2 + 0.1725a_S^3\big]. \end{aligned} \tag{A.15}$$

The scale dependence of $\overline{m}_q(\mu^2)$ is given by the scale dependence of $a_S = a_S(\mu^2)$. The renormalisation group independent mass parameters $\hat{m}_q$ are determined from the measured quark masses at fixed scales (cf. Table 4.1).

A.3 Electroweak form factors

The calculation of the electroweak form factors for lepton or quark flavours f, ρ_Z^f and κ_Z^f, absorbing the radiative corrections (cf. (4.4)–(4.6)), follows the ZFITTER procedure [6]. It includes two-loop electroweak corrections [6, 16, 45, 157–160]. We use the intermediate on-shell mass scheme [6], which lies between OMS-I and OMS-II. These latter two schemes are used to estimate the uncertainty arising from the renormalisation scheme ambiguity (see [59] for more information). The form factors in the intermediate scheme are given by

$$\rho_Z^f = \frac{1 + \delta\rho_{\text{rem}}^{f,[G]}}{1 + \delta\hat{\rho}^{(G)}(1 - \Delta\bar{r}_{\text{rem}}^{[G]})} + \delta\rho_{\text{rem}}^{f,G^2}, \tag{A.16}$$

$$\kappa_Z^f = \big(1 + \delta\kappa_{\text{rem}}^{f,[G]}\big)\left[1 - \frac{c_W^2}{s_W^2}\delta\hat{\rho}^{(G)}\big(1 - \Delta\bar{r}_{\text{rem}}^{[G]}\big)\right] + \delta\kappa_{\text{rem}}^{f,G^2}, \tag{A.17}$$

where the superscript (G) stands for the inclusion of all known terms, whereas $[G] = G + \alpha_S G$ includes the electroweak one-loop corrections together with all known orders in the strong coupling constant. These QCD corrections are taken from [161]. The parameter $\delta\hat{\rho}^{(G)}$ contains all known corrections to the Veltman parameter, defined by the ratio of effective couplings of neutral to charged currents [162, 163]. The subscript "rem" stands for "remainder". The correction $\Delta\bar{r}_{\text{rem}}^{[G]}$ is given by

$$\Delta\bar{r}_{\text{rem}}^{[G]} = \Delta\bar{r}_{\text{rem}}^{G} + \Delta r_{\text{rem}}^{G\alpha_S}, \tag{A.18}$$

with the one-loop remainder

$$\Delta\bar{r}_{\text{rem}}^{G} = \frac{\sqrt{2}G_F M_Z^2 s_W^2 c_W^2}{4\pi^2} \times \left\{-\frac{2}{3} + \frac{1}{s_W^2}\left(\frac{1}{6}N_C^f - \frac{1}{6} - 7c_W^2\right)\ln c_W^2\right.$$

$$+\frac{1}{s_W^2}\Bigg[\Delta\rho_W^F+\frac{11}{2}-\frac{5}{8}c_W^2\big(1+c_W^2\big)+\frac{9c_W^2}{4s_W^2}\ln c_W^2\Bigg]\Bigg\},\tag{A.19}$$

where $N_C^{f=q(\ell)}=3(1)$ is the colour factor, $s_W^2=\sin^2\theta_W$ and $c_W^2=\cos^2\theta_W$, and where $\Delta\rho_W^F$ is given by

$$\Delta\rho_W^F=\frac{1}{M_W^2}\big[\Sigma_{WW}^F(0)-\Sigma_{WW}^F\big(M_W^2\big)\big].\tag{A.20}$$

The terms $\Sigma_{WW}^F(0)$ and $\Sigma_{WW}^F(M_W^2)$ are the W boson self-energies discussed below.

For the purpose of illustration we give the formulae for the one-loop corrections of the electroweak form factors at the Z pole for vanishing external fermion masses [164]:

$$\delta\rho_{\mathrm{rem}}^{f,[G]}=\frac{\alpha}{4\pi s_W^2}\Bigg[\Sigma'_{ZZ}\big(M_Z^2\big)-\Delta\rho_Z^F-\frac{11}{2}+\frac{5}{8}c_W^2\big(1+c_W^2\big)-\frac{9}{4}\frac{c_W^2}{s_W^2}\ln c_W^2+2u_f\Bigg],\tag{A.21}$$

$$\delta\kappa_{\mathrm{rem}}^{f,[G]}=\frac{\alpha}{4\pi s_W^2}\Bigg[-\frac{c_W^2}{s_W^2}\Delta\rho^F+\Pi_{Z\gamma}^F\big(M_Z^2\big)+\frac{s_W^4}{c_W^2}Q_f^2V_{1Z}\big(M_Z^2\big)-u_f\Bigg],\tag{A.22}$$

where

$$u_f=\frac{1}{4c_W^2}\big[1-6|Q_f|s_W^2+12Q_f^2s_W^4\big]V_{1Z}\big(M_Z^2\big)+\Bigg[\frac{1}{2}-c_W^2-|Q_f|s_W^2\Bigg]V_{1W}\big(M_Z^2\big)+c_W^2V_{2W}\big(M_Z^2\big),$$

$$\Delta\rho_Z^F=\frac{1}{M_W^2}\big[\Sigma_{WW}^F(0)-\Sigma_{ZZ}^F\big(M_Z^2\big)\big].$$

The term $\Sigma_{ZZ}^F(M_W^2)$ is the Z boson self-energy. The vertex functions in the chiral limit are given by [16]

$$V_{1V}(s)=-\frac{7}{2}-2R_V-(3+2R_V)\ln(-\tilde{R}_V)+2(1+R_V)^2\big[\mathrm{Li}_2(1+\tilde{R}_V)-\mathrm{Li}_2(1)\big],\tag{A.23}$$

$$V_{2W}(s)=-\frac{1}{6}-2R_W-\Big(\frac{7}{6}+R_W\Big)\frac{L_{WW}(s)}{s}+2R_W(R_W+2)\mathcal{F}_3\big(s,M_W^2\big),\tag{A.24}$$

where Li_2 is the dilogarithm function, and where $\tilde{R}_V=R_V-i\gamma_V$, $\gamma_V=M_V\Gamma_V/s$, and $R_V=M_V^2/s$. The Z–γ mixing function in (A.22) is given by

$$\Pi_{Z\gamma}^F\big(M_Z^2\big)=2\sum_f N_C^f|Q_f|v_f\mathbf{I}_3\big(-s;m_f^2,m_f^2\big),\tag{A.25}$$

where $v_f=1-4Q_fs_W^2$, and where the index f runs over all fundamental fermions. The integrals $\mathcal{F}_3$ in (A.24) and $\mathbf{I}_3(Q^2;M_1^2,M_2^2)$ in (A.25) are given in Appendices C and D of Ref. [165].

For the two-loop corrections to the electroweak form factors, $\delta\rho_{\mathrm{rem}}^{f,G^2}$ and $\delta\kappa_{\mathrm{rem}}^{f,G^2}$ in (A.16) and (A.17), the interested reader is referred to the original literature [6, 16, 45, 157–160]. Because of missing two-loop corrections to the form factors ρ_Z^b and κ_Z^b occurring in $Z\to b\bar{b}$, an approximate expression is used, which includes the full one-loop correction and the known leading two-loop terms $\propto m_t^4$. Non-universal top contributions [6, 166, 167] must be taken into account in this channel due to a CKM factor close to 1 and the large mass difference of bottom and top quarks,

$$\tau_b=-2x_t\Bigg[1-\frac{\pi}{3}\alpha_s\big(m_t^2\big)+\frac{G_Fm_t^2}{8\pi^2\sqrt{2}}\tau^{(2)}\Big(\frac{m_t^2}{M_Z^2}\Big)\Bigg],\tag{A.26}$$

where the function $\tau^{(2)}(m_t^2/M_Z^2)$ is given in [166]. Since the first term in (A.26) represents one-loop corrections, it must be subtracted from the universal form factors to avoid double counting. Let ρ_b' and κ_b' be these corrected form factors (cf. Refs. [6, 166, 167] for the correction procedure), the form factors beyond one-loop are obtained by $\rho_b=\rho_b'(1+\tau_b)^2$ and $\kappa_b=\kappa_b'(1+\tau_b)^{-1}$.

A.3.1 Self-energies of W and Z boson

The W and Z boson self-energies $\sum_{WW}^F$ and $\sum_{ZZ}^F$ and on-shell derivative $\sum_{ZZ}^{\prime F}$ are the sums of bosonic and fermionic parts. The bosonic parts read [16, 168]

$$\frac{\sum_{WW}^{\mathrm{Bos},F}(0)}{M_W^2}=\frac{5c_W^2(1+c_W^2)}{8}-\frac{17}{4}+\frac{5}{8c_W^2}-\frac{r_W}{8}+\Big(\frac{9}{4}+\frac{3}{4c_W^2}-\frac{3}{s_W^2}\Big)\ln c_W^2+\frac{3r_W}{4(1-r_W)}\ln r_W,\tag{A.27}$$

$$\frac{\sum_{WW}^{\mathrm{Bos},F}(M_W^2)}{M_W^2}=-\frac{157}{9}+\frac{23}{12c_W^2}+\frac{1}{12c_W^4}-\frac{r_W}{2}+\frac{r_W^2}{12}+\frac{1}{c_W^2}\Big(-\frac{7}{2}+\frac{7}{12c_W^2}+\frac{1}{24c_W^4}\Big)\ln c_W^2+r_W\Big(-\frac{3}{4}+\frac{r_W}{4}-\frac{r_W^2}{24}\Big)\ln r_W+\Big(\frac{1}{2}-\frac{r_W}{6}+\frac{r_W^2}{24}\Big)\frac{L_{WH}(M_W^2)}{M_W^2}$$

$$+\left(-2c_W^2-\frac{17}{6}+\frac{2}{3c_W^2}+\frac{1}{24c_W^4}\right)\times\frac{L_{WZ}(M_W^2)}{M_W^2}, \tag{A.28}$$

$$\frac{\sum_{ZZ}^{\mathrm{Bos},F}(M_Z^2)}{M_W^2}=-8c_W^4-\frac{34c_W^2}{3}+\frac{35}{18}\left(1+\frac{1}{c_W^2}\right)-\frac{r_W}{2}+\frac{r_Z^2}{12c_W^2}+r_W\left(-\frac{3}{4}+\frac{r_Z}{4}-\frac{r_Z^2}{24}\right)\ln r_Z+\frac{5\ln c_W^2}{6c_W^2}+\left(\frac{1}{2}-\frac{r_Z}{6}+\frac{r_Z^2}{24}\right)\frac{L_{ZH}(M_Z^2)}{M_W^2}+\left(-2c_W^6-\frac{17}{6}c_W^4+\frac{2}{3}c_W^2+\frac{1}{24}\right)\times\frac{L_{WW}(M_Z^2)}{M_W^2}, \tag{A.29}$$

$$\sum_{ZZ}^{\prime\mathrm{Bos},F}(M_Z^2)=-4c_W^4+\frac{17c_W^2}{3}-\frac{23}{9}+\frac{5}{18c_W^2}-\frac{r_W}{2}+\frac{r_Wr_Z}{6}+r_W\left(-\frac{3}{4}+\frac{3r_Z}{8}-\frac{r_Z^2}{12}\right)\ln r_Z-\frac{1}{12c_W^2}\ln c_W^2+\frac{\ln r_Z}{2c_W^2}+\left(-c_W^6+\frac{7c_W^4}{6}-\frac{17c_W^2}{12}-\frac{1}{8}\right)\times\frac{L_{WW}(M_Z^2)}{M_W^2}+\left(\frac{1}{2}-\frac{5r_Z}{24}+\frac{r_Z^2}{12}+\frac{1}{2(r_Z-4)}\right)\times\frac{L_{ZH}(M_Z^2)}{M_W{}^2}, \tag{A.30}$$

where the shorthand notation $r_W=M_H^2/M_W^2$ and $r_Z=M_H^2/M_Z^2$ has been used. The function $L_{V_1V_2}(s)\equiv L(-s;M_{V_1}^2,M_{V_2}^2)$ is defined in (2.14) of Ref. [169].

The fermionic parts read [16, 168]

$$\frac{\sum_{WW}^{\mathrm{Fer},F}(M_W^2)}{M_W^2}=\sum_{f=f_u,f_d}N_C^f\left[-\frac{2s}{M_W^2}\mathbf{I}_3(\cdots)+\frac{m_{f_u}^2}{M_W^2}\mathbf{I}_1(\cdots)+\frac{m_{f_d}^2}{M_W^2}\mathbf{I}_1\big(-s;m_{f_d}^2,m_{f_u}^2\big)\right], \tag{A.31}$$

$$\frac{\sum_{ZZ}^{\mathrm{Fer},F}(M_Z^2)}{M_W^2}=\frac{1}{2c_W^2}\sum_f N_C^f\left[-\frac{s}{M_Z^2}\big(1+v_f^2\big)\times\mathbf{I}_3\big(-s;m_f^2,m_f^2\big)+\frac{m_f^2}{M_Z^2}\mathbf{I}_0\big(-s;m_f^2,m_f^2\big)\right], \tag{A.32}$$

$$\sum_{ZZ}^{\prime\mathrm{Fer},F}\big(M_Z^2\big)=-\sum_f N_C^f\left\{\frac{r_f}{2}\big[1-r_fM_W^2\mathcal{F}\times\big(-M_Z^2,m_f^2,m_f^2\big)\big]+\frac{1}{6c_W^2}\big(1+v_f^2\big)\left[\frac{1}{2}\ln\big(r_fc_W^2\big)+r_fc_W^2+\left(-\frac{1}{4c_W^2}+\frac{r_f}{2}-r_f^2c_W^2\right)\times M_W^2\mathcal{F}\big(-M_Z^2,m_f^2,m_f^2\big)\right]\right\}, \tag{A.33}$$

with $r_f=m_f^2/M_W^2$ and $v_f=1-4Q_fs_W^2$ (recalled from above), and where $(\cdots)$ in (A.31) stands for $(-s;m_{f_u}^2,m_{f_d}^2)$. The sums are taken over all fundamental up-type and down-type fermions of all $SU(2)\otimes U(1)$ doublets with masses m_{f_u} and m_{f_d}, respectively. The integrals $\mathbf{I}_n(Q^2;M_1^2,M_2^2)$ and $\mathcal{F}$ are given in Appendix D of Ref. [165].

A.4 Radiator functions

The radiator functions $R_V^q(s)$ and $R_A^q(s)$ absorb the final state QED and QCD corrections to the vector and axial-vector currents in hadronic Z decays. They also contain mixed QED $\otimes$ QCD corrections and finite quark-mass corrections expressed in terms of running masses. The following formulae are taken from [45]. They have been updated to take into account results from the recent 3NLO calculation of the massless QCD Adler function [17] (represented by the coefficient C_{04}). We have

$$R_V^q(s)=1+\frac{3}{4}Q_q^2\frac{\alpha(s)}{\pi}+a_S(s)-\frac{1}{4}Q_q^2\frac{\alpha(s)}{\pi}a_S(s)+\left[C_{02}+C_2^t\left(\frac{s}{m_t^2}\right)\right]a_S^2(s)+C_{03}a_S^3(s)+C_{04}a_S^4(s)+\delta_{C05}a_S^5(s)+\frac{\overline{m}_c^2(s)+\overline{m}_b^2(s)}{s}C_{23}a_S^3(s)+\frac{\overline{m}_q^2(s)}{s}\big[C_{21}^Va_S(s)+C_{22}^Va_S^2(s)+C_{23}^Va_S^3(s)\big]+\frac{\overline{m}_c^4(s)}{s^2}\left[C_{42}-\ln\frac{\overline{m}_c^2(s)}{s}\right]a_S^2(s)$$

$$
\begin{aligned}
&+\frac{\overline{m}_b^4(s)}{s^2}\left[C_{42}-\ln\frac{\overline{m}_b^2(s)}{s}\right]a_S^2(s)\\
&+\frac{\overline{m}_q^4(s)}{s^2}\left\{C_{41}^V a_S(s)\right.\\
&\left.+\left[C_{42}^V+C_{42}^{V,L}\ln\frac{\overline{m}_q^2(s)}{s}\right]a_S^2(s)\right\}\\
&+12\frac{\overline{m}_q'^4(s)}{s^2}a_S^2(s)-\frac{\overline{m}_q^6(s)}{s^3}\\
&\times\left\{8+\frac{16}{27}\left[155+6\ln\frac{\overline{m}_q^2(s)}{s}\right]a_S(s)\right\},
\end{aligned}
\tag{A.34}
$$

$$
\begin{aligned}
R_A^q(s)&=1+\frac{3}{4}Q_q^2\frac{\alpha(s)}{\pi}+a_S(s)-\frac{1}{4}Q_q^2\frac{\alpha(s)}{\pi}a_S(s)\\
&+\left[C_{02}+C_2^t\left(\frac{s}{m_t^2}\right)-\left(2I_3^q\right)\mathcal{I}^{(2)}\left(\frac{s}{m_t^2}\right)\right]a_S^2(s)\\
&+\left[C_{03}-\left(2I_3^q\right)\mathcal{I}^{(3)}\left(\frac{s}{m_t^2}\right)\right]a_S^3(s)\\
&+\left[C_{04}-\left(2I_3^q\right)\delta_{\mathcal{I}^{(4)}}\right]a_S^4(s)\\
&+\delta_{C05}a_S^5(s)+\frac{\overline{m}_c^2(s)+\overline{m}_b^2(s)}{s}C_{23}a_S^3(s)\\
&+\frac{\overline{m}_q^2(s)}{s}\left[C_{20}^A+C_{21}^A a_S(s)+C_{22}^A a_S^2(s)\right.\\
&\left.+6\left(3+\ln\frac{m_t^2}{s}\right)a_S^2(s)+C_{23}^A a_S^3(s)\right]\\
&-10\frac{\overline{m}_q^2(s)}{m_t^2}\left[\frac{8}{81}+\frac{1}{54}\ln\frac{m_t^2}{s}\right]a_S^2(s)\\
&+\frac{\overline{m}_c^4(s)}{s^2}\left[C_{42}-\ln\frac{\overline{m}_c^2(s)}{s}\right]a_S^2(s)\\
&+\frac{\overline{m}_b^4(s)}{s^2}\left[C_{42}-\ln\frac{\overline{m}_b^2(s)}{s}\right]a_S^2(s)\\
&+\frac{\overline{m}_q^4(s)}{s^2}\left\{C_{40}^A+C_{41}^A a_S(s)\right.\\
&\left.+\left[C_{42}^A+C_{42}^{A,L}\ln\frac{\overline{m}_q^2(s)}{s}\right]a_S^2(s)\right\}\\
&-12\frac{\overline{m}_q'^4(s)}{s^2}a_S^2(s),
\end{aligned}
\tag{A.35}
$$

where the finite quark-mass corrections are retained for charm and bottom quarks only, i.e., all lighter quarks are taken to be massless. This restricts the validity of the above formula to energies well above the strange-pair and below the top-pair production thresholds, which is sufficient for our use. The mass $\overline{m}_q'$ denotes the other quark mass, i.e., it is $\overline{m}_b$ if $q=c$ and $\overline{m}_c$ if $q=b$. The running of the quark masses is computed in the $\overline{\text{MS}}$ scheme according to (A.15). The two parameters $\delta_{\mathcal{I}^{(4)}}$ and $\delta_{C_{05}}$ represent the next unknown coefficients in the perturbative expansion. They are treated as theoretical errors within the *R*fit scheme and vary within the bounds obtained when assuming a geometric growth of the perturbative coefficients with the perturbative order, i.e., for a coefficient H one has $\delta_{H_n}=(H_{n-1}/H_{n-2})\cdot H_{n-1}$.

The expressions for the fixed-order perturbative coefficients $C_{ij}^{(V/A)}$ in (A.34) and (A.35) are given below.

Massless non-singlet corrections [17, 170–173]:

$$
C_{02}=\frac{365}{24}-11\zeta(3)+\left(-\frac{11}{12}+\frac{2}{3}\zeta(3)\right)n_f,
\tag{A.36}
$$

$$
\begin{aligned}
C_{03}&=\frac{87029}{288}-\frac{121}{8}\zeta(2)-\frac{1103}{4}\zeta(3)+\frac{275}{6}\zeta(5)\\
&+\left(-\frac{7847}{216}+\frac{11}{6}\zeta(2)+\frac{262}{9}\zeta(3)-\frac{25}{9}\zeta(5)\right)n_f\\
&+\left(\frac{151}{162}-\frac{1}{18}\zeta(2)-\frac{19}{27}\zeta(3)\right)n_f^2,
\end{aligned}
\tag{A.37}
$$

$$
C_{04}=-156.61+18.77n_f-0.7974n_f^2+0.0215n_f^3,
\tag{A.38}
$$

which for $n_f=5$ take the values $C_{02}=1.40923$, $C_{03}=-12.7671$ and $C_{04}=-80.0075$, exhibiting satisfactory convergence given that $\alpha_S(M_Z^2)/\pi\simeq 0.04$.

Quadratic massive corrections [174]:

$$
C_{23}=-80+60\zeta(3)+\left[\frac{32}{9}-\frac{8}{3}\zeta(3)\right]n_f,
\tag{A.39}
$$

$$
C_{21}^V=12,
\tag{A.40}
$$

$$
C_{22}^V=\frac{253}{2}-\frac{13}{3}n_f,
\tag{A.41}
$$

$$
\begin{aligned}
C_{23}^V&=2522-\frac{855}{2}\zeta(2)+\frac{310}{3}\zeta(3)-\frac{5225}{6}\zeta(5)\\
&+\left[-\frac{4942}{27}+34\zeta(2)-\frac{394}{27}\zeta(3)+\frac{1045}{27}\zeta(5)\right]n_f\\
&+\left[\frac{125}{54}-\frac{2}{3}\zeta(2)\right]n_f^2,
\end{aligned}
\tag{A.42}
$$

$$
C_{20}^A=-6,
\tag{A.43}
$$

$$
C_{21}^A=-22,
\tag{A.44}
$$

$$
\begin{aligned}
C_{22}^A&=-\frac{8221}{24}+57\zeta(2)+117\zeta(3)\\
&+\left[\frac{151}{12}-2\zeta(2)-4\zeta(3)\right]n_f,
\end{aligned}
\tag{A.45}
$$

$$
C_{23}^A=-\frac{4544045}{864}+1340\zeta(2)+\frac{118915}{36}\zeta(3)-127\zeta(5)
$$

$$+\left[\frac{71621}{162}-\frac{209}{2}\zeta(2)\right.$$
$$\left.-216\zeta(3)+5\zeta(4)+55\zeta(5)\right]n_f$$
$$+\left[-\frac{13171}{1944}+\frac{16}{9}\zeta(2)+\frac{26}{9}\zeta(3)\right]n_f^2. \quad \text{(A.46)}$$

Quartic massive corrections [174]:

$$C_{42}=\frac{13}{3}-4\zeta(3), \quad \text{(A.47)}$$
$$C_{40}^V=-6, \quad \text{(A.48)}$$
$$C_{41}^V=-22, \quad \text{(A.49)}$$
$$C_{42}^V=-\frac{3029}{12}+162\zeta(2)+112\zeta(3)$$
$$+\left[\frac{143}{18}-4\zeta(2)-\frac{8}{3}\zeta(3)\right]n_f, \quad \text{(A.50)}$$
$$C_{42}^{V,L}=-\frac{11}{2}+\frac{1}{3}n_f, \quad \text{(A.51)}$$
$$C_{40}^A=6, \quad \text{(A.52)}$$
$$C_{41}^A=10, \quad \text{(A.53)}$$
$$C_{42}^A=\frac{3389}{12}-162\zeta(2)-220\zeta(3)$$
$$+\left[-\frac{41}{6}+4\zeta(2)+\frac{16}{3}\zeta(3)\right]n_f, \quad \text{(A.54)}$$
$$C_{42}^{A,L}=\frac{77}{2}-\frac{7}{3}n_f. \quad \text{(A.55)}$$

Power suppressed top-mass correction [174]:

$$C_2^t(x)=x\left(\frac{44}{675}-\frac{2}{135}\ln x\right). \quad \text{(A.56)}$$

Singlet axial-vector corrections [174]:

$$\mathcal{I}^{(2)}(x)=-\frac{37}{12}+\ln x+\frac{7}{81}x+0.0132x^2, \quad \text{(A.57)}$$
$$\mathcal{I}^{(3)}(x)=-\frac{5075}{216}+\frac{23}{6}\zeta(2)+\zeta(3)$$
$$+\frac{67}{18}\ln x+\frac{23}{12}\ln^2 x. \quad \text{(A.58)}$$

Singlet vector correction [174]:

$$R_V^h(s)=\left(\sum_f v_f\right)^2(-0.41317)a_S^3(s). \quad \text{(A.59)}$$

References

1. G. Alexander et al. (LEP Collaborations: ALEPH, DELPHI, L3 and OPAL), Phys. Lett. B **276**, 247 (1992)
2. S. Abachi et al. (D0 Collaboration), Phys. Rev. Lett. **74**, 2632 (1995). hep-ex/9503003
3. F. Abe et al. (CDF Collaboration), Phys. Rev. Lett. **74**, 2626 (1995). hep-ex/9503002
4. LEP Electroweak Working Group, in *27th International Conference on High-Energy Physics, ICHEP 94*, Glasgow, Scotland, UK, 20–27 July 1994, CERN-PPE-94-187
5. A.B. Arbuzov et al., Comput. Phys. Commun. **174**, 728 (2006). hep-ph/0507146
6. D.Y. Bardin et al., Comput. Phys. Commun. **133**, 229 (2001). hep-ph/9908433
7. G. Montagna, O. Nicrosini, F. Piccinini, G. Passarino, Comput. Phys. Commun. **117**, 278 (1999). hep-ph/9804211
8. J. Erler, Phys. Rev. D **63**, 071301 (2001). hep-ph/0010153
9. http://cern.ch/Gfitter
10. R. Brun, F. Rademakers, Nucl. Instrum. Methods A **389**, 81 (1997)
11. M. Awramik, M. Czakon, A. Freitas, G. Weiglein, Phys. Rev. D **69**, 053006 (2004). hep-ph/0311148
12. M. Awramik, M. Czakon, A. Freitas, G. Weiglein, Phys. Rev. Lett. **93**, 201805 (2004). hep-ph/0407317
13. M. Awramik, M. Czakon, A. Freitas, J. High Energy Phys. **11**, 048 (2006). hep-ph/0608099
14. R. Boughezal, J.B. Tausk, J.J. van der Bij, Nucl. Phys. B **713**, 278 (2005). hep-ph/0410216
15. R. Boughezal, J.B. Tausk, J.J. van der Bij, Nucl. Phys. B **725**, 3 (2005). hep-ph/0504092
16. D.Y. Bardin et al. (Electroweak working group), hep-ph/9709229, Prepared for Workshop Group on Precision Calculations for the Z Resonance (2nd meeting held March 31, 3rd meeting held June 13), Geneva, Switzerland, 14 January 1994, CERN-YELLOW-95-03A
17. P.A. Baikov, K.G. Chetyrkin, J.H. Kühn, arXiv:0801.1821, SFB-CPP-08-04, TTP08-01
18. M. Davier, S. Descotes-Genon, A. Hoecker, B. Malaescu, Z. Zhang, arXiv:0803.0979, CERN-OPEN-2008-006
19. ATLAS Collaboration, Physics TDR, vol. II, CERN-LHCC-99-15, 1999
20. CMS Collaboration, Physics TDR, vol. II, CERN-LHCC-06-21, 2006
21. A. Djouadi et al., arXiv:0709.1893
22. J. Charles et al. (CKMfitter Group), Eur. Phys. J. C **41**, 1 (2005). hep-ph/0406184
23. A. Hoecker, H. Lacker, S. Laplace, F. Le Diberder, Eur. Phys. J. C **21**, 225 (2001). hep-ph/0104062
24. J. Charles, in *School of Statistics, SOS 2008*, Strasbourg, France, June 30–July 4 2008
25. L. Demortier, CDF-MEMO-STATISTICS-PUBLIC-8662, June 2007
26. S.S. Wilks, Ann. Math. Stat. **9**, 60 (1938)
27. J. Neyman, Philos. Trans. R. Soc. Lond. Ser. A **226**, 333 (1937). Reprinted in A Selection of Early Statistical Papers on J. Neyman, U. of California Press, Berkeley, 1967
28. G.J. Feldman, R.D. Cousins, Phys. Rev. D **57**, 3873 (1998). physics/9711021
29. J. Conrad, O. Botner, A. Hallgren, C. Perez de los Heros, Phys. Rev. D **67**, 012002 (2003). hep-ex/0202013
30. G. Punzi, physics/0511202
31. R.L. Berger, D.D. Boos, J. Am. Stat. Assoc. **89**, 1012 (1994)
32. M.J. Silvapulle, J. Am. Stat. Assoc. **91**, 1690 (1996). Erratum: **92**, 801 (1997)
33. F. James, M. Roos, Comput. Phys. Commun. **10**, 343 (1975)
34. N. Reid, Prepared for PHYSTAT 2003: Statistical Problems in Particle Physics, Astrophysics, and Cosmology, Menlo Park, CA, 8–11 September 2003, PHYSTAT-2003-THAT001
35. W.A. Rolke, A.M. Lopez, J. Conrad, Nucl. Instrum. Methods A **551**, 493 (2005). physics/0403059

36. K. Cranmer, physics/0511028
37. The Gfitter code is available at the CERN CVS repository. Contact the authors for a copy
38. A. Hoecker et al., physics/0703039, CERN-OPEN-2007-007
39. LEP Electroweak Working Group (LEP EWWG), Status of March 2008. http://lepewwg.web.cern.ch/LEPEWWG/
40. M. Goodman's, Neutrino-Oscillation-Industry web page. http://neutrinooscillation.org/
41. M. Bona et al. (UTfit Collaboration), J. High Energy Phys. **07**, 028 (2005). hep-ph/0501199
42. NASA's Lambda archive. http://lambda.gsfc.nasa.gov/
43. R. Lafaye, T. Plehn, D. Zerwas, hep-ph/0404282, Contribution to LHC-LC Study Group, G. Weiglein et al., CERN-TH-2003-313
44. P. Bechtle, K. Desch, P. Wienemann, Comput. Phys. Commun. **174**, 47 (2006). hep-ph/0412012
45. D.Y. Bardin, G. Passarino (Clarendon, Oxford, 1999)
46. The ALEPH, DELPHI, L3, OPAL, SLD Collaborations, the LEP Electroweak Working Group, the SLD Electroweak and Heavy Flavour Working Groups, Phys. Rep. **427**, 257 (2006). hep-ex/0509008
47. J. Erler, P. Langacker, Phys. Lett. B **667**, 1 (2008). Review article in Particle Data Group, Review of Particle Physics 2008
48. G. Passarino, M.J.G. Veltman, Nucl. Phys. B **160**, 151 (1979)
49. A. Sirlin, Phys. Rev. D **22**, 971 (1980)
50. K.I. Aoki, Z. Hioki, M. Konuma, R. Kawabe, T. Muta, Prog. Theor. Phys. Suppl. **73**, 1 (1982)
51. K.G. Chetyrkin, M. Faisst, J.H. Kühn, P. Maierhofer, C. Sturm, Phys. Rev. Lett. **97**, 102003 (2006). hep-ph/0605201
52. Y. Schroder, M. Steinhauser, Phys. Lett. B **622**, 124 (2005). hep-ph/0504055
53. R. Boughezal, M. Czakon, Nucl. Phys. B **755**, 221 (2006). hep-ph/0606232
54. M. Awramik, M. Czakon, A. Freitas, B.A. Kniehl, 0811.1364
55. A. Czarnecki, J.H. Kühn, Phys. Rev. Lett. **77**, 3955 (1996). hep-ph/9608366
56. R. Harlander, T. Seidensticker, M. Steinhauser, Phys. Lett. B **426**, 125 (1998). hep-ph/9712228
57. D.Y. Bardin, S. Riemann, T. Riemann, Z. Phys. C **32**, 121 (1986)
58. B.A. Kniehl, F. Madricardo, M. Steinhauser, Phys. Rev. D **62**, 073010 (2000). hep-ph/0005060
59. M. Goebel, Diploma thesis, University Hamburg, 2008
60. P. Skands, D. Wicke, Eur. Phys. J. C **52**, 133 (2007). hep-ph/0703081
61. D. Wicke, P.Z. Skands, 0807.3248
62. A.H. Hoang, A. Jain, I. Scimemi, I.W. Stewart, 0803.4214
63. A.H. Hoang, I.W. Stewart, 0808.0222
64. C. Amsler et al. (Particle Data Group), Phys. Lett. B **667**, 1 (2008)
65. Tevatron Electroweak Working Group, and others, 0808.1089, FERMILAB-TM-2413-E
66. K. Hagiwara, A.D. Martin, D. Nomura, T. Teubner, Phys. Lett. B **649**, 173 (2007). hep-ph/0611102
67. A. Hoecker, W. Marciano, Phys. Lett. B **667**, 1 (2008). Review article in Particle Data Group, Review of Particle Physics 2008
68. J. Alcaraz et al. (ALEPH Collaboration), hep-ex/0612034
69. CDF, and others, 0808.0147, FERMILAB-TM-2415
70. V.M. Abazov et al. (CDF Collaboration), Phys. Rev. D **70**, 092008 (2004). hep-ex/0311039
71. R. Barate et al. (The ALEPH, DELPHI, L3 and OPAL Collaborations, and LEP Working Group for Higgs Boson Searches), Phys. Lett. B **565**, 61 (2003). hep-ex/0306033
72. The TEVNPH Working Group for the CDF and D0 Collaborations, 0804.3423, FERMILAB-PUB-08-069-E
73. G. Bernardi et al. (Tevatron New Phenomena Higgs Working Group), 0808.0534, FERMILAB-PUB-08-270-E
74. T. Read, in *1st Workshop on Confidence Limits*, CERN, Geneva, Switzerland, 17–18 January 2000, CERN-2000-005
75. T. Junk, Nucl. Instrum. Methods A **434**, 435 (1999). hep-ex/9902006
76. A.L. Read, J. Phys. G **28**, 2693 (2002)
77. C.S. Wood et al., Science **275**, 1759 (1997)
78. J. Guena, M. Lintz, M.A. Bouchiat, physics/0412017
79. N.H. Edwards, S.J. Phipp, P.E.G. Baird, S. Nakayama, Phys. Rev. Lett. **74**, 2654 (1995)
80. P.A. Vetter, D.M. Meekhof, P.K. Majumder, S.K. Lamoreaux, E.N. Fortson, Phys. Rev. Lett. **74**, 2658 (1995)
81. P.L. Anthony et al. (SLAC E158), Phys. Rev. Lett. **95**, 081601 (2005). hep-ex/0504049
82. G.P. Zeller et al. (NuTeV Collaboration), Phys. Rev. Lett. **88**, 091802 (2002). hep-ex/0110059
83. K.J. Eskola, H. Paukkunen, J. High Energy Phys. **06**, 008 (2006). hep-ph/0603155
84. S. Davidson, S. Forte, P. Gambino, N. Rius, A. Strumia, J. High Energy Phys. **02**, 037 (2002). hep-ph/0112302
85. K.S. McFarland, S.-O. Moch, in *Proceedings of Mini-Workshop on Electroweak Precision Data and the Higgs Mass*, Zeuthen, Germany, 28 February–1 March, 2003. hep-ph/0306052
86. M. Beneke, M. Jamin, 0806.3156
87. K. Maltman, T. Yavin, 0807.0650
88. M. Davier, A. Hoecker, Phys. Lett. B **435**, 427 (1998). hep-ph/9805470
89. H. Burkhardt, B. Pietrzyk, Phys. Rev. D **72**, 057501 (2005). hep-ph/0506323
90. G. Abbiendi et al. (OPAL Collaboration), Eur. Phys. J. C **45**, 1 (2006). hep-ex/0505072
91. M. Acciarri et al. (L3 Collaboration), Phys. Lett. B **476**, 40 (2000). hep-ex/0002035
92. P. Achard et al. (L3 Collaboration), Phys. Lett. B **623**, 26 (2005). hep-ex/0507078
93. G. Abbiendi et al. (OPAL Collaboration), Eur. Phys. J. C **33**, 173 (2004). hep-ex/0309053
94. J. Alcaraz et al. (The ALEPH, DELPHI, L3, OPAL Collaborations, and the LEP Electroweak Working Group), 0712.0929, CERN-PH-EP-2007-039
95. S. Haywood et al., in *CERN Workshop on Standard Model Physics (and more) at the LHC (Final Plenary Meeting)*, Geneva, Switzerland, 14–15 October 1999, CERN-TH-2000-102. hep-ph/0003275
96. I. Borjanovic et al., Eur. Phys. J. C **39**(2), 63 (2005). hep-ex/0403021
97. V. Buge et al., J. Phys. G **34**, N193 (2007)
98. N. Besson, M. Boonekamp, E. Klinkby, T. Petersen, S. Mehlhase, 0805.2093
99. A.H. Hoang et al., Eur. Phys. J. Direct C **2**, 1 (2000). hep-ph/0001286
100. K.G. Chetyrkin, M. Steinhauser, Nucl. Phys. B **573**, 617 (2000). hep-ph/9911434
101. R. Hawkings, K. Mönig, Eur. Phys. J. Direct C **1**, 8 (1999). hep-ex/9910022
102. M. Winter, LC-PHSM-2001-016
103. F. Jegerlehner, in *2nd ECFA/DESY Study 1998-2001*, 1851, DESY-01-029. hep-ph/0105283
104. H.E. Haber, G.L. Kane, T. Sterling, Nucl. Phys. B **161**, 493 (1979)
105. H.E. Haber, D. O'Neil, Phys. Rev. D **74**, 015018 (2006). hep-ph/0602242
106. S. Davidson, H.E. Haber, Phys. Rev. D **72**, 035004 (2005). hep-ph/0504050
107. J.M. Cline, P.-A. Lemieux, Phys. Rev. D **55**, 3873 (1997). hep-ph/9609240
108. J.F. Gunion, H.E. Haber, G.L. Kane, S. Dawson, *The Higgs Hunter's Guide* (Perseus, Cambridge, 1990). SCIPP-89/13, UCD-89-4, BNL-41644

109. J.F. Gunion, H.E. Haber, G.L. Kane, S. Dawson, hep-ph/9302272
110. L.F. Abbott, P. Sikivie, M.B. Wise, Phys. Rev. D **21**, 1393 (1980)
111. LEP Higgs Working Group for Higgs boson searches, hep-ex/0107031
112. L. Michel, Proc. Phys. Soc. A **63**, 514 (1950)
113. W. Fletschwe, H.-J. Gerber, Phys. Lett. B **667**, 1 (2008). Review article in Particle Data Group, Review of Particle Physics 2008
114. A. Stahl, Phys. Lett. B **667**, 1 (2008). Review article in Particle Data Group, Review of Particle Physics 2008
115. H.E. Haber, H.E. Logan, Phys. Rev. D **62**, 015011 (2000). hep-ph/9909335
116. M. Misiak et al., Phys. Rev. Lett. **98**, 022002 (2007). hep-ph/0609232
117. E. Barberio et al. (Heavy Flavor Averaging Group), 0808.1297
118. P. Gambino, M. Misiak, Nucl. Phys. B **611**, 338 (2001). hep-ph/0104034
119. P. Gambino, M. Misiak, private communication
120. A. Gray et al. (HPQCD). Phys. Rev. Lett. **95**, 212001 (2005). hep-lat/0507015
121. J. Charles et al. (CKMfitter Group), Updated results for ICHEP 2008 conference available at http://ckmfitter.in2p3.fr
122. W.-S. Hou, Phys. Rev. D **48**, 2342 (1993)
123. B. Aubert et al. (BABAR Collaboration), Phys. Rev. D **77**, 011107 (2008). 0708.2260
124. B. Aubert et al. (BABAR Collaboration), Phys. Rev. D **76**, 052002 (2007). 0705.1820
125. P. Chang, Rare decays and new physics, in *34th International Conference on High Energy Physics (ICHEP 2008)*, Philadelphia, USA, 29 Jully–5 August 2008
126. M. Mazur, *B* decays with tau leptons in the final state, in *10th International Workshop on Tau Lepton Physics (Tau 2008)*, Novosibirsk, Russia, 22–25 September 2008
127. B. Aubert et al. (BABAR Collaboration), 0807.4187
128. M. Antonelli et al. (FlaviaNet Working Group on Kaon Decays), 0801.1817, FERMILAB-PUB-08-101-T
129. E. Blucher, W. Marciano, Phys. Lett. B **667**, 1 (2008). Review article in Particle Data Group, Review of Particle Physics 2008
130. J.F. Kamenik, F. Mescia, Phys. Rev. D **78**, 014003 (2008). 0802.3790
131. B. Aubert et al. (BABAR Collaboration), Phys. Rev. Lett. **100**, 021801 (2008). 0709.1698
132. A.G. Akeroyd et al. (SuperKEKB Physics Working Group), hep-ex/0406071
133. S. Hashimoto et al. (eds.), KEK-REPORT-2004-4
134. Super KEKB Project, Super KEKB Home Page http://superb.kek.jp/
135. M. Bona et al., 0709.0451
136. M. Flechl, 0710.1761, and references therein
137. P.W. Higgs, Phys. Rev. Lett. **13**, 508 (1964)
138. F. Englert, R. Brout, Phys. Rev. Lett. **13**, 321 (1964)
139. J.R. Ellis, G.L. Fogli, E. Lisi, Phys. Lett. B **343**, 282 (1995)
140. P.J. Mohr, B.N. Taylor, D.B. Newell, Rev. Mod. Phys. **80**, 633 (2008). 0801.0028
141. M. Steinhauser, Phys. Lett. B **429**, 158 (1998). hep-ph/9803313
142. D. Nomura, T. Teubner, Private communication, 2007
143. J.H. Kühn, M. Steinhauser, Phys. Lett. B **437**, 425 (1998). hep-ph/9802241
144. K.G. Chetyrkin, J.H. Kühn, M. Steinhauser, Phys. Lett. B **371**, 93 (1996). hep-ph/9511430
145. K.G. Chetyrkin, J.H. Kühn, M. Steinhauser, Nucl. Phys. B **482**, 213 (1996). hep-ph/9606230
146. K.G. Chetyrkin, J.H. Kühn, M. Steinhauser, Nucl. Phys. B **505**, 40 (1997). hep-ph/9705254
147. G. t'Hooft, M. Veltman, Nucl. Phys. B **44**, 189 (1972)
148. W.A. Bardeen, A.J. Buras, D.W. Duke, T. Muta, Phys. Rev. D **18**, 3998 (1978)
149. T. van Ritbergen, J.A.M. Vermaseren, S.A. Larin, Phys. Lett. B **400**, 379 (1997). hep-ph/9701390
150. M. Czakon, Nucl. Phys. B **710**, 485 (2005). hep-ph/0411261
151. K.G. Chetyrkin, B.A. Kniehl, M. Steinhauser, Phys. Rev. Lett. **79**, 2184 (1997). hep-ph/9706430
152. G.M. Prosperi, M. Raciti, C. Simolo, Prog. Part. Nucl. Phys. **58**, 387 (2007)
153. W. Bernreuther, W. Wetzel, Nucl. Phys. B **197**, 228 (1982). Erratum: Nucl. Phys. B **513**, 758 (1998)
154. W. Wetzel, Nucl. Phys. B **196**, 259 (1982)
155. G. Rodrigo, A. Pich, A. Santamaria, Phys. Lett. B **424**, 367 (1998). hep-ph/9707474
156. J.A.M. Vermaseren, S.A. Larin, T. van Ritbergen, Phys. Lett. B **405**, 327 (1997). hep-ph/9703284
157. G. Degrassi, S. Fanchiotti, F. Feruglio, B.P. Gambino, A. Vicini, Phys. Lett. B **350**, 75 (1995). hep-ph/9412380
158. G. Degrassi, F. Feruglio, A. Vicini, S. Fanchiotti, P. Gambino, hep-ph/9507286
159. G. Degrassi, P. Gambino, A. Vicini, Phys. Lett. B **383**, 219 (1996). hep-ph/9603374
160. G. Degrassi, P. Gambino, Nucl. Phys. B **567**, 3 (2000). hep-ph/9905472
161. B.A. Kniehl, Nucl. Phys. B **347**, 86 (1990)
162. D.A. Ross, M.J.G. Veltman, Nucl. Phys. B **95**, 135 (1975)
163. M.J.G. Veltman, Nucl. Phys. B **123**, 89 (1977)
164. A.A. Akhundov, D.Y. Bardin, T. Riemann, Nucl. Phys. B **276**, 1 (1986)
165. D.Y. Bardin et al., Z. Phys. C **44**, 493 (1989)
166. R. Barbieri, M. Beccaria, P. Ciafaloni, G. Curci, A. Vicere, Nucl. Phys. B **409**, 105 (1993)
167. J. Fleischer, O.V. Tarasov, F. Jegerlehner, Phys. Lett. B **319**, 249 (1993)
168. D.Y. Bardin, P.K. Khristova, O.M. Fedorenko, Nucl. Phys. B **197**, 1 (1982)
169. D.Y. Bardin, P.K. Khristova, O.M. Fedorenko, Nucl. Phys. B **175**, 435 (1980)
170. K.G. Chetyrkin, A.L. Kataev, F.V. Tkachov, Phys. Lett. B **85**, 277 (1979)
171. M. Dine, J.R. Sapirstein, Phys. Rev. Lett. **43**, 668 (1979)
172. W. Celmaster, R.J. Gonsalves, Phys. Rev. Lett. **44**, 560 (1980)
173. S.G. Gorishnii, A.L. Kataev, S.A. Larin, Phys. Lett. B **273**, 141 (1991)
174. K.G. Chetyrkin, J.H. Kühn, A. Kwiatkowski, hep-ph/9503396